

**USE OF A GEOGRAPHIC INFORMATION SYSTEM TO EXTRACT
TOPOGRAPHY FOR MODELING FLOW IN THE COLORADO RIVER
THROUGH MARBLE AND GRAND CANYONS**

by

ELEANOR R. GRIFFIN

B.S., United States Military Academy, 1980

A thesis submitted to the
Faculty of the Graduate School of the
University of Colorado in partial fulfillment
of the requirement for the degree of
Master of Science
Department of Geological Sciences

1997

Grand Canyon Monitoring
and Research Center

JUN 30 1997

Received
Flagstaff, AZ

**USE OF A GEOGRAPHIC INFORMATION SYSTEM TO EXTRACT
TOPOGRAPHY FOR MODELING FLOW IN THE COLORADO RIVER
THROUGH MARBLE AND GRAND CANYONS**

by

ELEANOR R. GRIFFIN

B.S., United States Military Academy, 1980

A thesis submitted to the
Faculty of the Graduate School of the
University of Colorado in partial fulfillment
of the requirement for the degree of
Master of Science
Department of Geological Sciences

1997

JUN 30 1997

Received
Flagstaff, AZ

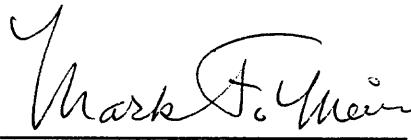
This thesis for the Master of Science degree by

Eleanor R. Griffin

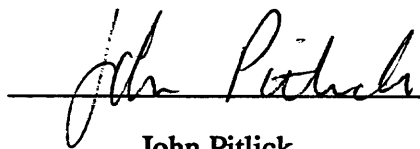
has been approved for the

Department of Geological Sciences

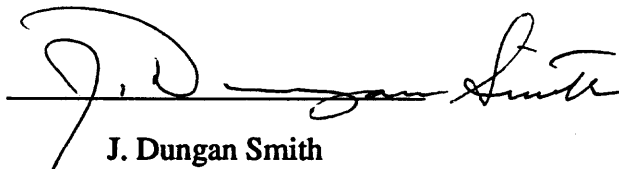
by



Mark F. Meier



John Pitlick



J. Dungan Smith

Date 4/7/97

Griffin, Eleanor R. (M.S., Geological Sciences)

Use of a Geographic Information System to Extract Topography for Modeling Flow in
the Colorado River through Marble and Grand Canyons

Thesis directed by J. Dungan Smith, U.S. Geological Survey

The presence and operation of Glen Canyon Dam have a strong impact on the riparian habitat along the Colorado River downstream from the dam through Marble and Grand Canyons. Experience has shown that the present operating conditions, although less extreme than those employed prior to 1990, are contributing to the erosion of beaches downstream from the dam, and not allowing periodic renewal of these beaches. The changes in riparian habitat are of great concern to researchers studying the effects of the operation of the dam on biological systems and beach erosion, as well as to those who use sand bars for recreational activities. The observed effects of the present flow conditions have resulted in a proposal to conduct controlled floods as a means of redistributing sediment through the system. The ability to model flow and sediment transport through Marble and Grand Canyons is needed in order to predict the effects of such controlled floods.

Efforts to model flow and sediment transport in the Colorado River through Marble and Grand Canyons have been limited by a lack of information on the detailed topography through this reach, especially for stages expected during the proposed controlled floods. Such topographic data have been obtained from aerial photographs for several selected reaches covering about 20% of the river corridor from Lees Ferry to Diamond Creek, and have been entered into a geographic information system (GIS) database. A method is presented here for extracting topography from the GIS database, and using this topography to derive a characteristic channel shape for the 362-km reach between Lees Ferry and Diamond Creek. Hydraulic properties associated with this channel shape were derived from hydrographs computed from the

records of streamflow-gaging stations recorded during an experimental high flow release from Glen Canyon Dam in March and April, 1996. Channel roughness as a function of stage was then calculated for the new channel shape over the range of discharge of the high flow release (226 m³/s to 1,270 m³/s).

An existing one-dimensional unsteady flow model was modified with the new channel shape and roughness functions and applied to flows above 790 m³/s to test its accuracy. These tests showed the new functions result in significant improvement of the model predictions for high flows. The flow model can now be used to provide a hydrodynamic foundation upon which researchers can determine the most environmentally sound method of operating Glen Canyon Dam.

ACKNOWLEDGEMENTS

This work was funded by the U.S. Geological Survey in cooperation with the Bureau of Reclamation as part of the Glen Canyon Environmental Studies.

Jim Dungan Smith suggested the thesis topic and provided me the opportunity and inspiration to work on this project. Because of his willingness to share ideas as well as his knowledge and insight into physical processes, this has been an extremely rewarding learning experience. Mark Meier, who chaired my thesis committee, and John Pitlick, who participated as a member of the committee, provided support, raised interesting questions, and offered helpful suggestions throughout this process.

Sam Jansen, formerly of the USGS Water Resources Division in Tucson, Arizona, taught me the basics of ARC/INFO and Arc Macro Language programming, which greatly reduced the amount of time required for this project. In addition, he provided a general approach that served as the basis for the method used to extract the cross-sections from the GIS data.

Steve Wiele's willingness to share his insight and knowledge, discuss the project, read manuscripts, and offer suggestions for different approaches substantially improved the final product. One particularly significant suggestion Steve made was to use the falling limb of the hydrographs from the 1996 high flow release from Glen Canyon Dam to derive the channel roughness relation.

Discussions with many others working on related GCES studies, including Julie Graf of the USGS Water Resources Division in Tucson, and Ned Andrews and David Topping of the USGS in Boulder, were also helpful. The opportunity to participate in field work directed by Julie Graf and Ned Andrews enabled me to actually see some of the reach being modeled and directly observe the streamflow-channel characteristics

of this reach. This experience was valuable later in making decisions concerning methods used to average the cross-sections and in evaluating the results.

I extend my greatest appreciation to all those mentioned above as well as to my family and friends, who were supportive throughout this process.

CONTENTS

CHAPTER			
1.	INTRODUCTION.....		1
	Background.....		1
	GCES/GIS Data.....		4
	Pre-Dam Geomorphic Processes		8
	Purpose and Scope.....		9
2.	METHOD.....		10
	Derivation of the Channel Geometry.....		10
	Limitations of the GIS Data.....		16
	Density of Cross-Sections.....		17
	Computing the Average Channel Shape.....		24
	Division by Morphologically Similar Reaches.....		25
	Estimation of the Channel Shape below the 140 m ³ /s Water Surface.....		26
	Method used to Average the Individual Cross-sections within a GIS Reach		31
	Morphologically Similar Reach RM 0 - 11		41
	Morphologically Similar Reach RM 11 - 23		44
	Morphologically Similar Reach RM 23 - 50		48
	Morphologically Similar Reach RM 50 - 63.3		50
	Morphologically Similar Reach RM 63.3 - 77		51
	Morphologically Similar Reach RM 77 - 107		54
	Morphologically Similar Reach RM 107 - 140		56
	Morphologically Similar Reach RM 140 - 169		58
	Morphologically Similar Reach RM 169 - 190		58
	Morphologically Similar Reach RM 190 - 225		60
	Computing the Single Weighted Average Channel Shape.....		63

	Discussion of the Break in Slope of the Average Channel Shape.....	65
	Specification of the Channel Shape for the Flow Model.....	75
	Estimation of the Channel Roughness.....	76
	Determination of the Friction Coefficient using Measured Wave Speeds	79
	Finding β for a specific discharge.....	86
3.	RESULTS	91
	Application of the Revised Flow Model.....	91
	Application of the Revised Model to the 1996 High Flow Release	91
	Application of the Revised Model to Normal Dam Operations	98
	Application of the Revised Model to Two Pre-dam Flood Events	101
4.	SUMMARY AND CONCLUSIONS.....	104
	Future Work.....	105
	REFERENCES	108
	APPENDIX	
	A. DISTRIBUTION OF THE GIS REACHES IN RELATION TO RIVER LEVEL GEOLOGY	111

TABLES

Table

1.	Statistics for average shapes calculated using different cross-section spacings.....	22
2.	Summary of the GIS cross-section data	24
3.	Statistics for the GIS reaches.....	38
4.	Comparison of average widths at 140 m ³ /s	41
5.	Calculated weighting factors for the average shapes representing the morphologically similar reaches	64
6.	Geometric and hydraulic properties of the average channel shape from the GIS cross-sections.....	89
7.	Error of the original and revised models on the rising limb of the 1996 high flow release	92
8.	Error of the original and revised models on the falling limb of the 1996 high flow release	93

FIGURES

Figure		
1.	Map of the study area showing gaging station locations.....	2
2.	Locations of the GCES/GIS reaches	5
3.	Contour coverage for a segment of GCES/GIS Site 3.....	7
4.	Hydrograph computed from stage records and the stage-discharge relation at streamflow-gaging station Colorado River at Lees Ferry during a flood event in 1927	11
5.	Three-dimensional surface model (TIN surface) for a segment of GCES/GIS Site 3	13
6.	Distribution of cross-sections within a segment of GCES/GIS Site 3	15
7.	Comparison of average shapes calculated for GIS Site 9, RM 143-145, using different cross-section spacings	19
8.	Comparison of average shapes calculated for GIS Site 7, RM 120-123, using different cross-section spacings	20
9.	Comparison of average shapes calculated for GIS Site 5, RM 63.3-72, using different cross-section spacings	21
10.	Comparison of the average shape calculated for all the Wilson cross-sections with the average shape calculated in reaches where the river-level rock is limestone.....	28
11.	Comparison of the average shape calculated from the GIS Site 6 cross-sections with average shapes calculated using the Wilson cross-sections.....	30
12.	Comparison of the average channel shapes below the 140 m ³ /s water surface calculated from the GIS and Wilson cross-sections for morphologically similar reach RM 63.3 to 77.....	32
13.	Comparison of the average channel shape calculated for GIS Site 10, RM 179 to 181, using three different methods tested.....	33
14.	Example of a single cross-section extracted from the GIS data.....	36
15.	Comparison of the average shapes calculated from the Wilson cross-sections and the GIS cross-sections for morphologically similar reach RM 0 to 11	43
16.	Comparison of the average channel shapes calculated from the Wilson cross-sections for RM 11 to 23 and for RM 77 to 107.....	45

17.	Comparison of the average shapes calculated from the GIS Site 6 cross-sections and the Wilson cross-sections for the reaches RM 0 to 225, RM 11 to 23, and RM 77 to 107.....	46
18.	Comparison of the average shapes calculated from the Wilson cross-sections and the GIS cross-sections for morphologically similar reach RM 11 to 23	47
19.	Comparison of the average shapes calculated from the Wilson cross-sections and the GIS cross-sections for morphologically similar reach RM 23 to 50	49
20.	Comparison of the average shapes calculated from the Wilson cross-sections and the GIS cross-sections for morphologically similar reach RM 50 to 63.3	52
21.	Comparison of the average shapes calculated from the Wilson cross-sections and the GIS cross-sections for morphologically similar reach RM 63.3 to 77	53
22.	Comparison of the average shapes calculated from the Wilson cross-sections and the GIS cross-sections for morphologically similar reach RM 77 to 107	55
23.	Comparison of the average shapes calculated from the Wilson cross-sections and the GIS cross-sections for morphologically similar reach RM 107 to 140	57
24.	Comparison of the average shapes calculated from the Wilson cross-sections and the GIS cross-sections for morphologically similar reach RM 140 to 169	59
25.	Comparison of the average shapes calculated from the Wilson cross-sections and the GIS cross-sections for morphologically similar reach RM 169 to 190	61
26.	Comparison of the average shapes calculated from the Wilson cross-sections and the GIS cross-sections for morphologically similar reach RM 190 to 225	62
27.	Comparison of the average channel shape calculated for the entire 362-km (225-mile) reach using the GIS cross-sections and the average channel shape calculated from the Wilson cross-sections.....	66
28.	Examples showing the average channel shape above the 140 m ³ /s water surface	69
29.	Wilson cross-section S-9, at RM 7.4, shown with no vertical exaggeration.....	72
30.	Roughness relation for the original channel shape from the average of the Wilson cross-sections	78

31.	Hydrographs computed from the records of the streamflow-gaging stations at Lees Ferry (RM 0) and above Diamond Creek near Peach Springs (RK 362, RM 225) for the falling limb of the 1996 high flow release	80
32.	Wave speed calculated from the records of the streamflow-gaging stations at Lees Ferry and above Diamond Creek, recorded during the falling limb of the 1996 high flow release	82
33.	Comparison of wave speed calculated from the records of the streamflow-gaging stations at Lees Ferry and above Diamond Creek during the falling limb of the 1996 high flow release and the calculated least-squares regression curves	84
34.	Roughness as a function of hydraulic radius calculated for the new channel shape from the average of the GIS cross-sections compared to the roughness relation for the original channel shape.....	87
35.	Predicted discharge as a function of stage for the average channel shape calculated from the GIS cross-sections	90
36.	Calculated hydrographs and hydrographs computed from stage records and the stage-discharge relation at streamflow-gaging station Colorado River above the Little Colorado River near Desert View (RK 98, RM 61) for the 1996 high flow release	95
37.	Calculated hydrographs and hydrographs computed from stage records and the stage-discharge relation at streamflow-gaging station Colorado River near Grand Canyon (RK 142, RM 88) for the 1996 high flow release	96
38.	Calculated hydrographs and hydrographs computed from stage records and the stage-discharge relation at streamflow-gaging station Colorado River above Diamond Creek near Peach Springs (RK 362, RM 225) for the 1996 high flow release	97
39.	Calculated hydrographs and hydrographs determined from stage records and the stage-discharge relation at Colorado River streamflow-gaging stations during a period of normal dam operations.....	99
40.	Calculated hydrographs and hydrographs determined from stage records and the stage-discharge relation at Colorado River near Grand Canyon (RK 142, RM 88) for two flood events in 1927	103

CHAPTER 1

INTRODUCTION

Background

Glen Canyon Dam on the Colorado River near Page, Arizona was completed in 1963, eliminating the primary sand source and natural floods through the Marble and Grand Canyons for the foreseeable future. Completion of this dam and its subsequent operation for power generation have resulted in significant changes in the riparian environment from the dam to Lake Mead, 386 kilometers (km) downstream (figure 1). In 1983, the Glen Canyon Environmental Studies (GCES) were initiated to investigate the effects of operation of the dam on riparian habitat within this 386 km reach. These studies were concerned with environmental changes affecting fish and wildlife, vegetation, and beaches resulting from the new flow conditions and erosion, deposition, and transport of fine sediment, dominantly sand.

The research conducted by the U.S. Geological Survey (USGS) in support of the GCES included the development of a one-dimensional unsteady flow model to route the dam releases downstream to Lake Mead (Wiele and Smith, 1996). This model was developed using data that included measured channel cross-sections, reach-averaged velocities determined by dye tracing, channel slope, and streamflow-gaging station information obtained during research flow B. Research flow B was one of a series of controlled dam releases during 1990 and 1991 that fluctuated between a specified minimum and maximum discharge on a daily cycle for a period of 11 days. Streamflow-gaging station information obtained during research flow B and two other research flows was used to check the accuracy of the model results. This information consisted of measurements of stage and the associated stage-discharge relations at the gaging stations. The one-dimensional model is based on large-scale, reach-averaged

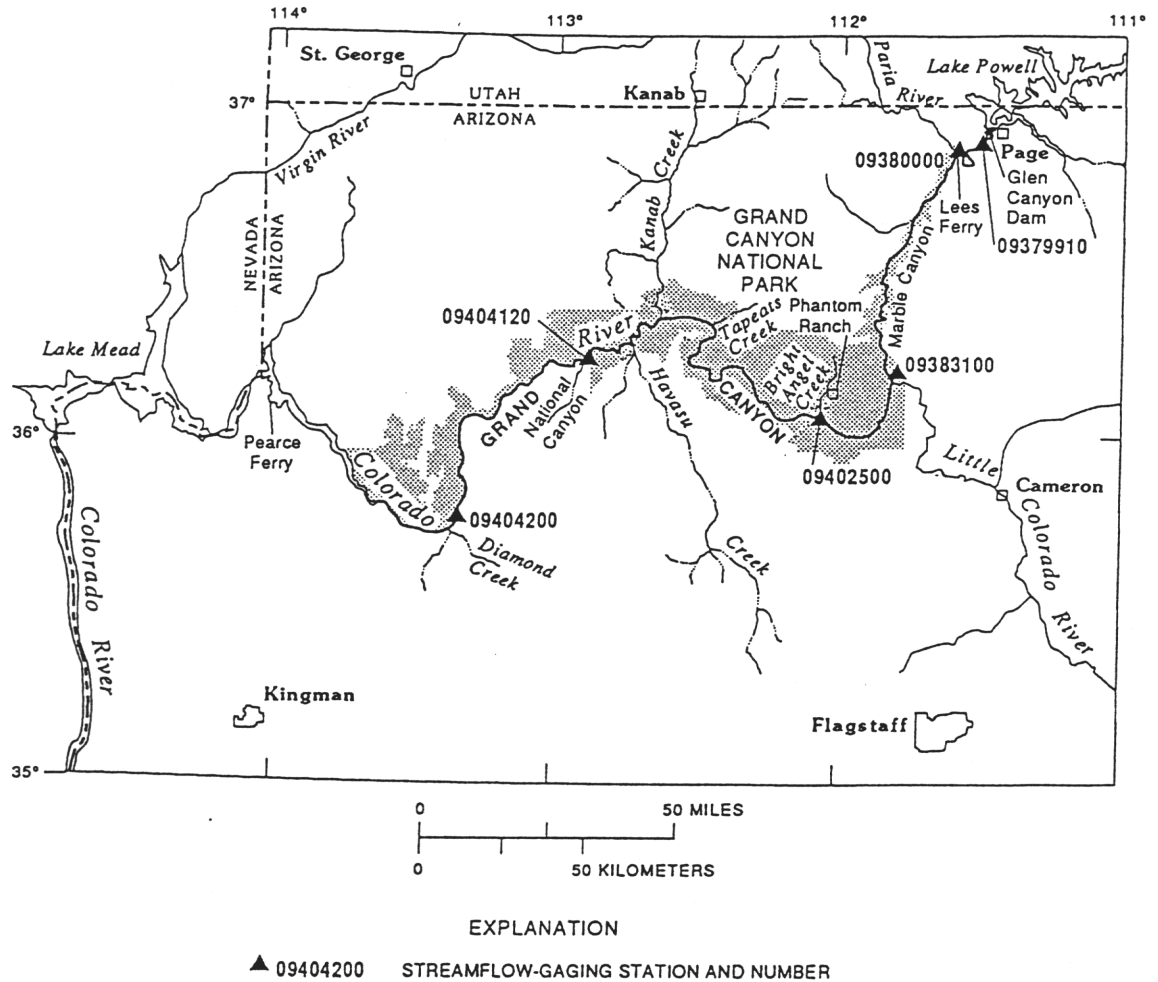


Figure 1. Map of the study area, showing the locations of six mainstem streamflow-gaging stations on the Colorado River between Glen Canyon Dam and Lake Mead (modified from Graf, 1995).

channel properties, including a single characteristic cross-section and an average slope (0.0015) for the entire 386 km reach.

The model solves numerically a combined form of the continuity and momentum equations derived by Lighthill and Whitham (1955) in order to predict the speed and shape of the discharge wave as it progresses from Glen Canyon Dam downstream through the Marble and Grand Canyons. This enables the model to calculate discharge hydrographs at desired locations downstream from the dam, using the dam release as an upstream boundary condition. The calculated discharge hydrographs are used by

researchers as part of their analysis of the effects of the dam releases on various physical and biological systems downstream.

The channel shape used in the model was developed using a reach-averaged channel geometry derived from 199 cross-sections measured by Wilson (1986). These cross-sections were measured at 199 locations between Lees Ferry (River Kilometer (RK) and River Mile (RM) 0)¹ and Diamond Creek (RK 362, RM 225), at discharges close to 790 m³/s (28,000 ft³/s). Digitized versions of these cross-sections were made available by the Bureau of Reclamation (T. Randle, BOR, written communication). A non-dimensional roughness coefficient was derived from velocity and cross-section measurements at known discharges and wave speed measured during research flow B (Wiele and Smith, 1996). When the model was applied to flows above 790 m³/s (28,000 ft³/s), hydraulic geometry in the model was extrapolated, because this was the maximum discharge for which velocity and cross-section measurements were available. Detailed topographic information is unavailable for most of the river corridor between Glen Canyon Dam and Lake Mead for flows above this level (Smith and Wiele, 1995).

The inability to model flows above 790 m³/s has been a serious deficiency, because observations have shown that flows with discharges below this level are not renewing the riparian habitat. Bathymetric surveys (Graf et. al., 1995b) within limited reaches have shown that a large volume of sand is available at times on the channel bed, particularly after high tributary inflows. However, the range of discharges in the Colorado River released from Glen Canyon Dam under normal operations have not been sufficient to move this sand from the bed to the channel margins. As a result, the sand is carried through the system and finally deposited at the bottom of Lake Mead. If

1. The primary units in this paper are metric. Because the location on the river is commonly given in river miles upstream (-) or downstream (+) from Lees Ferry, Arizona, locations and distances are given in both river kilometers and river miles. The use of cubic feet per second for discharge is also common and is clearly associated with stage at specific points along the river. Therefore, discharges are given in cubic meters per second and cubic feet per second.

Glen Canyon Dam is to be operated in a manner that will minimize its negative impact on the downstream environment, controlled floods must be used as a management tool and the dam operators need to be able to model flow and sediment transport at discharges higher than $790 \text{ m}^3/\text{s}$. Detailed information concerning the channel geometry and roughness at stages above those encountered with discharges at or below $790 \text{ m}^3/\text{s}$ is needed to be able to model the higher flows.

The ability to obtain field measurements of channel cross-section is limited by the scale and remoteness of the river corridor, resulting in a high cost associated with each set of measurements. Additional considerations are the need to protect a fragile riparian environment and areas considered sacred by local Native Americans. Therefore, other approaches are needed to obtain channel cross-section information. A method for extracting channel shape from topography developed from aerial photography and entered into a geographic information system (GIS) database is presented here.

GCES/GIS Data

Thirteen reaches through Marble and Grand Canyons have been selected as long-term monitoring sites for the GCES (figure 2). These reaches vary in length from 3.2 to 19.3 km and add up to approximately 98 km, 74 km of which are between Lees Ferry and Diamond Creek (Werth et al., 1993). As part of the support for extensive scientific studies in these areas, the Bureau of Reclamation (BOR) obtained aerial photographs of the selected reaches during periods of low flow, $140 \text{ m}^3/\text{s}$ ($5,000 \text{ ft}^3/\text{s}$), in June and July, 1990 and 1991. Topography was determined from these aerial photographs and used to create a GIS database (Werth et al., 1993). The data extend from the top of the old high water zone (OHWZ) river-right to the top of the OHWZ river-left. The OHWZ is identified by a relatively stable band of riparian shrubs just above the $2,800 \text{ m}^3/\text{s}$ ($100,000 \text{ ft}^3/\text{s}$) waterline (Carothers and Brown, 1991).

Long-Term Monitoring Sites	
SITE	LOCATION RIVER MILE
1	GLEN CANYON DAM to -10.5
2	LEE'S FERRY -4 to 2
3	PRESIDENT HARDING 42 to 48
4	NARROVEAP 51 to 56
5	LCR to CADEMÁS 60 to 72
6	GRANITE to CRYSTAL 93 to 98
7	BLACKTAIL 120 to 123
8	TATEATS & DEER CREEK 133 to 138
9	KIMMIB CREEK 143 to 145
10	LAVA FALLS 179 to 181
11	GRANITE PARK 207 to 210
12	DIAMOND CREEK 225 to 230
13	COLUMBINE FALLS 273 to 276

Special Study Sites	
14	HIDDEN SLOUGH -10.4 to -4.1
15	LCR LCR 7.5 to 12
16	MASEY'S PARADISE 29.0 to 42.0
17	BADGER 2.0 to 9.0

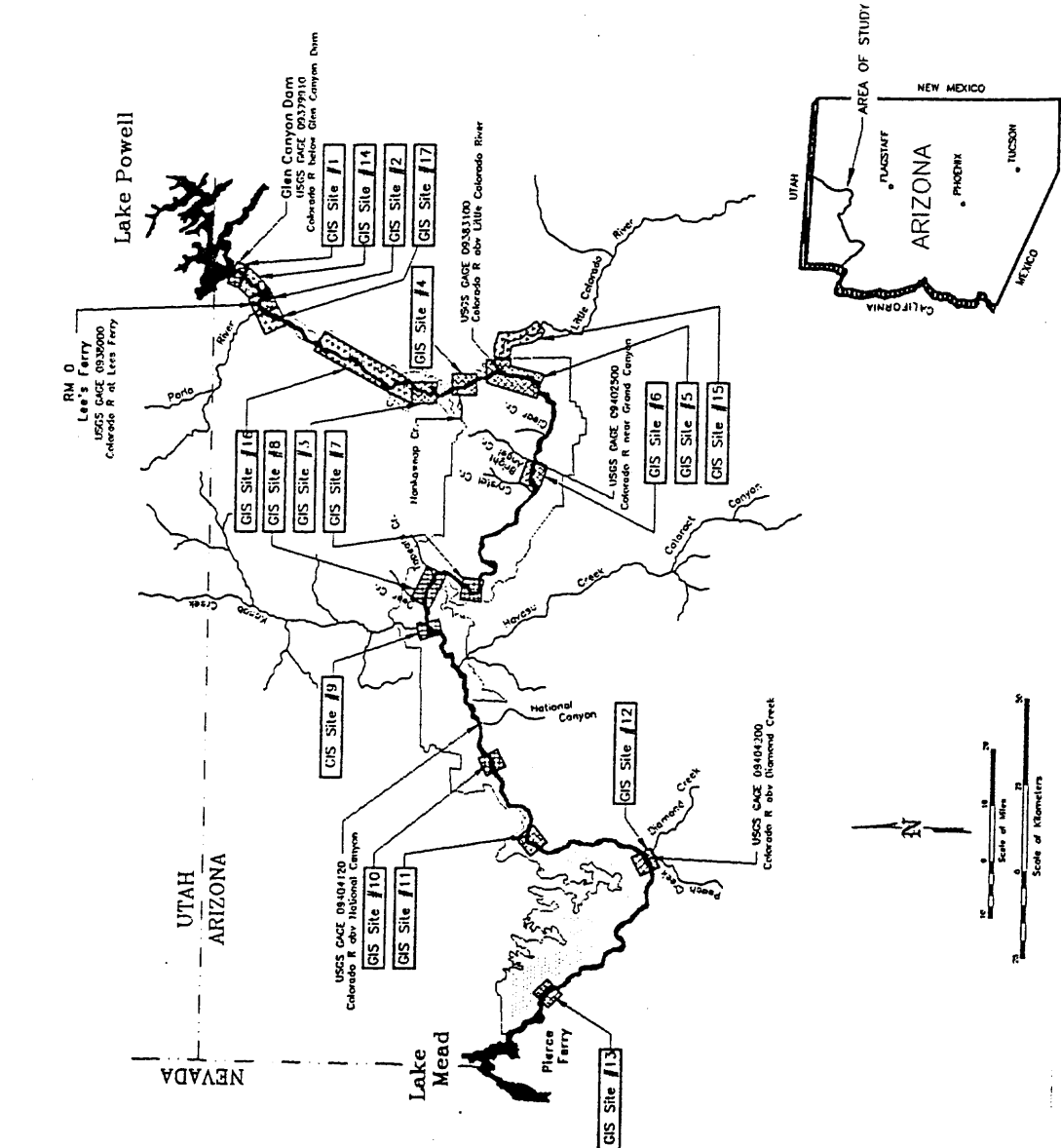
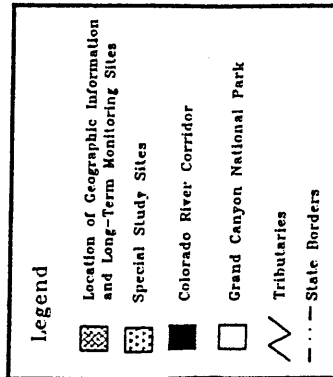


Figure 2. Locations of the GCES long-term monitoring sites, referred to in this report as the GCES/GIS reaches (from Werth et. al., 1993)

Criteria used to select the long-term monitoring sites included representation of ecological diversity and areas where special studies or critical resources were located (Werth et al., 1993). Critical resources include cultural resources (such as archeological sites) and beaches. The archeological sites are concentrated in areas where the river is accessible from the rim. In many cases, access is through side canyons with debris fans at the river. Debris fans also support many of the larger beaches along the river. As a result, several of the long-term monitoring sites are located in reaches much wider than the river on average. This characteristic of the GCES/GIS reaches was an important consideration when using them to compute a reach-averaged channel shape.

The GCES/GIS database was developed using ARC/INFO GIS software and is maintained as ARC/INFO coverages (Werth et al., 1993). The coverages were developed from a 1:2,400 orthophoto grid base map and contain lines (arcs) identifying elevation contours. Contour lines at 0.5-meter intervals were identified where possible, with 1.0-meter vertical accuracy and 2.0m horizontal accuracy (figure 3). Map coordinates are in the Arizona State Plane Coordinate System, in meters. With these ARC/INFO coverages, detailed channel cross-sections within the study reaches were extended to higher stages than was possible with the Wilson cross-sections.

Previous work using this database identified the river centerline and calculated river width at $140 \text{ m}^3/\text{s}$ as a function of distance downstream in each GIS reach (Furey and Smith, personal commun., 1994). A statistical analysis was then performed on the river width as a function of distance downstream, which showed there is no significant correlation between variance in river width and distance downstream within a particular GIS reach. Therefore, the minimum separation of cross-sections in the downstream direction needed to derive an accurate average channel shape could not be determined from these results. However, there was a strong correlation between mean river width and bedrock geology.

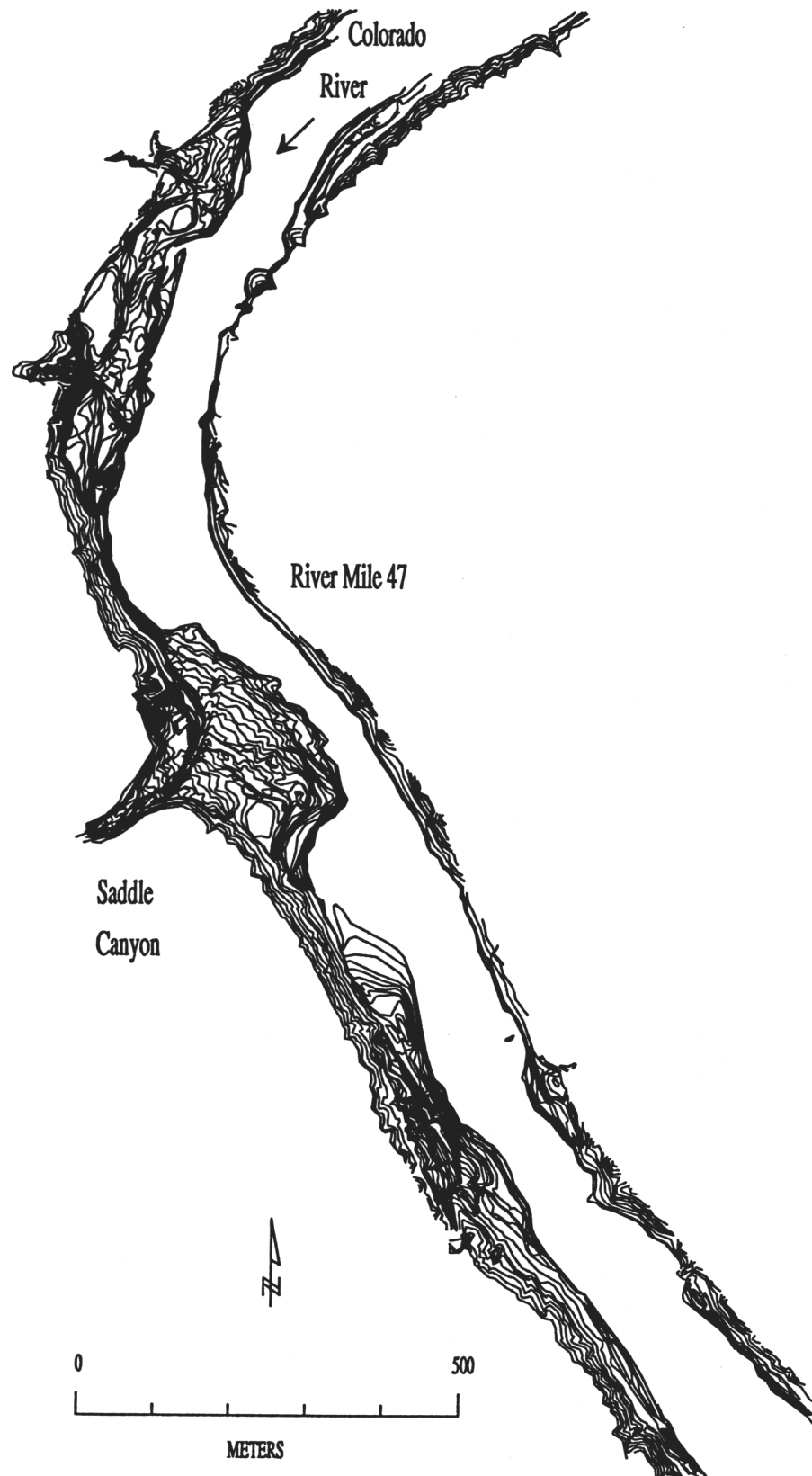


Figure 3. Contour coverage for a segment of GCES/GIS Site 3. Contours are at 0.5-meter intervals where possible, but are not continuous through steep slopes.

The Arizona District Office of the USGS has also performed bathymetric surveys of several of the GIS reaches. These data have been entered into a compatible database, so that the information can be combined with the topography above the river surface at $140 \text{ m}^3/\text{s}$ ($5,000 \text{ ft}^3/\text{s}$) to determine the complete channel geometry. This has only been done for segments of five of the GIS reaches, including one that extends about 10 km (6.5 miles) from the mouth of the Little Colorado River to Tanner Rapid (Graf et al, 1995a).

Pre-dam Geomorphic Processes

Physically-based flow and sediment transport models can be used to calculate pre-dam flow conditions in the Colorado River through the Grand Canyon to gain a better understanding of the hydrologic conditions that existed then. Stage measurements and discharges computed from the records from USGS streamflow-gaging stations at Lees Ferry (station 09380000, Colorado River at Lees Ferry) and near Grand Canyon (station 09402500, Colorado River near Grand Canyon), dating from 1895 and 1922 to the present, respectively, are available (Schmidt and Graf, 1990) and can be used in conjunction with such models as a basis for estimating the pre-dam hydrology of this reach.

Questions that might be addressed using these physically-based models concern rates and large-scale effects of geomorphic processes, including bank erosion, scouring of deep pools below rapids, and movement of large boulders on the bed and in debris fans. These processes all affected the rate of downcutting of the Grand Canyon during one or more periods of regional uplift. Estimates of the time interval during which the Grand Canyon was cut range from about 2 to 5 million years. Based on geologic evidence including the examination and dating of lava deposits within the Grand Canyon, this excavation occurred between six and one million years ago (Lucchitta, in Beus and Morales, 1990). A better understanding of pre-dam hydrologic

conditions may lead to knowledge of the rates at which downcutting through bedrock can occur on a large scale and, ultimately, a process-based estimate of the length of time it took to form the Grand Canyon.

Purpose and Scope

The purpose of my work was to derive river channel geometry within the GCES/GIS reaches along the Colorado River between Lees Ferry and Lake Mead from the ARC/INFO database and to relate stage from the average cross-section to discharge using a reach-averaged roughness. As part of this work, the derived channel geometry and roughness were integrated into an existing one-dimensional unsteady flow model to extend its capability to flows up to about 13,900 m³/s (490,000 ft³/s). In order to check its accuracy, the modified model was applied to normal dam releases, an experimental high flow release, and pre-dam flood events. The maximum discharge which can be modeled using this topography is well above the pre-dam (1921 - 1962) mean annual peak discharge of 2,640 m³/s (93,400 ft³/s) (Schmidt and Graf, 1990).

The modified flow model will provide input to a three-dimensional flow and sediment transport model (Wiele et al., 1996) which predicts the pool-scale transport of sediment in selected reaches downstream from the two main sediment-contributing tributaries (the Paria and Little Colorado Rivers). The flow and sediment transport modeling efforts are designed to route water and sediment downstream during high flows, providing information that can be used to predict the effects of future high flow events. The results of this effort, then, support the modeling of flow and sediment transport through Marble and Grand Canyons for flows above 790 m³/s (28,000 ft³/s). The model results ultimately will be used by researchers to predict the effects of high flow releases from Glen Canyon Dam on the riparian environment downstream from the dam.

CHAPTER 2

METHOD

Derivation of the Channel Geometry

During the development of the previous version of the one-dimensional flow model, Wiele and Smith (1996) determined that the use of a single average cross-section for the entire 386 km reach worked well in predicting the progress of daily flood waves with peaks below about $790 \text{ m}^3/\text{s}$ ($28,000 \text{ ft}^3/\text{s}$). This is a consequence of the length of the diurnal discharge wave, which is 100 to 200 km, or one-quarter to one-half the length of the modeled reach. A typical average wave speed for these daily flood waves is about 2 m/s.

A single average channel shape should also work well for modeling flows of greater discharge, because the higher phase speed of the wave, combined with a sufficiently long wave period, increases the wavelength. For example, a flood event in 1927 recorded by the gaging station at Lees Ferry lasted for a period of about 7 days between June 28th and July 5th (figure 4). Digitized streamflow-gaging station records for this event and the associated stage-discharge relation are available (D. Topping, U.S. Geological Survey, Boulder, personal commun., 1996). During this flood, the discharge increased from about $1,690 \text{ m}^3/\text{s}$ ($59,700 \text{ ft}^3/\text{s}$) to about $3,610 \text{ m}^3/\text{s}$ ($127,000 \text{ ft}^3/\text{s}$) over about 70 hours. Discharge remained near the peak for only about 5 hours, then began a slow, steady decrease back to about $1,690 \text{ m}^3/\text{s}$ over a period of almost 4 days. The average wave speed estimated for this flood is on the order of 3.7 m/s. Because of the wave period and speed, the wavelength was on the order of 2,000 km. Therefore, the progress of this flood wave was influenced by the average channel shape for the entire 386-km reach. For the quasi-steady flow associated with a

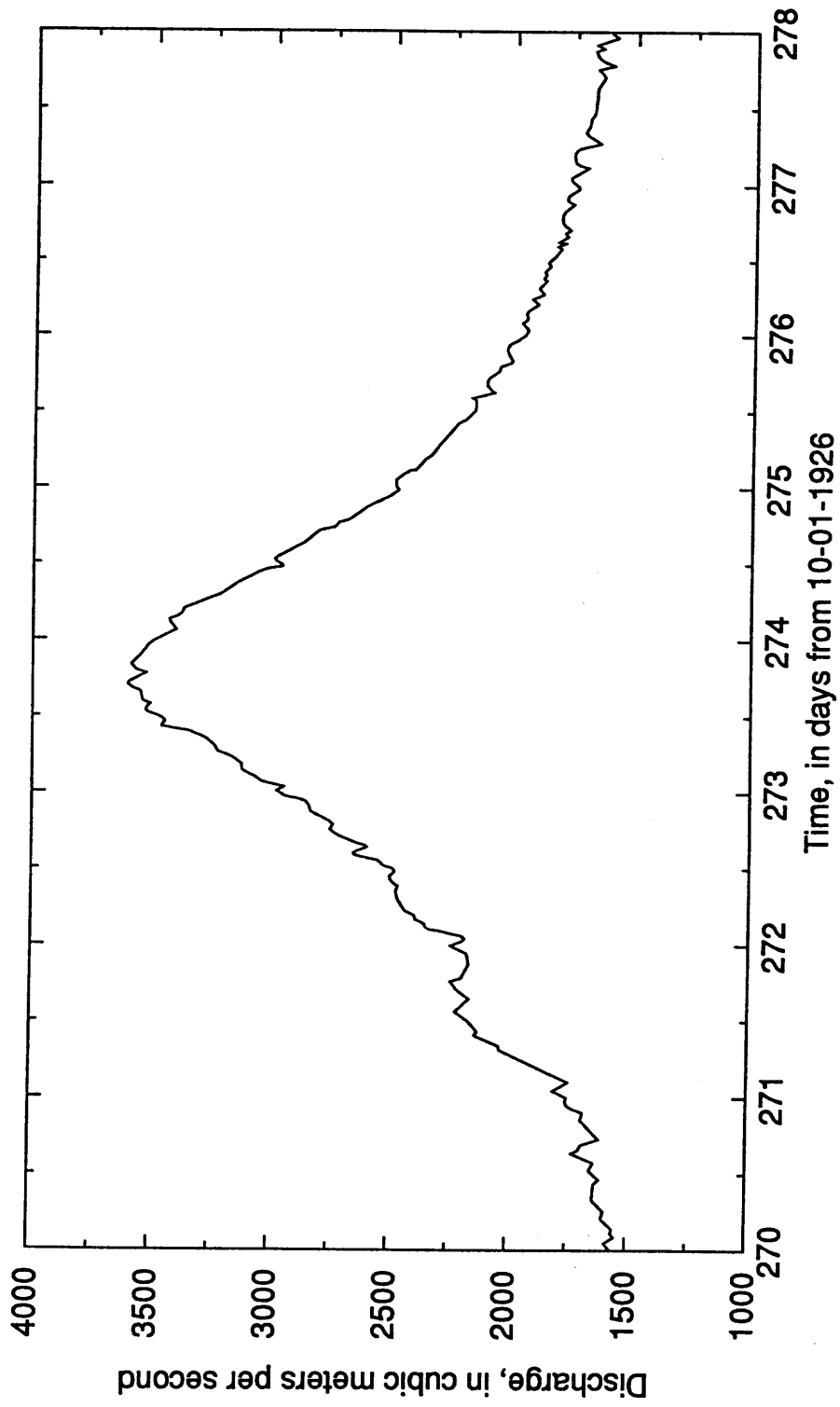


Figure 4. Hydrograph computed from stage records and the stage-discharge relation at streamflow-gaging station Colorado River at Lees Ferry (RM 0) during a flood event in June and July, 1927.

controlled flood, local information concerning stage-discharge relations is also of considerable importance. Therefore, the ability to estimate channel shape and roughness at particular locations is also needed.

The first step in this project was to use ARC/INFO to retrieve a dense set of cross-sections extending from the river's edge at a discharge of $140 \text{ m}^3/\text{s}$ to the top of the zone in which there are data in the GCES/GIS database. The cross-section information was retrieved by first creating a three-dimensional surface model for each individual GCES/GIS reach using the topographic information contained in the appropriate ARC/INFO coverage. A triangulated irregular network (TIN) coverage was created for each GCES/GIS reach using an ARC program (Environmental Systems Research Institute, Inc.(ESRI), 1994). Delaunay triangulation (McCullagh and Ross, 1980), in which sample points are connected to their two nearest neighbors to form triangles, is used in the ARC program to create the TIN. In the GCES/GIS data, the vertices and nodes which lie along the contour arcs, where elevation has been identified photogrammetrically, serve as the sample points. These points are generally spaced 5 to 10 m (planimetric distance) apart. A mesh network of lines parallel to the x- and y-axes was then draped over the surface to display the three-dimensional surface model (figure 5).

Once the TIN surface was created, interpolated values of elevation at desired points could be identified using a breakline bivariate quintic interpolation algorithm (ESRI, 1994). The algorithm, originally developed by Akima (1978) and modified by ESRI, uses a bivariate fifth-degree polynomial in x and y to perform the interpolation. This interpolation method creates a smooth surface model in which the normal to the surface varies continuously within each triangle. Because the geometry of neighboring triangles is considered when the elevation is interpolated, abrupt changes in the surface normal across an edge between triangles are avoided (ESRI, 1994).

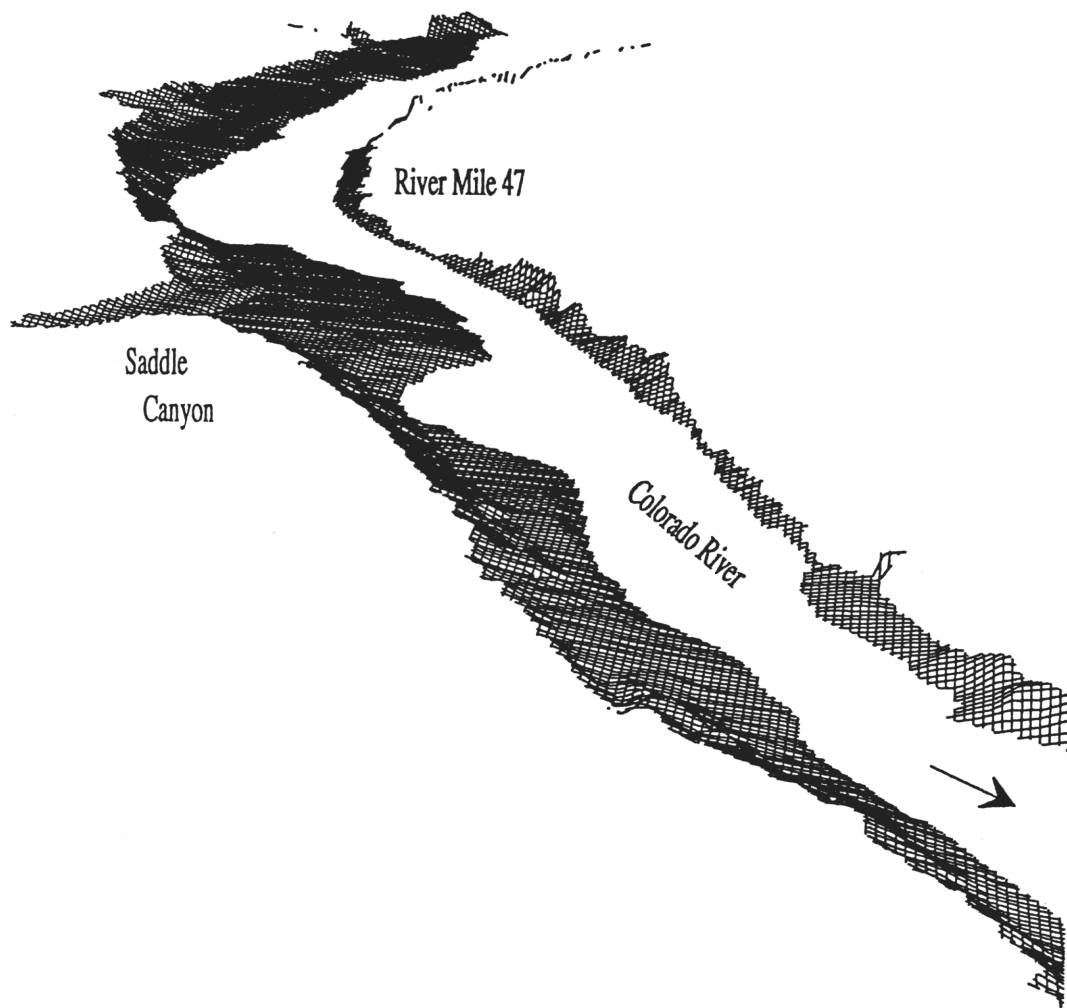


Figure 5. Three-dimensional surface model (TIN surface) for a segment of GCES/GIS Site 3. This is a perspective drawing looking upstream (generally north) with no vertical exaggeration. Mesh spacing is 5.0 meters.

A centerline for the 140 m³/s water surface was identified to use as a reference for the orientation of the cross-section lines and to set the spacing of the cross-sections. The centerline was specified by manually adding an arc (by eye) to the contour coverage within each GCES/GIS reach. The centerline arc was then used to create an ASCII file with x and y coordinates for nodes spaced 10 m apart along the centerline. This file was used to identify equally spaced points along the centerline at the desired interval for the cross-sections (20 m), and x and y coordinates were calculated for left- and right-bank endpoints for cross-section lines at that interval, perpendicular to the centerline (figure 6). Cross-section endpoints were calculated to extend out from the centerline far enough to capture all of the available data within a given reach. The distance of the endpoints from the centerline varied greatly between the narrower and wider reaches, from 100 m within Site 9, in the Muav Gorge near Kanab Creek, to 600 m within the Furnace Flats section of Site 5 (Muav Gorge and Furnace Flats reaches identified by Schmidt and Graf, 1990).

A file containing the cross-section endpoints was then used as input to a program run in ARCPLOT (ESRI, 1994), which computed the elevation at equally-spaced intervals (planimetric) along the cross-section line. In most cases, the spacing of the points along the line was 1.0 m. However, in areas where a cliff face extends from the water surface to the top of the OHWZ, the sampling distance was reduced to 0.5m in order to obtain at least two points for that bank, indicating the highest and lowest elevations of the bank. The output of this program was a file containing the x and y coordinates, distance from the left-bank endpoint, and the elevation at each point for the set of cross-section lines through the GCES/GIS reach.

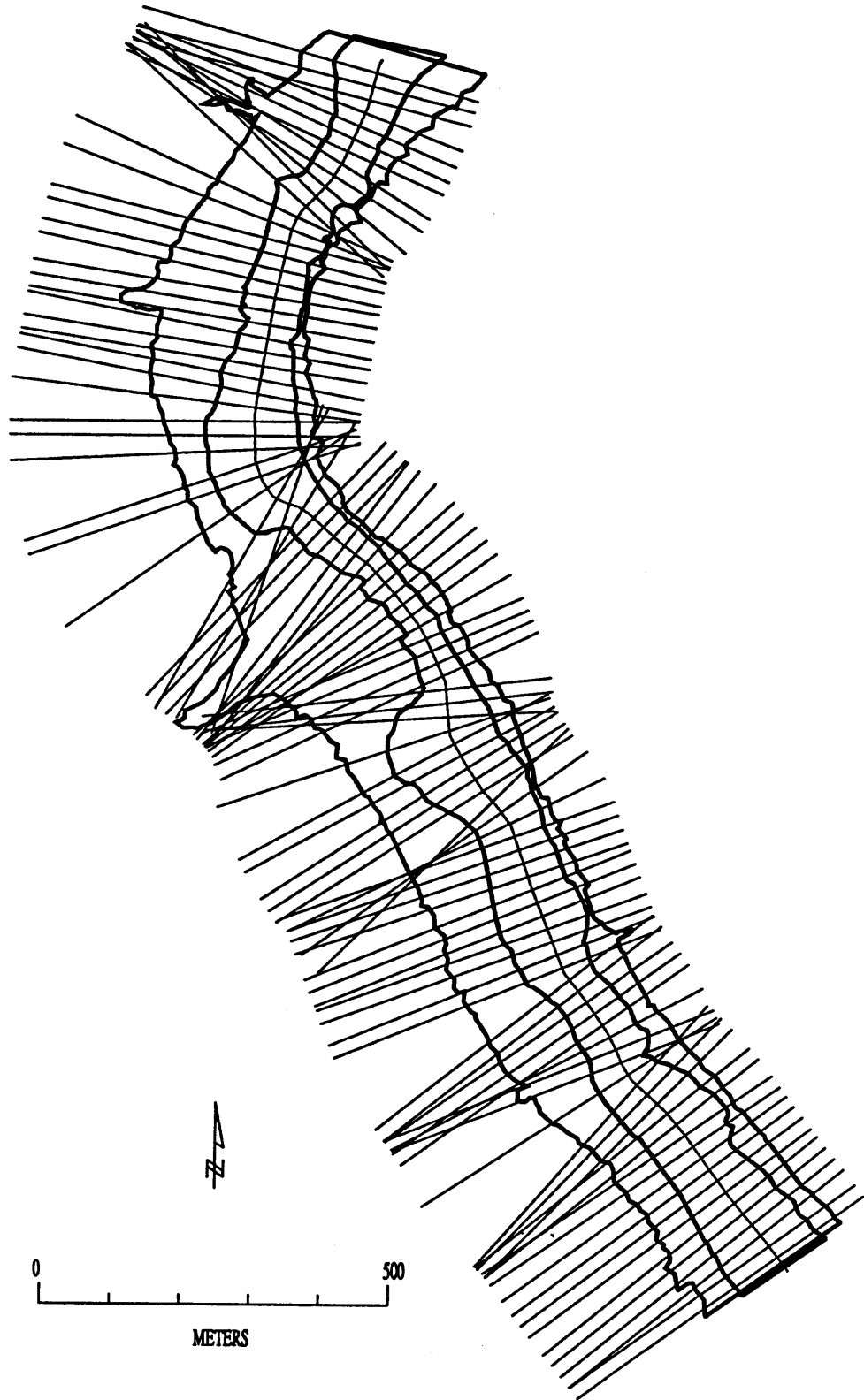


Figure 6. Distribution of cross-sections within a segment of GCES/GIS Site 3. Left and right-bank boundaries are shown, along with the $140 \text{ m}^3/\text{s}$ centerline.

The output cross-section data file was run through a program to filter out points with no elevation data and to identify the separate cross-sections. Also, for some reaches, the data did not extend up to the same maximum elevation on both banks. In those cases, only the data up to the lower of the two maximum elevations were retained. The cross-sections were then averaged to obtain a single average shape for each GCES/GIS reach. Details of the method used to average the cross-sections are discussed below.

Limitations of the GIS Data

There are two limitations of the GIS data that affect the retrieval of accurate cross-section data. One limitation is that the contour lines are not continuous through each reach. Where slopes become very steep, several contour lines may disappear within a short distance. In some areas, for example where a near-vertical cliff face extends from the water surface to the highest elevation included for that bank, only one or two contour lines are shown. The cliff face is also indicated simply with a breakline assigned no elevation in some areas. To represent these areas in the sets of cross-sections, the GIS data needed to be modified to provide boundaries with high and low elevations for these reaches. Arcs were added parallel to and within a short distance (about 1m) of an existing contour line or the breakline and assigned either the water-surface elevation or the highest elevation for that reach, as appropriate. The breakline itself was then assigned either the highest or lowest elevation of adjacent topography.

Another limitation of the GIS data for use in obtaining the average channel shape is that they do not extend below the 140 m³/s water surface. As a result, the shape of the channel below this water surface had to be estimated. This was done by adding an average shape obtained from the Wilson cross-sections below the 140 m³/s water surface, rescaled to the water surface width of the cross-section being averaged. A detailed discussion concerning how the estimated shape was obtained is provided in

the section "Computing the Average Channel Shape," below.

Density of the Cross-Sections

An initial estimate of the density of the cross-sections needed to represent accurately the average shape of the channel through each reach was one tenth of the river top width. This estimate is based on observed streamwise variations in channel width (Furey and Smith, personal commun.). The average top width for the GCES/GIS reaches was estimated to be about 200 m for some of the narrower reaches. A 20 m spacing of the cross-sections along the 140 m³/s water surface centerline was then estimated to be sufficient to provide a reasonably accurate shape for each reach.

In order to check whether or not the 20 m cross-section spacing was appropriate, the average shape was calculated for cross-sections spaced at 20 m, 60 m, 100 m, 120 m, 200 m and 400 m at the channel centerline for three of the GIS reaches. Average shapes and the standard deviation of the elevation were calculated for part of Site 5 (RM 63.3 to 72), Site 7 (RM 120 to 123), and Site 9 (RM 143-145). These reaches were chosen because they represented a broad range of reach lengths (8.7, 3, and 2 miles, or 14, 4.8, and 3.2 km, respectively) and average top widths (359 m, 196 m, and 135 m, respectively). Average channel shapes with cross-section spacings of 500 m and 600 m were also computed for the Site 5 reach because of its much greater length.

The sample size used to compute the average shape for each reach was dependent upon the length of the reach and the cross-section spacing. Therefore, the number of cross-sections used to compute the average shape was reduced with each increase in cross-section spacing. At 20 m spacing, the number of cross-sections averaged was 695 for Site 5, 261 for Site 7, and 180 for Site 9, while at 200 m spacing, these numbers were reduced to 67, 25, and 18, respectively. The greater the number of cross-sections within a given morphologically similar reach, the greater the resolution of the

average shape for that reach. By comparing the average shape calculated with different cross-section spacings, the number of cross-sections within a given reach needed to accurately determine the average shape was found.

The variability in mean channel shape found with different cross-section spacings was compared in two ways for the three GIS reaches. The first comparison was made with dimensions of width retained, while the second was made with width normalized in the cross-stream direction by dividing by the average top width. The average shapes computed for Sites 7 and 9 were averaged about the center of the 140 m³/s water surface, so that the computed average shape is symmetric. Reasons for averaging the left and right sides of the channel in these reaches are discussed later in this paper. For each of the three reaches, the mean section computed is essentially the same for cross-section spacings up to about 100 m (figures 7 - 9; table 1). For the shortest reach, Site 9 (RM 143 to 145), the average shape is well-defined with as few as 30 cross-sections spaced 120 m apart (figure 7). The difference between the mean top width of this shape and the average shape computed for Site 9 with 20 m cross-section spacing is about 1.8% (2.4 m), while the difference in width of the 140 m³/s water surface for the two average shapes is about 1.5% (0.86 m). With 200 m cross-section spacing, the difference in mean top width increases to 5.9%, while the difference in the calculated width of the 140 m³/s water surface is only 0.3%.

The minimum cross-section spacing for Site 7 (RM 120 to 123) that produces nearly the same shape as the average with 20 m cross-section spacing is 100 m (52 cross-sections; figure 8). With this spacing, the mean top width is about 1.1% (2.1 m) different from the mean top width of the average shape with 20 m cross-section spacing. The difference in the mean width of the 140 m³/s water surface for these two shapes is 0.74% (0.54 m). For Site 7, increasing the cross-section spacing to 120 m results in an increase in the difference in mean top width to 4.5%. The difference in the calculated mean water surface width remains low, at 0.8%.

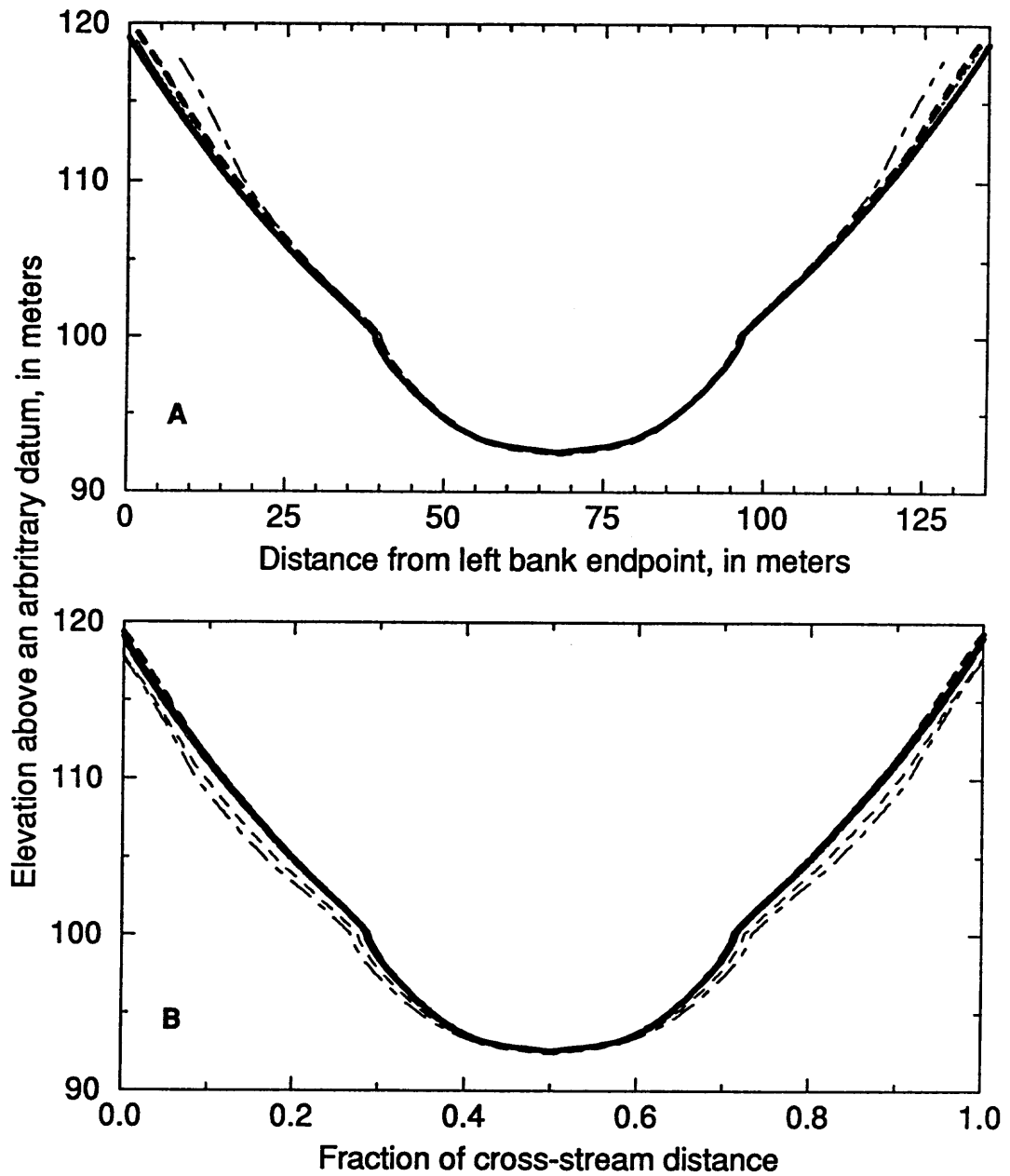
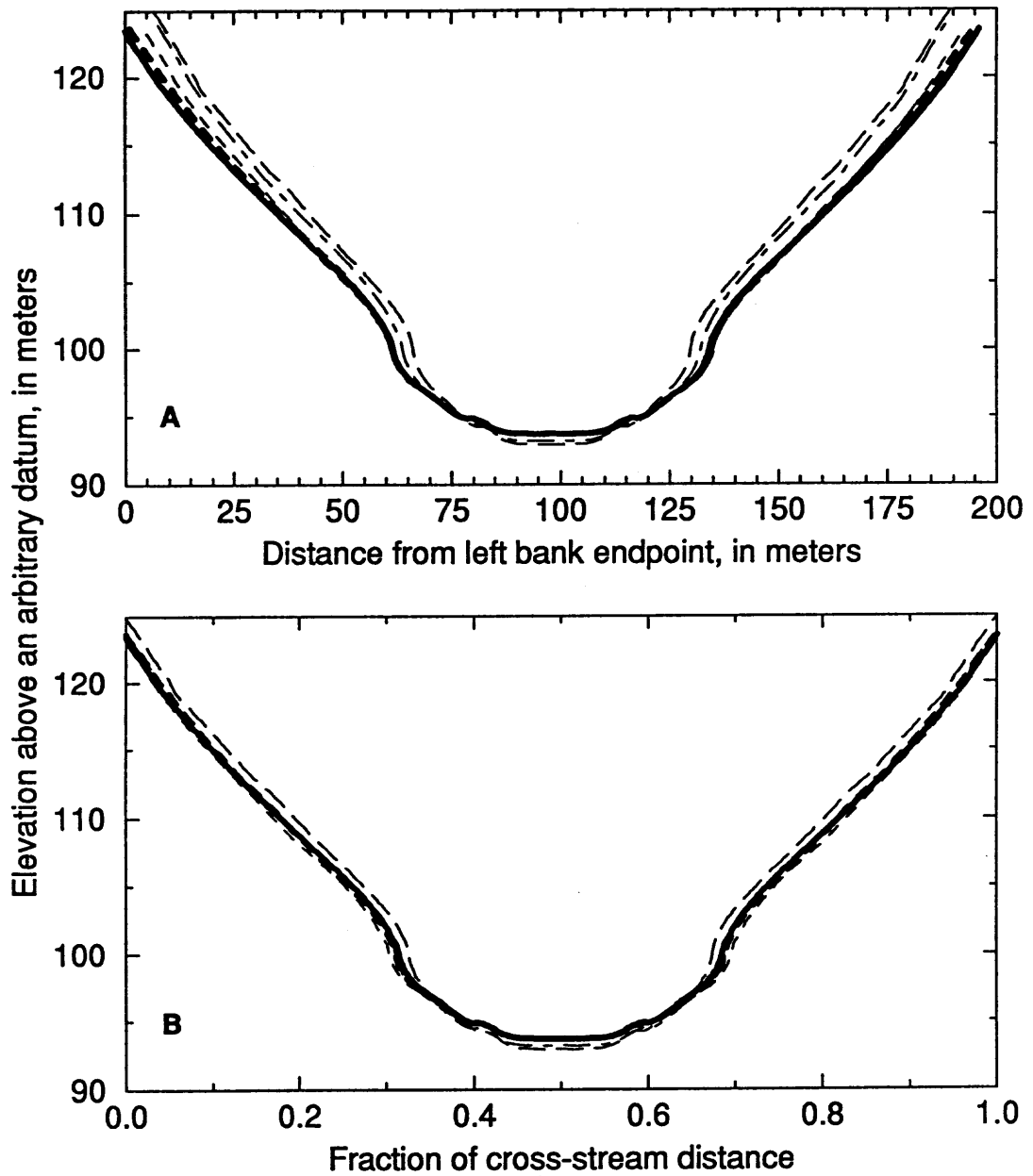


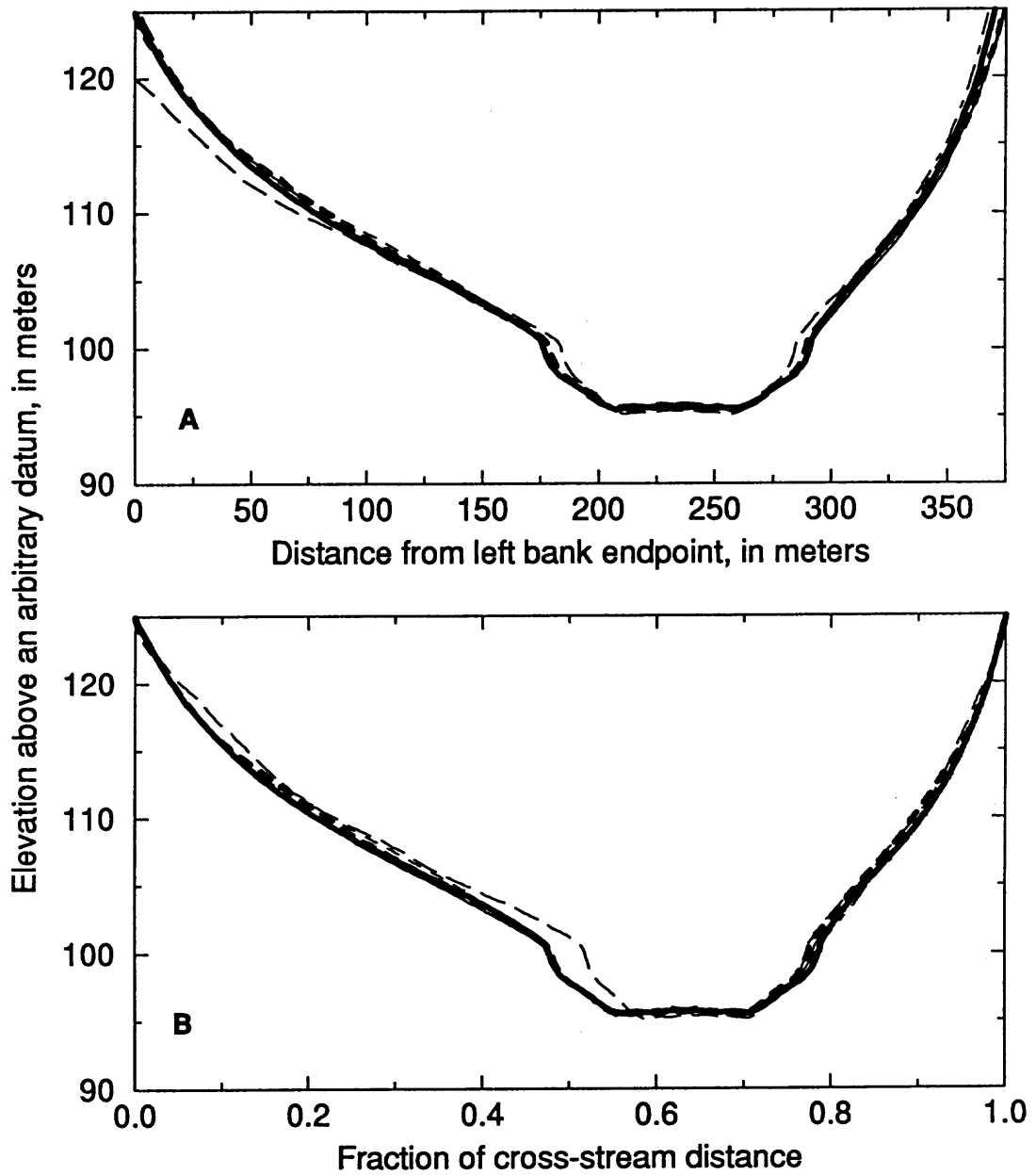
Figure 7. Comparison of average shapes calculated for GIS Site 9, RM 143 to 145, using different cross-section spacings. A, with dimensions of width retained. B, with each average shape divided by its top width.



EXPLANATION

- 261 cross-sections with 20m spacing
- 86 cross-sections with 60m spacing
- - - 52 cross-sections with 100m spacing
- - - 43 cross-sections with 120m spacing
- - - 25 cross-sections with 200m spacing
- - - 12 cross-sections with 400m spacing

Figure 8. Comparison of average shapes calculated for GIS Site 7, RM 120 to 123, using different cross-section spacings. A, with dimensions of width retained. B, with each average shape divided by its top width.



EXPLANATION

- 695 cross-sections with 20m spacing
- 137 cross-sections with 100m spacing
- - - 67 cross-sections with 200m spacing
- - - 32 cross-sections with 400m spacing
- - - 26 cross-sections with 500m spacing
- - - 20 cross-sections with 600m spacing

Figure 9. Comparison of average shapes calculated for GIS Site 5, RM 63.3 to 72, using different cross-section spacings. A, with dimensions of width retained. B, with each average shape divided by its top width.

Table 1. Statistics for average shapes calculated using different cross-section spacings

GIS reach	Cross-section spacing (m)	Number of cross-sections averaged	Mean top width (m)	Standard deviation of the top width (m)	Mean elevation (m)	Mean standard deviation of elevation (m)
Site 5 (RM 63.3 - 72)	20	695	370.2	144.2	105.9	6.814
	100	137	373.8	144.0	106.0	5.252
	200	67	373.5	142.3	106.2	5.508
	400	32	371.1	143.1	106.2	6.436
	500	26	364.2	139.7	106.0	4.504
	600	20	395.7	158.8	106.6	4.461
Site 7 (RM 120 - 123)	20	261	196.1	64.44	105.6	4.375
	60	86	194.7	62.34	105.5	4.269
	100	52	194.0	67.37	105.5	4.166
	120	43	187.2	51.75	105.2	4.359
	200	25	180.8	53.06	105.4	4.332
	400	12	182.8	54.74	106.2	3.991
Site 9 (RM 143 - 145)	20	180	135.5	45.33	102.8	3.222
	60	60	133.0	41.70	102.5	3.245
	100	36	132.8	40.22	102.6	3.225
	120	30	133.1	41.88	102.8	3.192
	200	18	127.6	34.89	102.0	3.058
	400	9	119.8	28.52	101.6	3.357

The longest reach used for the comparison of variability in mean shape with different cross-section spacings is part of Site 5, from RM 63.3 to RM 72 (figure 9). In this case, even with 500 m cross-section spacing (26 cross-sections), there is still only a 1.6% difference (6.01 m) between the mean top width and the mean top width calculated with 20 m cross-section spacing. At the 140 m³/s water surface, the difference in widths of the two average shapes is only 0.19 m (0.17%). However, the average shape computed from 20 cross-sections spaced 600 m apart has a mean top width that differs by 6.9% from the average shape computed with 20 m cross-section spacing, and the difference in the width of the 140 m³/s water surface is 12.2%. Therefore, a cross-section spacing of about 500 m or less is needed to calculate accurately the average shape of this 14-km (8.7-mile) reach.

Because the mean shape is the same for various cross-section spacings of 100 m or less in each of these three reaches, the 20 m spacing is considered to provide an accurate representation of the mean channel shape. With an increase in spacing beyond 100 m, the mean width as a function of stage begins to vary for Sites 7 and 9, but remains very similar to the shape with 20 m spacing for Site 5. In fact, cross-section spacings of up to 500m produce essentially the same shape for Site 5 (figure 9). The lack of change in the mean shape for Site 5 is likely a function of the length of the reach, 8.7 miles (14 km), and the large number of cross-sections being averaged, even with cross-sections spaced up to 500 m apart. Although these results indicate the mean shape remains essentially the same with up to 100 m cross-section spacing, all cross-sections were retained for the computation of the single average shape.

Computing the Average Channel Shape

A total of 4,039 cross-sections were extracted from the data in the 10 GCES/GIS reaches (table 2). The total distance covered by the GIS data between Lees Ferry and Diamond Creek is 75 km (47 miles). Some of the reaches extend slightly beyond the range shown in river miles, so that the total distance is almost 47 miles rather than the 46 miles obtained by summing the reach lengths in river miles. Also, the distance along the centerline of the 140 m³/s water surface is slightly greater than the distance in river miles. Therefore, the number of cross-sections shown in the table multiplied by the 20 m spacing at the channel center results in a greater distance than that shown in kilometers for some reaches. The elevation range shown in the table is that from the average 140 m³/s water-surface elevation to the average highest elevation within the reach. The water surface slope for each reach was determined from the difference between the water-surface elevation at the upstream and downstream limits of the reach divided by the distance along the 140 m³/s water surface centerline.

Table 2. Summary of the GIS cross-section data

GIS Site	Reach (RM)	Distance (km)	Number of cross-sections	Average elevation range (m)	140 m ³ /s water surface slope
2	0 - 2	3.54	187	14.63	.0017
3	42 - 48	9.65	537	20.30	.0007
4	51 - 56	8.05	432	19.11	.0016
5*	60 - 72	20.1	970	24.73	.0016
6	93 - 99	9.65	553	22.54	.0028
7	120 - 123	4.83	261	23.42	.0016
8	133 - 138	8.05	458	21.10	.0021
9	143 - 145	3.22	180	19.11	.0028
10	179 - 181	3.22	185	20.51	.0031
11	207 - 210	4.83	275	22.05	.0022

*Excludes a section at the mouth of the Little Colorado River about 500 m in length.

Although the data nominally extend from bank to bank at the top of the pre-dam high water zone (OHWZ), in some areas the data extend beyond those limits, while in others, they do not extend that far. As a result, the highest elevation cannot be correlated to a specific discharge for all GIS reaches. The only elevation that can be associated with a specific discharge is that of the 140 m³/s water surface. Therefore, elevation within each cross-section was adjusted so that the water surface was set to an arbitrary reference elevation before the cross-sections were averaged. Also, the center of the 140 m³/s water surface was used as a reference for the center of the channel for each cross-section, and the cross-sections were averaged about that center for each reach except Site 5, from RM 63.3 to RM 72. The reason for not averaging the shape of this reach about the channel center is discussed in the next section. The cross-sections were used to compute a mean shape for each GCES/GIS reach, then a single weighted average shape was calculated from the mean shapes of 10 selected morphologically similar reaches, described in detail below.

Division by Morphologically Similar Reaches

Smith and Wiele (1995) identified 10 morphologically similar reaches between Glen Canyon Dam and Lake Mead based on river level geology and channel geometry, using the cross-sections from the Wilson data set to delineate characteristic reaches for channel geometry. Their divisions are similar to those for the eleven morphologic zones defined by Schmidt and Graf (1990). Ten morphologically similar reaches are used here also (shown in Appendix A), but are different from those of Smith and Wiele in two cases. The first case is for the reach RM 50 to 77, which was identified as a single morphologically similar reach by Smith and Wiele. This reach is covered extensively by GIS data from Site 4 (RM 51 to 56) and Site 5 (RM 60 to 72). A distinct change in channel morphology occurs at RM 63.3, where the river bed changes from Tapeats Sandstone to the PreCambrian sedimentary rocks of the Unkar Group. The

channel becomes very wide at this point, with alternating bars not common through most of the 362-km (225-mile) reach. Because the GIS coverage of this reach is so extensive, for the purpose of this study, the reach was split it into two morphologically similar reaches: 1) RM 50 to 63.3, where the river level rocks are Bright Angel Shale and Tapeats Sandstone; and 2) RM 63.3 to 77, in the Unkar Group.

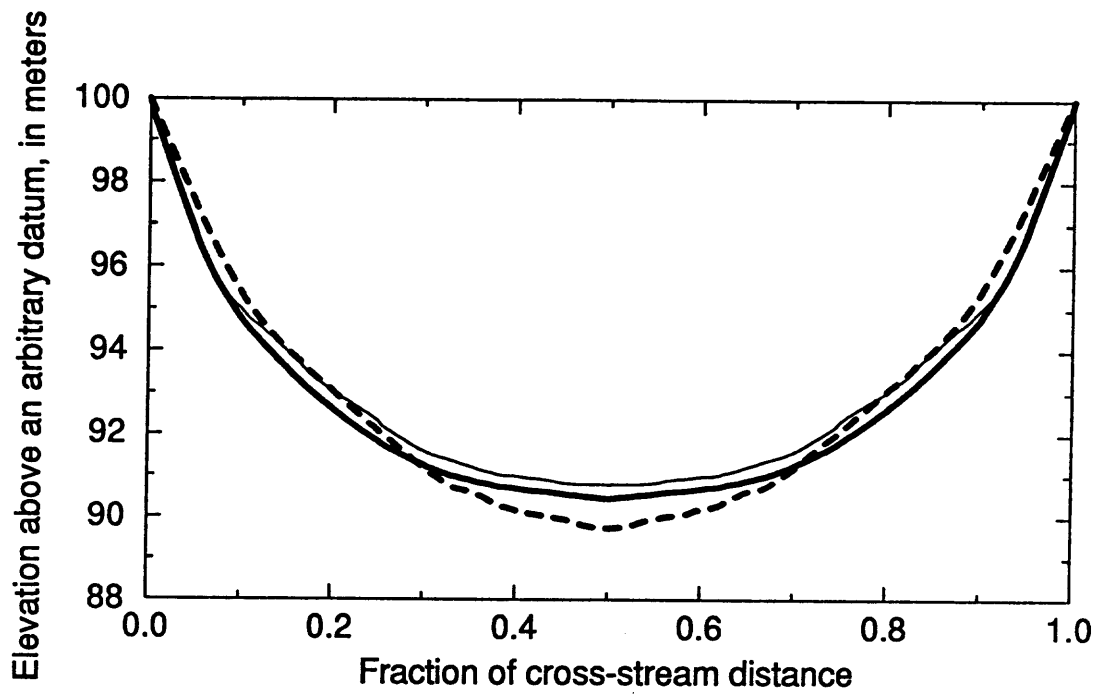
The second difference in morphologically similar reaches is for RM 107 to 140, where Smith and Wiele (1995) identified two separate morphologically similar reaches. Their reaches were: RM 107 to 117, with mixed PreCambrian rocks at river level; and RM 117 to 140, which includes a mix of basal Cambrian and mixed PreCambrian rocks. There are no GIS data within the reach RM 107 to 117. Also, because the river level geology of the entire reach between RM 107 and 140 alternates between several different rock types, the best approach for this study was considered to be to leave this as a single reach, represented by several GIS reaches (described in detail below). Appendix A shows the distribution of the GIS and morphologically similar reaches used in this report in relation to river-level rock type.

Estimation of the Channel Shape Below the 140 m³/s Water Surface

As discussed in the section on the limitations of the GIS data, the shape of the channel below the 140 m³/s water surface had to be estimated. The first choice was to use the average shape of the Wilson cross-sections within the same morphologically similar reach to estimate this segment of the channel shape. This was possible in some cases, but not in others where discharge as a function of stage for the average shape for the particular reach was not known. Smith and Wiele (1995) provided the geometric and hydraulic properties for 7 hydraulically characterized reaches, which correspond to the 10 morphologically similar reaches in some cases. For the purpose of their study, however, in some of these cases it was appropriate to combine the profiles from several reaches with similar channel shape in order to improve the resolution of the

shape. The same combinations of reaches are not necessarily appropriate here because of the distribution of the GIS reaches. Therefore, the average shapes from the 7 hydraulically characterized reaches could not be used to estimate an average shape below the $140 \text{ m}^3/\text{s}$ water surface in every case. Where the specific reach-averaged shapes from the Wilson cross-sections could be used, they were. The exceptions are described below. Details concerning the shape added to each cross-section below the $140 \text{ m}^3/\text{s}$ water surface are provided in the descriptions of the average shapes for the morphologically similar reaches, appearing later in this section.

In four cases, the average shape of all the 199 Wilson cross-sections was used to estimate the channel shape below the $140 \text{ m}^3/\text{s}$ water surface instead of the average of the Wilson cross-sections within the particular reach. These are where the dominant rock types at river level are either limestone (Site 3, RM 42-48; Site 8, RM 133-138; and Site 9, RM 143-145) or the schist and granite of the Granite Gorge (Site 6, RM 93-99). The average shape computed from all the Wilson cross-sections is very similar to the average shape of the Wilson cross-sections within the limestone reaches (figure 10). The relation between stage and discharge for the average shape of all the Wilson cross-sections is well-defined, while the same relation for the average shapes of particular limestone reaches could only be estimated roughly. Therefore, the average of all the Wilson cross-sections was considered to be a better estimate of the shape of the channel at $140 \text{ m}^3/\text{s}$ in the reaches with limestone at river level.



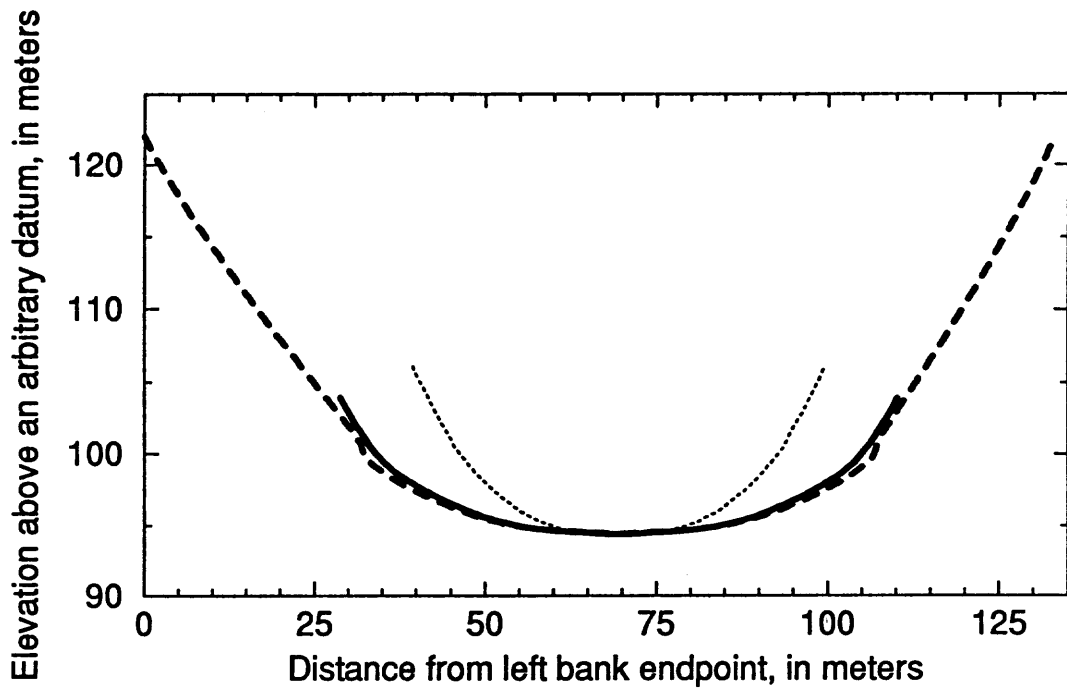
EXPLANATION

- Average shape from all the Wilson cross-sections, RM 0-225
- Average shape from 23 Wilson cross-sections, RM 23-50
- - - Average shape from 26 Wilson cross-sections, RM 140-169

Figure 10. Comparison of the average shape calculated for all the Wilson cross-sections, RM 0 to 225, with the average shapes calculated from the Wilson cross-sections in reaches where the river-level rock is limestone.

The only other case where the average shape of all the Wilson cross-sections was used rather than an average shape from the cross-sections in the particular morphologically similar reach is for Site 6, RM 93 to 99, within the Granite Gorge. The average width of the GIS cross-sections in Site 6 is much wider than the average of the Wilson cross-sections between RM 77 and 107 (figure 11). In fact, the average width of these GIS cross-sections at $140 \text{ m}^3/\text{s}$ (75.01 m) is much closer to that of the average of all the Wilson cross-sections (71.29 m) than that of the average of the Wilson cross-sections, RM 77-107 (46.26 m). Because of this difference in channel width, the width of the average shape from the GIS cross-sections at $140 \text{ m}^3/\text{s}$ was re-scaled to match that of the Wilson cross-sections, RM 77 to 107. Using the average shape from all the Wilson cross-sections below the $140 \text{ m}^3/\text{s}$ water surface resulted in a reasonable shape when this re-scaling was applied, whereas using the average shape from the Wilson cross-sections between RM 77 and 107 did not. Therefore, it was necessary to use the average shape of all the Wilson cross-sections to estimate the channel shape below the $140 \text{ m}^3/\text{s}$ water surface in this case, also.

The average shapes of the channel in other reaches, such as where Tapeats Sandstone is at river level, are much different than the average of all the Wilson cross-sections. For those reaches, an average shape from the Wilson cross-sections for the same morphologically similar reach or for more than one reach with similar river-level geology was added to each GIS cross-section below the $140 \text{ m}^3/\text{s}$ water surface. An estimate of the center depth of the channel within the morphologically similar reaches at $140 \text{ m}^3/\text{s}$ was made based on the geometric and hydraulic properties of the hydraulically characterized reaches given by Smith and Wiele (1995).



EXPLANATION

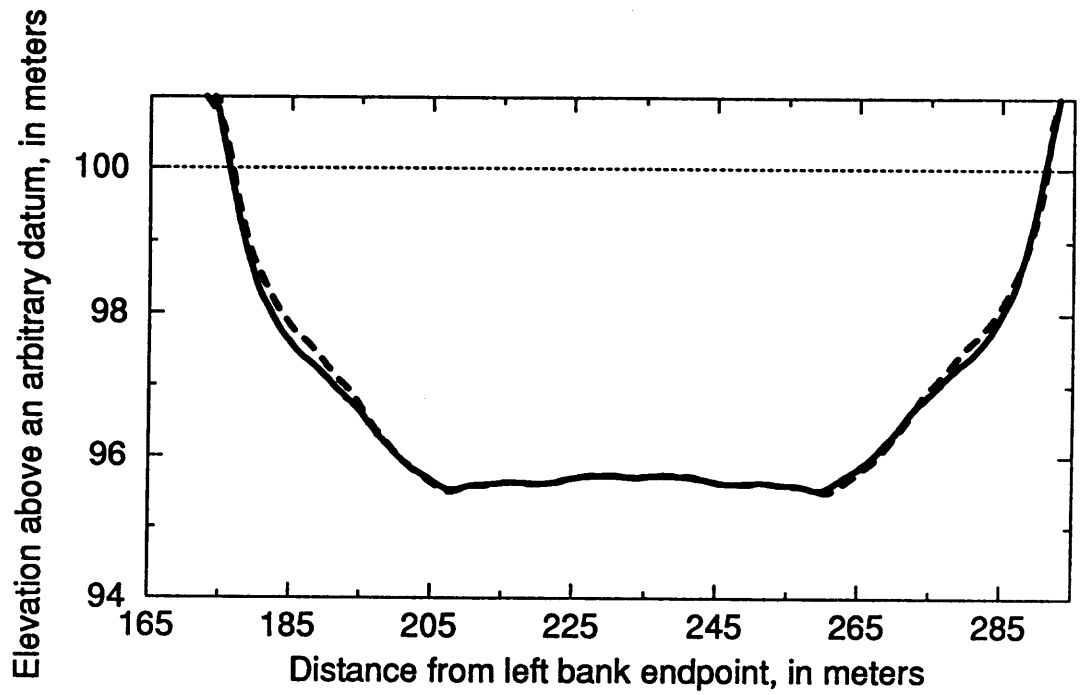
- - - Average shape from the Site 6 GIS cross-sections
- Average shape from all the Wilson cross-sections, RM 0-225
- Average shape from 29 Wilson cross-sections, RM 77-107

Figure 11. Comparison of the average shape calculated from the GIS Site 6 cross-sections, RM 93 to 99, with the average shape calculated using all the Wilson cross-sections and the average of the Wilson cross-sections in the Granite Gorge, RM 77 to 107.

In order to check whether or not this approach is reasonable, the average shape calculated for the 15 Wilson cross-sections between RM 63.3 and RM 77 was compared to the average shape computed from the GIS data with the estimated average shape from the Wilson cross-sections in this reach added to each cross-section below the 140 m³/s water surface. The estimated shape below the 140 m³/s water surface is nearly the same as the average shape calculated using the Wilson cross-sections (figure 12). Therefore, this method appears to provide a reasonable estimate of the channel shape below the 140 m³/s water surface.

Method used to Average the Individual Cross-Sections within a GIS Reach

Several different schemes for averaging the cross-sections within a single GIS reach were tried before one was found that resulted in a reasonably accurate average shape. The first attempt involved computing a simple average of the elevation at equally-spaced points along each cross-section line. The individual cross-sections were first normalized in the cross-stream direction by dividing the cross-stream location by the cross-section top width. Elevations at fractions of cross-stream distance were then averaged. Because of the large variation in the location of the thalweg through each reach, the use of a simple average of the cross-sections results in the shape below the 140 m³/s water surface being averaged out (figure 13). Therefore, this method was not considered appropriate for use in this project.



EXPLANATION

- Average of 15 Wilson cross-sections, RM 63.3 to 77
- - - Average shape from the GIS Site 5 cross-sections, RM 63.3 to 72
- Estimated 140 cms water surface

Figure 12. Comparison of the average channel shapes calculated from the GIS and Wilson cross-sections for morphologically similar reach RM 63.3 to 77. The width of the average shape from the GIS cross-sections at 140 m³/s was multiplied by 1.11 to match the width of the Wilson cross-sections at the same stage. The average channel shape from the 15 Wilson cross-sections was averaged about its center.

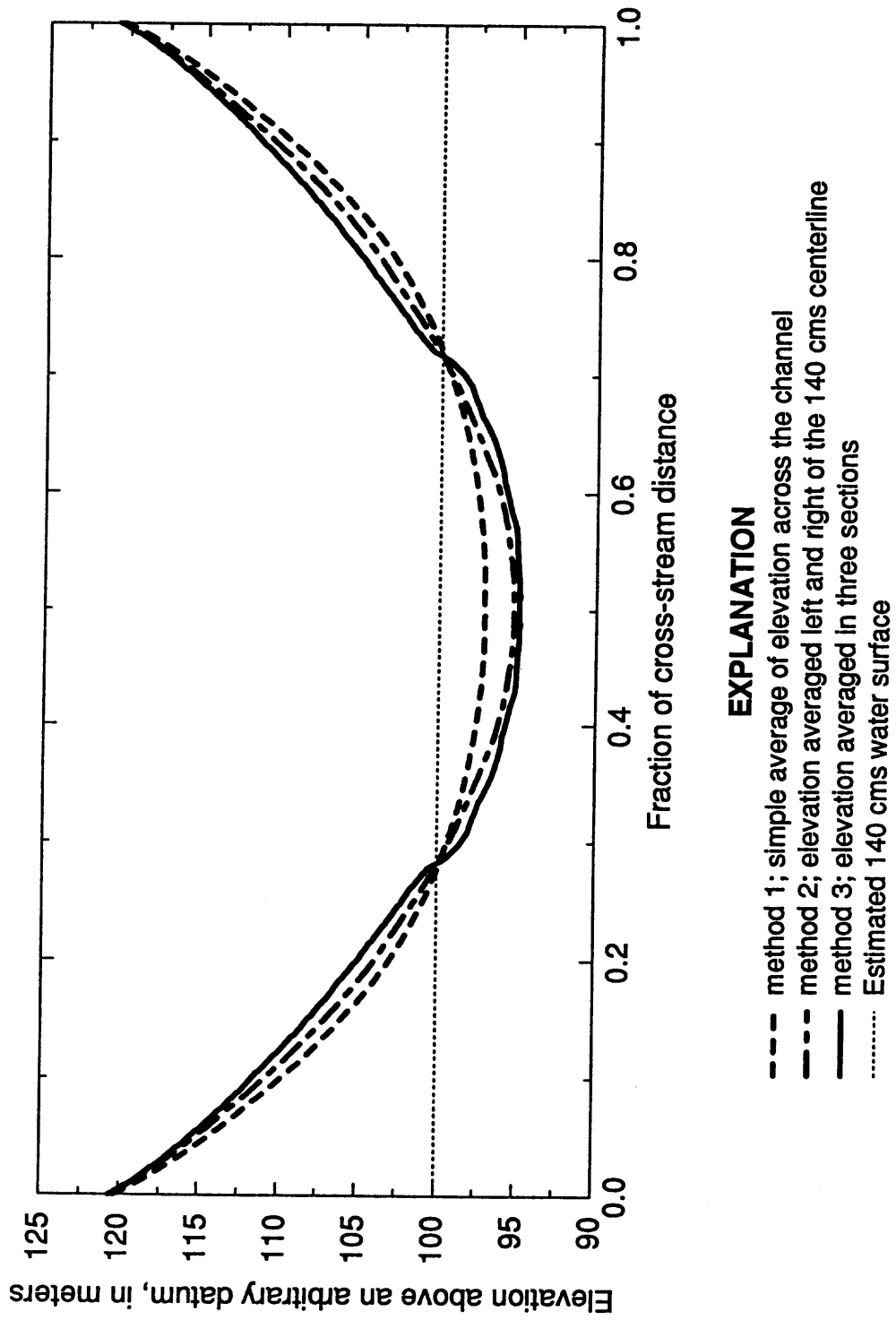


Figure 13. Comparison of the average channel shape calculated for GIS Site 10, RM 179 to 181, using three different methods tested. The first two methods did not provide sufficient resolution of the channel shape. The third method shown is the one used to calculate the average channel shape in this study.

Another method tested for computing the average shape involved dividing each cross-section into left and right sections, with the center of the $140 \text{ m}^3/\text{s}$ water surface assumed to be the center of the channel, then averaging about the center of the channel. Width was normalized in a similar manner, but in this case, the fraction of cross-stream distance ranged from 0 to 0.5 from the left-bank endpoint to the center of the $140 \text{ m}^3/\text{s}$ water surface, and from 0.5 to 1 from the center of the water surface to the right-bank endpoint. Average elevation at each fraction of cross-stream distance through the left and right sides of the channel was then found, and width re-scaled by the average widths of the left and right sides of the channel. This method also resulted a loss of resolution of channel shape near the center, however. Also, the average shape for each reach below the $140 \text{ m}^3/\text{s}$ water surface found using this method was well-rounded, regardless of the estimated shape added below the water surface (figure 13). In addition, for reaches where the average shape was not symmetric, the average width of the $140 \text{ m}^3/\text{s}$ water surface in the GIS cross-sections, which was calculated separately, was not accurately reflected in the reach-averaged shape. While this second method of averaging the cross-sections was an improvement over the first, it still did not produce an adequate representation of the reach-averaged channel shape.

The averaging method resulting in the most accurate average channel shape was applied and is described here. Before averaging the elevation for all the cross-sections in a reach, the information for each cross-section was first adjusted to apply a consistent reference elevation. The minimum elevation for each cross-section is at the $140 \text{ m}^3/\text{s}$ water surface. Because this is the only elevation for which discharge is known, the $140 \text{ m}^3/\text{s}$ water surface was chosen as the reference and arbitrarily set to 100 m. The cross-sections within a particular GIS reach were then averaged in 3 sections: 1) the left bank GIS data; 2) the segment below the $140 \text{ m}^3/\text{s}$ water surface, where the shape had to be estimated; and 3) the right bank GIS data. Details of the procedure used to adjust each cross-section within a given set before computing the

average shape for that GIS reach are provided below.

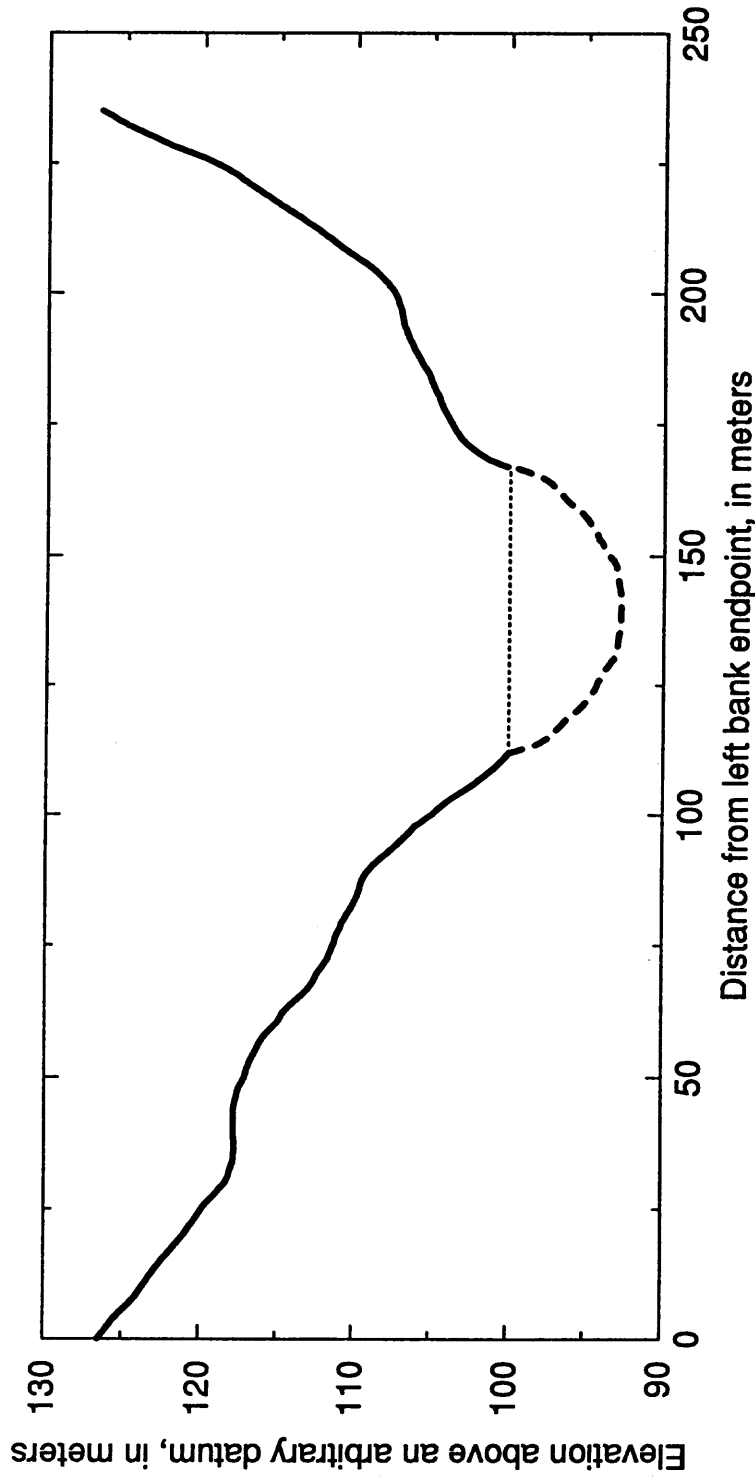
1) Elevation values along the cross-section were adjusted by subtracting the water-surface elevation for that cross-section from the elevation at each point, then adding 100m so that the water-surface elevation was set to 100 m.

2) Each cross-section was separated into three parts: from the top of the left bank to the left bank water's edge at $140 \text{ m}^3/\text{s}$; from the left edge of the water to the right edge of the water; and from the water's edge on the right bank to the top of the right bank.

3) An average shape from the Wilson cross-sections below the $140 \text{ m}^3/\text{s}$ water surface was rescaled to the width of the water surface at $140 \text{ m}^3/\text{s}$ for the cross-section being averaged, then added between the left and right edges of the water (figure 14). (The depth at each point was adjusted by the same amount as the width, so that the cross-section area for a discharge of $140 \text{ m}^3/\text{s}$ remained the same as for the average of the Wilson cross-sections at this discharge). The average shape added to each cross-section was dependent on river-level geology and similarities in channel shape among reaches as found by Smith and Wiele (1995). Specific shapes added within each reach are discussed in detail in the next section.

4) The values for distance (y) along the cross-section line were then rescaled by dividing the distance from the left-most point of each of the three segments by the width of the corresponding segment (i.e., left bank, $140 \text{ m}^3/\text{s}$ water surface, and right bank). This resulted in a range of y values from 0 to 1 for each of the three segments.

5) Values of elevation were interpolated for equally spaced points within each of the three segments, so that an average elevation at each fraction of cross-stream distance could be computed.



EXPLANATION

- Shape of a single cross-section in the Site 10 GIS data
- - - Estimated shape from the average of 16 Wilson cross-sections, RM 169-190
- 140 cms water surface

Figure 14. Example of a single cross-section extracted from the GIS data, with the estimated shape from the Wilson cross-sections added below the 140 m²/s water surface.

After the adjustments described above were made for each cross-section, the elevations at each fraction of cross-stream distance (from 0 to 1) for each of the three segments were averaged for all the cross-sections in the GIS reach. The average width of each segment was found, and width restored to the average shape by multiplying the fraction of cross-stream distance within each third of the channel by the average width of that segment, then adding that value to the distance from the left-bank endpoint of the first point in the segment (i.e., for the left bank, the distance from the left-bank endpoint of the first point in that segment is 0, while the right-bank y values were added to the distance from the left-bank endpoint to the right edge of the 140 m³/s water surface). The mean standard deviation of the elevation was found, along with an average width and standard deviation of the width for the set of cross-sections (table 3). The result of this method of averaging is that the average width of the 140 m³/s water surface is accurately reflected in the average shape for a given reach, and the channel shape below that water surface agrees well with the average shape of the Wilson cross-sections within the morphologically similar reach.

Average ratios of top width to mean depth for each GIS reach (table 3) were compared to the ratios found by Schmidt and Graf (1990) for the corresponding morphologic zone. This comparison shows less than 10% difference for some reaches and significant differences for others. Several factors contribute to the difference where there is a discrepancy. For example, in GIS Site 11 (RM 207 - 210) the Vishnu Schist is at river level. The average channel width-to-depth ratio determined by Schmidt and Graf for the Lower Canyon (RM 160 - 213.8) was 8.1, while the average ratio obtained from the GIS cross-sections was 18.6, indicating a much wider, shallower reach. In this case, the GIS cross-sections extend sufficiently far enough above the 140 m³/s water surface to encounter a change in geology. The transition into the Tapeats Sandstone results in a distinct widening of the channel above the Vishnu Schist, resulting in a higher ratio of width-to-depth than at lower stages.

Table 3. Statistics for the GIS reaches

GIS Reach (River miles)	GIS Reach (River kilometers)	Dominant rock type at river level	Average maximum depth, \bar{h} (meters)	Mean depth, \bar{h} (meters)	Mean standard deviation of the depth, \bar{s}_h (meters)	\bar{s}_h/h	Average OHWZ top width, \bar{b} (meters)	Standard deviation of the OHWZ top width, s_b (meters)	s_b/\bar{b}	Average ratio of top width to mean depth
42 - 48	68 - 77	Muav Limestone	24.80	17.21	3.458	0.139	207.8	41.86	0.201	12.8
51 - 56	82 - 90	Bright Angel Shale	25.02	16.15	2.443	0.098	270.7	44.13	0.163	16.8
60 - 63.3	97 - 102	Tapeats Sandstone	29.87	21.21	5.428	0.182	193.6	37.68	0.195	9.13
63.3 - 72	102 - 116	PreCambrian Sedimentary rocks	29.47	18.79	6.814	0.231	358.8	144.2	0.402	19.1
93 - 99	150 - 159	Vishnu Schist and Zoroaster Granite	27.64	19.67	2.415	0.087	133.0	23.84	0.179	6.76
120 - 123	193 - 198	Tapeats Sandstone	29.85	17.97	4.375	0.147	196.0	64.44	0.329	10.9
133 - 138	214 - 222	Bass Limestone	27.66	17.48	3.476	0.126	159.5	53.55	0.336	9.12
143 - 145	230 - 233	Cambrian limestones	26.56	16.31	3.222	0.121	134.8	45.33	0.336	8.26
179 - 181	288 - 291	Lava over Cambrian sedimentary rocks	25.79	16.97	3.275	0.127	192.0	41.01	0.214	11.3
207 - 210	333 - 338	Vishnu Schist	27.09	15.92	2.939	0.108	317.7	120.9	0.381	20.0
0 - 225	0 - 362		26.01	17.70	1.932	0.074	225.2	72.99	0.324	12.7

In some cases, the average shapes for the morphologically similar reaches initially obtained from the GIS data were not symmetric about the center of the channel. This is generally the result of the presence of tributaries with wide side canyons and associated debris fans on one side of the river within the limited GIS reach. For example, Kanab Creek enters the Colorado River on the right bank at RM 143.5, within GIS Site 9 (RM 143-145). There are no other major side canyons within this GIS reach, so the average shape computed for Site 9 is asymmetric. Over the distance of the morphologically similar reach (in this case RM 140 to 169), the number and size of side canyons on either side of the river are expected to balance out, resulting in a symmetric average shape for the longer reach. This assumption is supported by the symmetric average shapes computed from the Wilson cross-sections. Therefore, the average shapes computed using the GIS cross-sections were averaged left and right to produce a symmetric shape for every reach except RM 63.3 to 77. Along the left bank through much of this reach, identified as Furnace Flats by Schmidt and Graf (1990), is an extensive wide, flat area that clearly leads to an asymmetric average shape. Therefore, the average shape for this reach was not averaged left and right.

In two of the morphologically similar reaches, information from more than one GIS site is available. The first reach is RM 50 to 63.3, which includes GIS Site 4, RM 51 to 56, and part of Site 5, RM 60 to 63.3. The second reach extends from RM 107 to 140, including GIS Site 7, RM 120 to 123, and Site 8, RM 133 to 138. In addition, the Vishnu Schist is at river level through a large part of this reach, so the average channel shape from Site 6, RM 93-99, in the Granite Gorge, was also used to compute the average shape for RM 107 to 140. In other cases, the single GIS reach within the morphologically similar reach was considered to be not representative of the average shape for that reach, for reasons discussed below. In those cases, a representative shape from another GIS reach (or reaches) with similar river-level geology was used to represent the desired morphologically similar reach.

For each of the morphologically similar reaches, the width of the average shape from the GIS cross-sections at $140 \text{ m}^3/\text{s}$ was compared to the width of the average shape of the Wilson cross-sections in that reach. Although widely-spaced (about 1 mile, or 1.6 km apart), the Wilson cross-sections represent the entire morphologically similar reaches, and the average width of these cross-sections at $140 \text{ m}^3/\text{s}$ was assumed to be an accurate representation of the actual average width. The GIS cross-sections, on the other hand, represent limited segments of the morphologically similar reaches. While these cross-sections were found to work well in defining the average shape for the entire morphologically similar reach, they were not necessarily sufficient to determine the average width. For each morphologically similar reach, then, the width of the $140 \text{ m}^3/\text{s}$ water surface in the average shape from the GIS cross-sections was adjusted to match the width of the Wilson cross-sections for the same reach at $140 \text{ m}^3/\text{s}$ (table 4). Except for the average shape from GIS Site 6, which was used to represent both morphologically similar reaches RM 77 to 107 and RM 11 to 23, the difference in widths of the $140 \text{ m}^3/\text{s}$ water surface calculated from the GIS cross-sections is less than 12% of the average width of the Wilson cross-sections in the same reach. A detailed description of method used to derive the average shape for each morphologically similar reach is provided below.

Table 4. Comparison of average widths at 140 m³/s

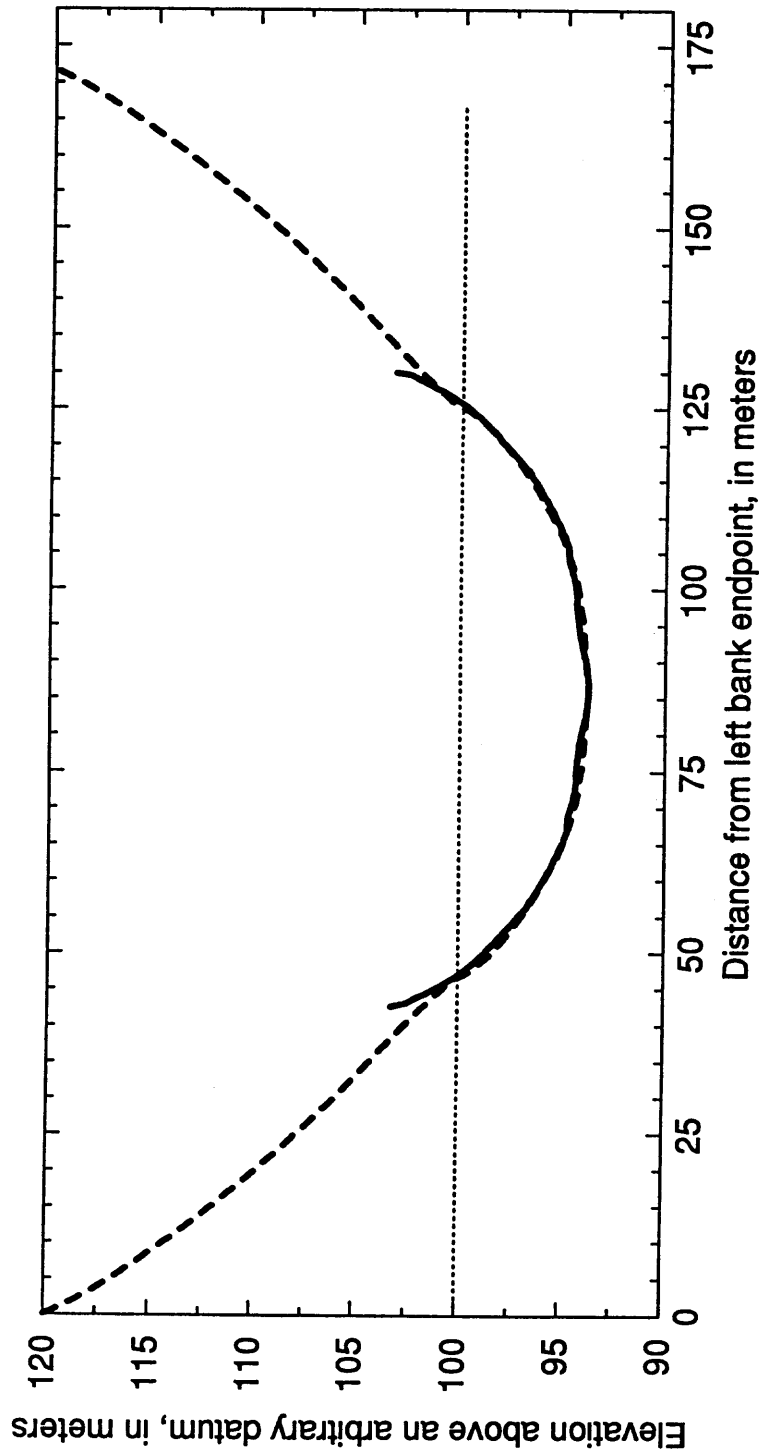
Morphologically similar reach (RM)	Number of Wilson cross-sections	Average width of the Wilson cross-sections at 140 m ³ /s (m)	Average width of the GIS cross-sections at 140 m ³ /s (m)	Percent difference in width at 140 m ³ /s	140 m ³ /s width adjustment factor
0 - 11	12	78.64	74.10	5.8	1.061
11 - 23	13	45.27	75.01	66	.6035
23 - 50	23	76.69	74.10	3.4	1.035
50 - 63.3	10	99.30	98.90	0.4	1.004
63.3 - 77	15	115.0	103.6	9.9	1.110
77 - 107	29	46.26	75.01	62	.6167
107 - 140	25	57.63	62.74	8.9	.9186
140 - 169	26	57.64	56.88	1.3	1.013
169 - 190	16	84.58	81.74	3.4	1.035
190 - 225	30	89.74	79.17	12	1.134

Morphologically Similar Reach RM 0 - 11:

The rock types at river level in this reach are primarily mixed Permian sedimentary rocks, including the Kaibab Limestone, Toroweap Limestone, and Coconino Sandstone (Smith and Wiele, 1995). Although a GIS reach (Site 2) is within this morphologically similar reach, it extends from RM 0 to 2, including the wide, shallow reach at the mouth of the Paria River. From RM 0 to 0.8, the river-level geology consists of the sandstone, siltstone and shale of the Moenkopi Formation. The rocks in this formation are much more easily eroded than the more resistant limestones and calcareously cemented sandstones which first appear at RM 0.8, resulting in a much wider channel than that found a short distance downstream. Just downstream from the Paria River mouth, the Colorado River channel becomes considerably more narrow as it enters Marble Canyon. GIS Site 2 is therefore not considered to be representative of

the average shape of the channel between RM 0 and 11.

Because the dominant rock type at river level in this reach is limestone, an average shape from the three GIS reaches located where limestone is at river level was chosen to represent the average shape for RM 0 to 11. These three GIS reaches are: Site 3, RM 42 - 48, in the Muav Limestone; Site 8, RM 133-138, in the Bass Limestone; and Site 9, RM 143-145, again in the Muav Limestone. The shape of the channel below the 140 m³/s water surface was estimated by adding the average shape from all the Wilson cross-sections at 140 m³/s to each cross-section in each of the three reaches. The average shapes of each of the three reaches were then weighted equally (by 0.333) to find the single average shape for the limestone reaches. The difference in width of this average shape at 140 m³/s and that of the average of the Wilson cross-sections is about 4.5 m, or 5.8%. The width of the average shape from Sites 3, 8, and 9 at 140 m³/s was then multiplied by 1.061, so that the width of the average shape from the GIS cross-sections at that discharge agreed with the width of the average of the Wilson cross-sections (table 4). A comparison of the average shape obtained for the three limestone reaches with the average shape of the Wilson cross-sections, RM 0 to 11, (figure 15) shows good agreement between the two shapes.



EXPLANATION

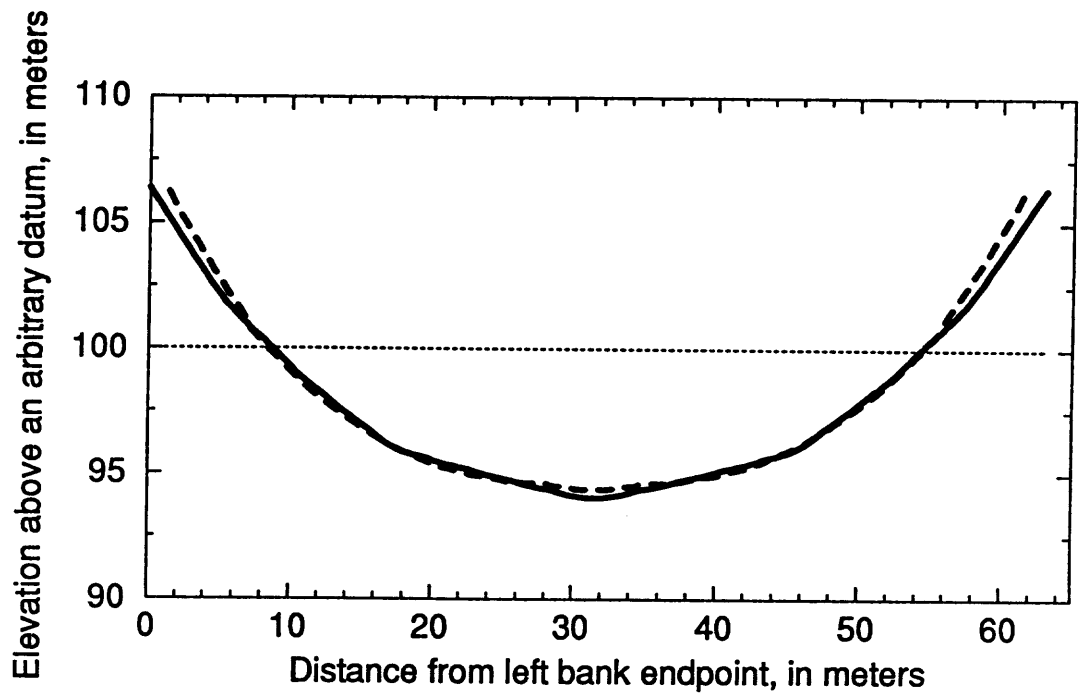
- Average of 12 Wilson cross-sections, RM 0 to 11
- - - Average shape from 3 GIS reaches in limestone
- Estimated 140 cms water surface

Figure 15. Comparison of the average shapes calculated from the Wilson cross-sections and the GIS cross-sections for morphologically similar reach RM 0 to 11. The width of the average shape of the GIS reaches in limestone at 140 m³/s was multiplied by 1.061 to match the width of the average shape from the Wilson cross-sections at that discharge

Morphologically Similar Reach RM 11 - 23:

In the reach RM 11 - 23, the Colorado River passes through the Pennsylvanian clastic rocks of the Supai Group, including the Esplanade Sandstone. There are no GIS data within this morphologically similar reach. However, Smith and Wiele (1995) found the average shape of the Wilson cross-sections within this reach to be very similar to the average shape of the channel obtained from the Wilson cross-sections in the Granite Gorge, RM 77 to 107 (figure 16). GIS Site 6, RM 93 to 99, provides an average shape for the Granite Gorge, so this shape is used to represent morphologically similar reach RM 11 to 23 as well. The average shape of all the Wilson cross-sections below $140 \text{ m}^3/\text{s}$ was added to each of the cross-sections within Site 6. In addition, Site 6 extends through a reach with an large number of rapids with their associated debris fans and wide side canyons. At high stages (those associated with discharges greater than about $850 \text{ m}^3/\text{s}$ ($30,000 \text{ ft}^3/\text{s}$)), the channel is much wider through the side canyons than it is on average in the Granite Gorge. Therefore, the GIS cross-sections through these side canyons were eliminated from the data set before the average shape for Site 6 was computed.

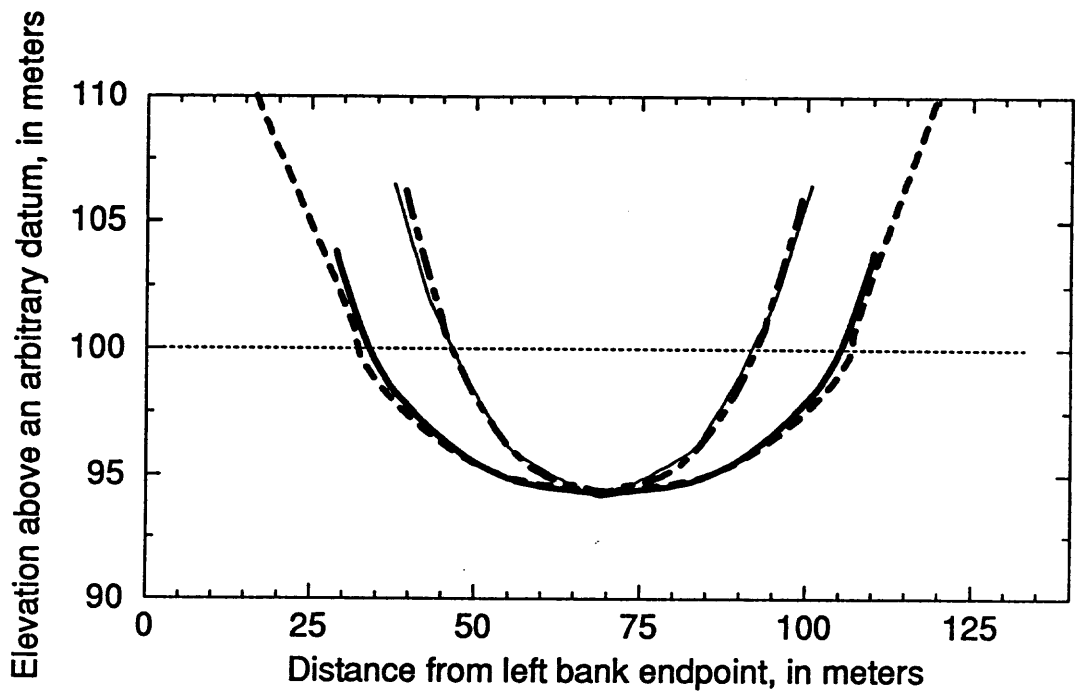
A comparison of the average shape of the GIS cross-sections in Site 6 with the average shape for the Wilson cross-sections between both RM 11 and 23 and RM 77 to 107 (figure 17) revealed a significant difference in the widths of the average shape from the GIS cross-sections and the average shapes of the Wilson cross-sections in the two morphologically similar reaches at $140 \text{ m}^3/\text{s}$. The difference in the average widths of the GIS cross-sections and the Wilson cross-sections between RM 11 and 23 at $140 \text{ m}^3/\text{s}$ was used to determine a factor (0.6035) applied to modify the width of the average shape of the GIS reach at the $140 \text{ m}^3/\text{s}$ water surface. The average shape from the GIS cross-sections with the modified width agrees well with the average shape of the Wilson cross-sections, RM 11 to 23 (figure 18).



EXPLANATION

- Average of 13 Wilson cross-sections, RM 11 to 23
- - - Average of 29 Wilson cross-sections, RM 77 to 107
- Estimated 140 cms water surface

Figure 16. Comparison of the average channel shape calculated from the Wilson cross-sections, RM 11 to 23, with the average shape from the Wilson cross-sections, RM 77 to 107. There are no GIS data in the reach RM 11 to 23. However, the similarities in the two average shapes shown here indicate the average shape from morphologically similar reach RM 77 to 107 can be used to estimate the average shape for this reach also.



EXPLANATION

- Average shape from all the Wilson cross-sections, RM 0 to 225
- Average of 13 Wilson cross-sections, RM 11 to 23
- - - Average of 29 Wilson cross-sections, RM 77 to 107
- . - . Average shape from the GIS Site 6 cross-sections, RM 93 to 99
- Estimated 140 cms water surface

Figure 17. Comparison of the average channel shape calculated from the GIS Site 6 (RM 93 to 99) cross-sections with the average shapes calculated for all the Wilson cross-sections and those between RM 11 to 23 and RM 77 to 107. The average width of the GIS cross-sections agrees much more closely with that of the average of all the Wilson cross-sections.

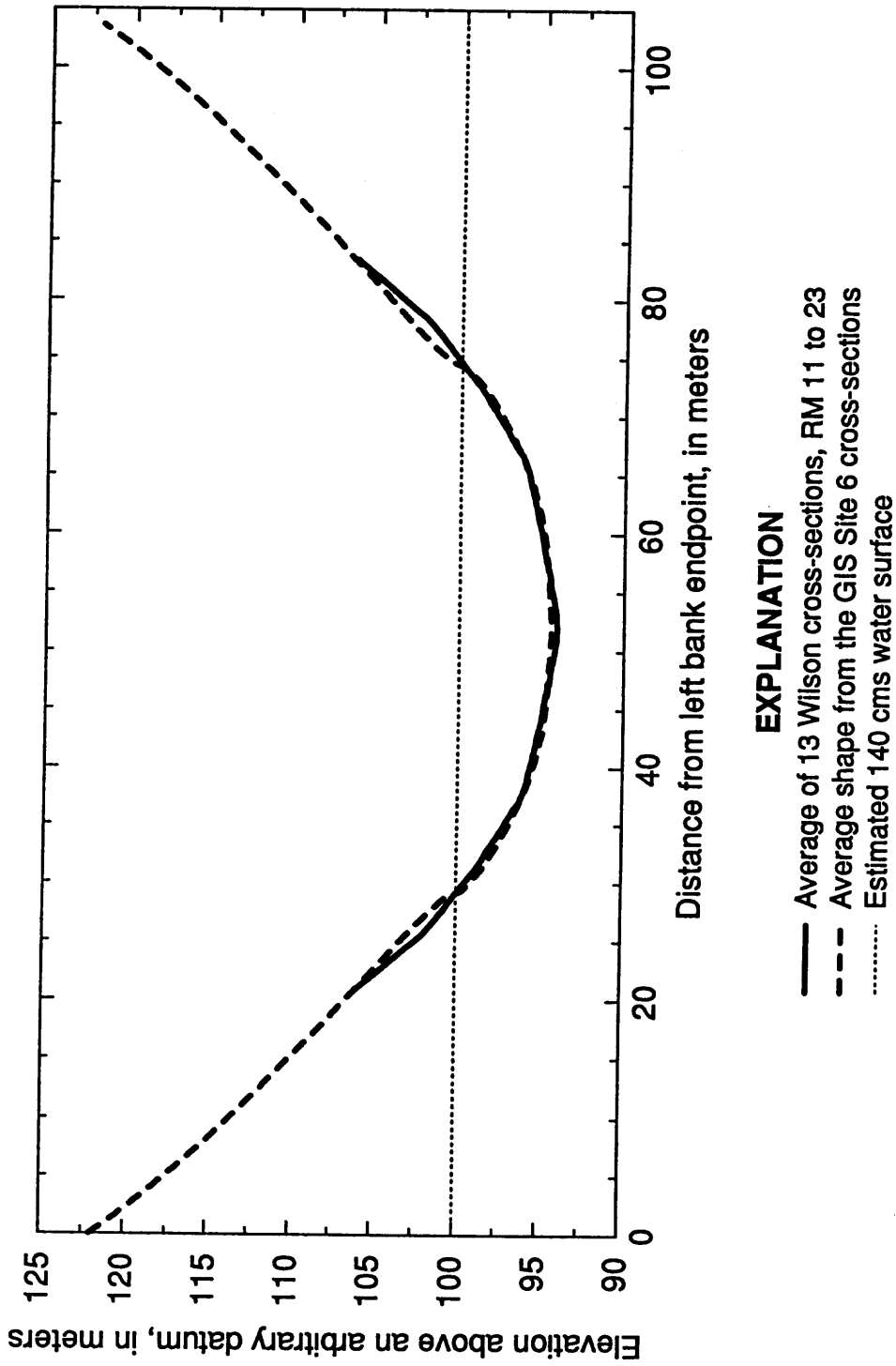
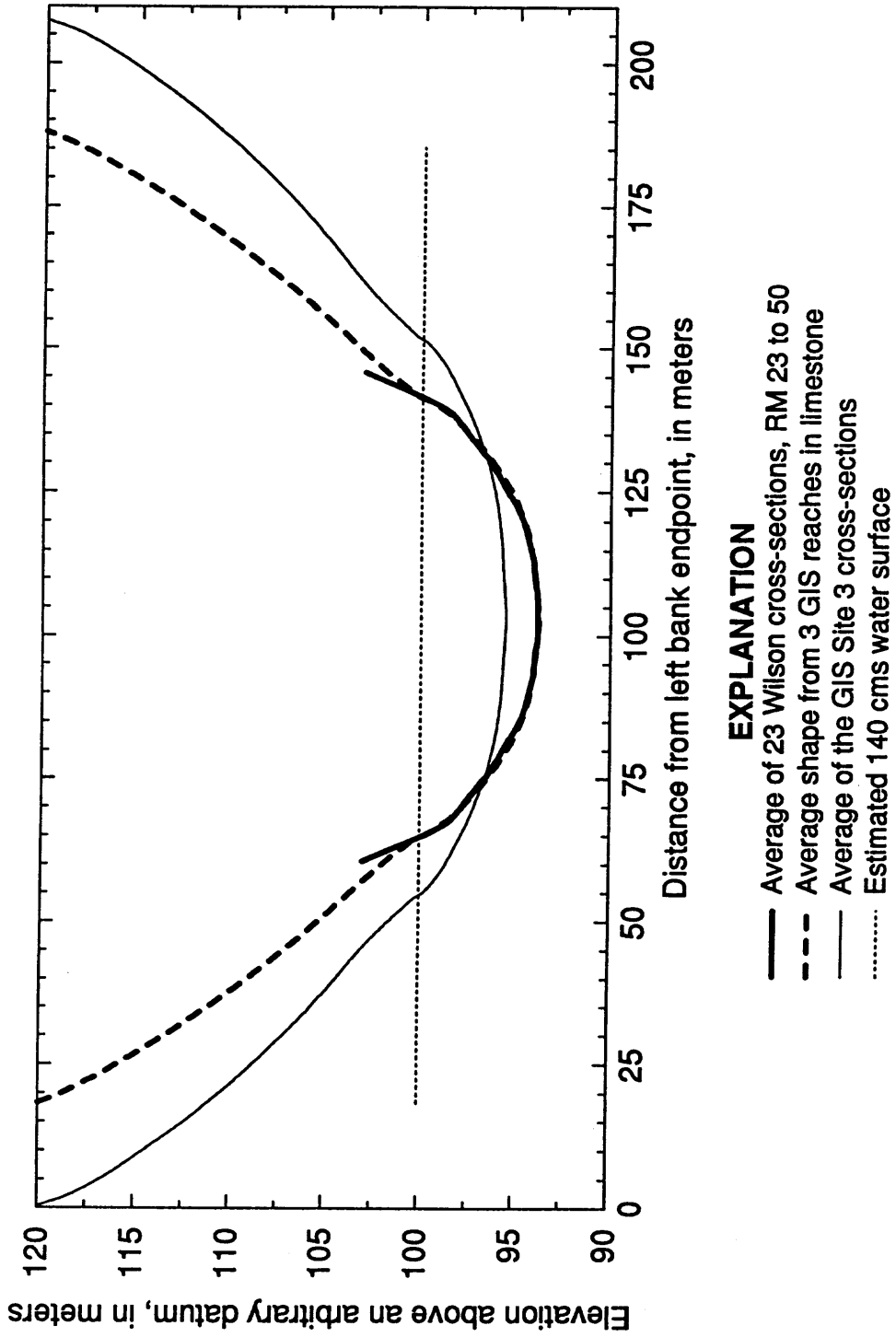


Figure 18. Comparison of the average shapes calculated from the Wilson cross-sections and the GIS cross-sections for morphologically similar reach RM 11 to 23. The width of the average shape of the GIS Site 6 cross-sections at 140 m³/s was multiplied by 0.6035 to match the width of the average shape from the Wilson cross-sections at that discharge.

Morphologically Similar Reach RM 23 - 50:

Within this reach, the Colorado River travels through the Redwall Limestone into the Muav Limestone. GIS Site 3, RM 42 - 48, is entirely within the Muav Limestone. While Smith and Wiele (1995) found the average shape of the Wilson cross-sections in each of the limestone reaches to be similar, the Site 3 GIS reach is anomalously wide. The average shape of the GIS cross-sections in this reach is similar to but much wider than those of the other two limestone reaches (Sites 8 and 9). GIS Site 3 is located in part along the Eminence Break Fault, at a large bend in the river around Point Hansbrough, which contributes to a wider-than-average shape. A comparison of the average shape of Site 3 with the average shape of the Wilson cross-sections, RM 23 - 50 (figure 19) shows the difference in the two shapes. The average shape of the three limestone reaches, however, agrees well with the average shape of the Wilson cross-sections in this reach. Therefore, the average shape from Sites 3, 8, and 9, as described for morphologically similar reach RM 0 to 11, is used to represent this morphologically similar reach also. The difference in channel width at $140 \text{ m}^3/\text{s}$ between the average shape computed from GIS Sites 3, 8, and 9 and the average shape computed from the Wilson cross-sections, RM 23-50 is 2.6 m. Therefore, the average width at $140 \text{ m}^3/\text{s}$ was adjusted by multiplying by 1.035, so that the average width of the Site 3, 8, and 9 GIS cross-sections matches that of the average shape of the Wilson cross-sections at that discharge.



EXPLANATION

- Average of 23 Wilson cross-sections, RM 23 to 50
- - - Average shape from 3 GIS reaches in limestone
- Average of the GIS Site 3 cross-sections
- Estimated 140 cms water surface

Figure 19. Comparison of the average shapes calculated from the Wilson cross-sections and the GIS cross-sections for morphologically similar reach RM 23 to 50. The average shape from the GIS reaches in limestone is used to represent this reach rather than the GIS Site 3 cross-sections for reasons discussed in the text. The width of the average shape of the three GIS reaches in limestone at 140 m³/s was multiplied by 1.035 to match the width of the average shape from the Wilson cross-sections at that discharge.

Morphologically Similar Reach RM 50 - 63.3:

The dominant rock types at river level in this reach are Bright Angel Shale and Tapeats Sandstone. The Bright Angel Shale forms talus-covered slopes, while the Tapeats Sandstone forms cliffs. There are GIS reaches in both of the two rock types, with Site 4 in the shale, between RM 51 and 56, and part of Site 5 (RM 60 to 63.3) in the Tapeats Sandstone. The cross-sections in these two GIS reaches were therefore averaged to obtain an average shape for the morphologically similar reach. A large side canyon enters the Colorado River channel at Nankoweap Rapid (RM 52). Because a wide, relatively flat debris fan is present here, which is not characteristic of the average shape between RM 50 and 63.3, cross-sections extending through this debris fan were excluded from the sample set. The total number of cross-sections from Site 4 used to calculate the average shape, then, is 262. The cross-sections from Site 5 in a reach about 500 m long at the mouth of the Little Colorado River (RM 61.5) were also excluded for similar reasons, so that the total number of cross-sections from Site 5 between RM 60 and 63.3 was 270.

The average shapes of the Wilson cross-sections within this reach and the reach RM 169 to 190, which is also in the Bright Angel Shale and Tapeats Sandstone, show that both have a relatively broad, flat bottom. This shape is distinctly different from the average of all the Wilson cross-sections. There are only 10 Wilson cross-sections in the reach RM 50 to 63.3, and 16 in the reach RM 169 to 190. To improve the resolution of the channel shape, then, the cross-sections in these two similar reaches were combined to obtain an average shape at $140 \text{ m}^3/\text{s}$. This shape was then added to each of the cross-sections in Site 4 and to those in Site 5 from RM 60 to 63.3. A single average shape for this morphologically similar reach was found by averaging all the cross-sections in these two reaches. The difference in channel width at $140 \text{ m}^3/\text{s}$ between this average shape (98.9 m) and that of the average of the 10 Wilson cross-sections between RM 50 and 63.3 (99.3 m) is about 0.4 m. Therefore, the width of the

average of the GIS cross-sections at $140 \text{ m}^3/\text{s}$ was multiplied by 1.004, so the two widths agree. The average shape from the GIS cross-sections agrees well with the average shape from the Wilson cross-sections, RM 50 to 63.3 (figure 20).

Morphologically Similar Reach RM 63.3 - 77:

The morphology of this reach is determined by PreCambrian sedimentary rocks of the Unkar Group. This group consists of a variety of rock types, including basalt, sandstone, quartzite, shale, and limestone, with much of the rock heavily eroded. The reach includes the area identified by Schmidt and Graf (1990) as Furnace Flats, a particularly wide reach containing many large sand and cobble bars. There are numerous bends in the river through the reach, which contribute significantly to the resulting wide average shape for RM 63.3 to 77. This reach is well-represented by the cross-sections of GIS Site 5, from RM 63.3 to RM 72. The characteristic shape of the channel bottom identified by the Wilson cross-sections through this reach is that of a wide channel with a symmetric rise in the center. This rise is the result of the presence of alternating bars through the reach (J.D. Smith, U.S. Geological Survey, personal commun.), which are not common elsewhere in the canyon. The shape of the channel below the $140 \text{ m}^3/\text{s}$ water surface therefore was estimated using the average shape obtained from the 15 Wilson cross-sections in the reach RM 63.3 to 77.

The average shape of the channel obtained from the GIS cross-sections in Site 5 is more narrow than the average shape of the Wilson cross-sections in this reach. Therefore, the representative shape from the GIS cross-sections was modified by multiplying its width at $140 \text{ m}^3/\text{s}$ by a constant factor (1.11) derived from the difference in the width of the two average shapes at this discharge. Adjustment of the water surface width by this factor results in good agreement between the two average shapes (figure 21).

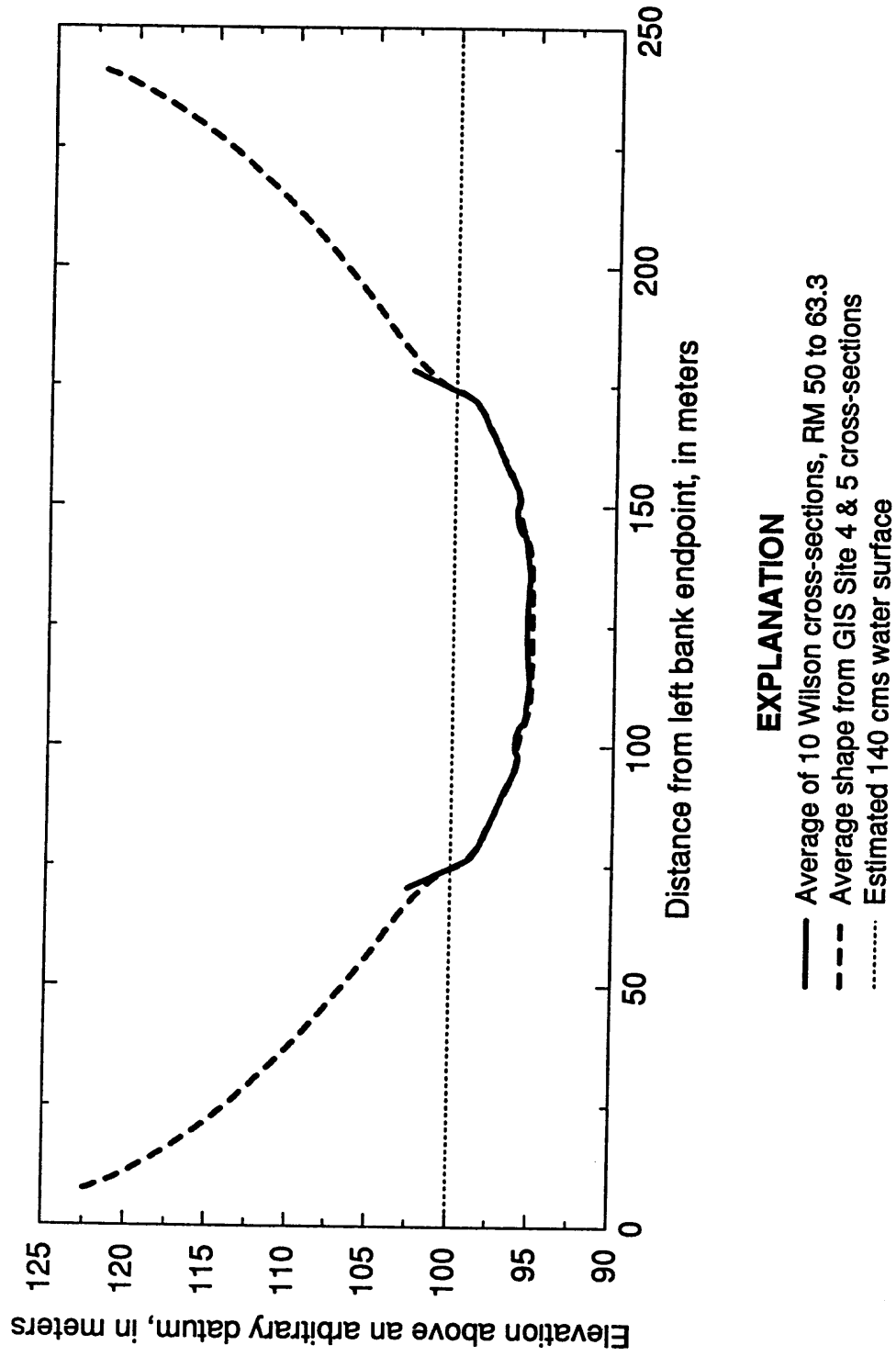


Figure 20. Comparison of the average shapes calculated from the Wilson cross-sections and the GIS cross-sections for morphologically similar reach RM 50 to 63.3. The width of the average shape of the GIS Site 4 and 5 cross-sections at 140 m³/s was multiplied by 1.004 to match the width of the average shape from the Wilson cross-sections at that discharge.

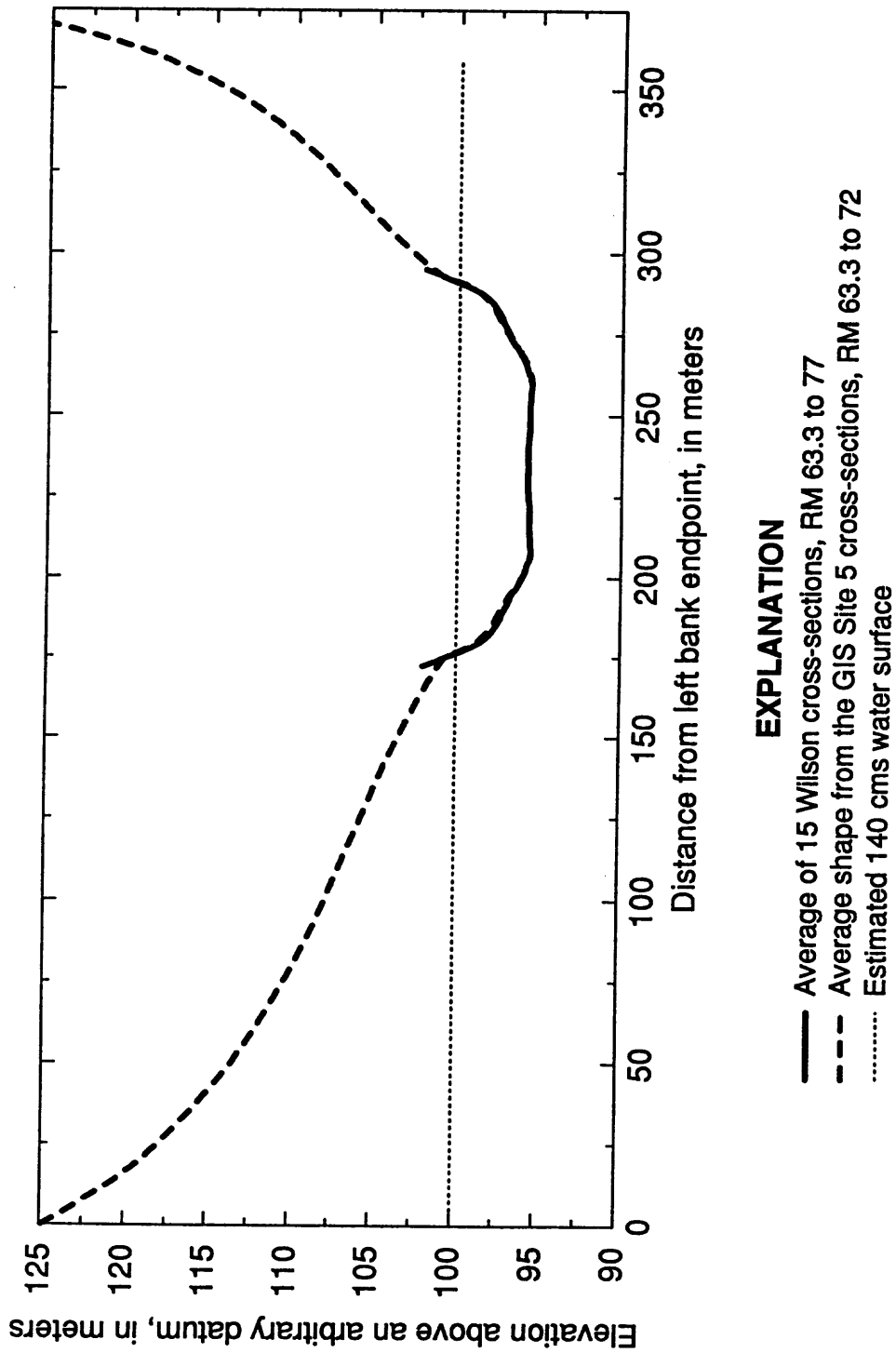


Figure 21. Comparison of the average shapes calculated from the Wilson cross-sections and the GIS cross-sections for morphologically similar reach RM 63.3 to 77. The width of the average shape of the GIS Site 5 cross-sections at 140 m³/s was multiplied by 1.11 to match the width of the average shape from the Wilson cross-sections at that discharge. This reach includes the area known as Furnace Flats, which is an extensive wide, flat area along the left bank, leading to an asymmetric average channel shape.

Morphologically Similar Reach RM 77 - 107:

Between RM 77 and 107, the Colorado River cuts through the Vishnu Schist and Zoroaster Granite in the Granite Gorge. GIS data are available from Site 6, RM 93 to 99, extending from Granite Rapid to Crystal Rapid. GIS Site 6 includes several major rapids and their associated debris fans and side canyons. Cross-sections through these debris fans and side canyons were deleted from the set used to compute the average shape for this reach for the reasons already discussed in the description of morphologically similar reach RM 11 - 23. The average shape added to each cross-section below the $140 \text{ m}^3/\text{s}$ water surface is the average of all the Wilson cross-sections.

The average shape obtained from the GIS cross-sections in Site 6 is much wider than the average of the Wilson cross-sections between RM 77 and 107, as noted previously. Therefore, the width of the average of the GIS cross-sections was adjusted by multiplying the width of the $140 \text{ m}^3/\text{s}$ water surface by 0.6167. The adjusted average shape for Site 6 agrees well with the average shape of the 29 Wilson cross-sections in this reach (figure 22).

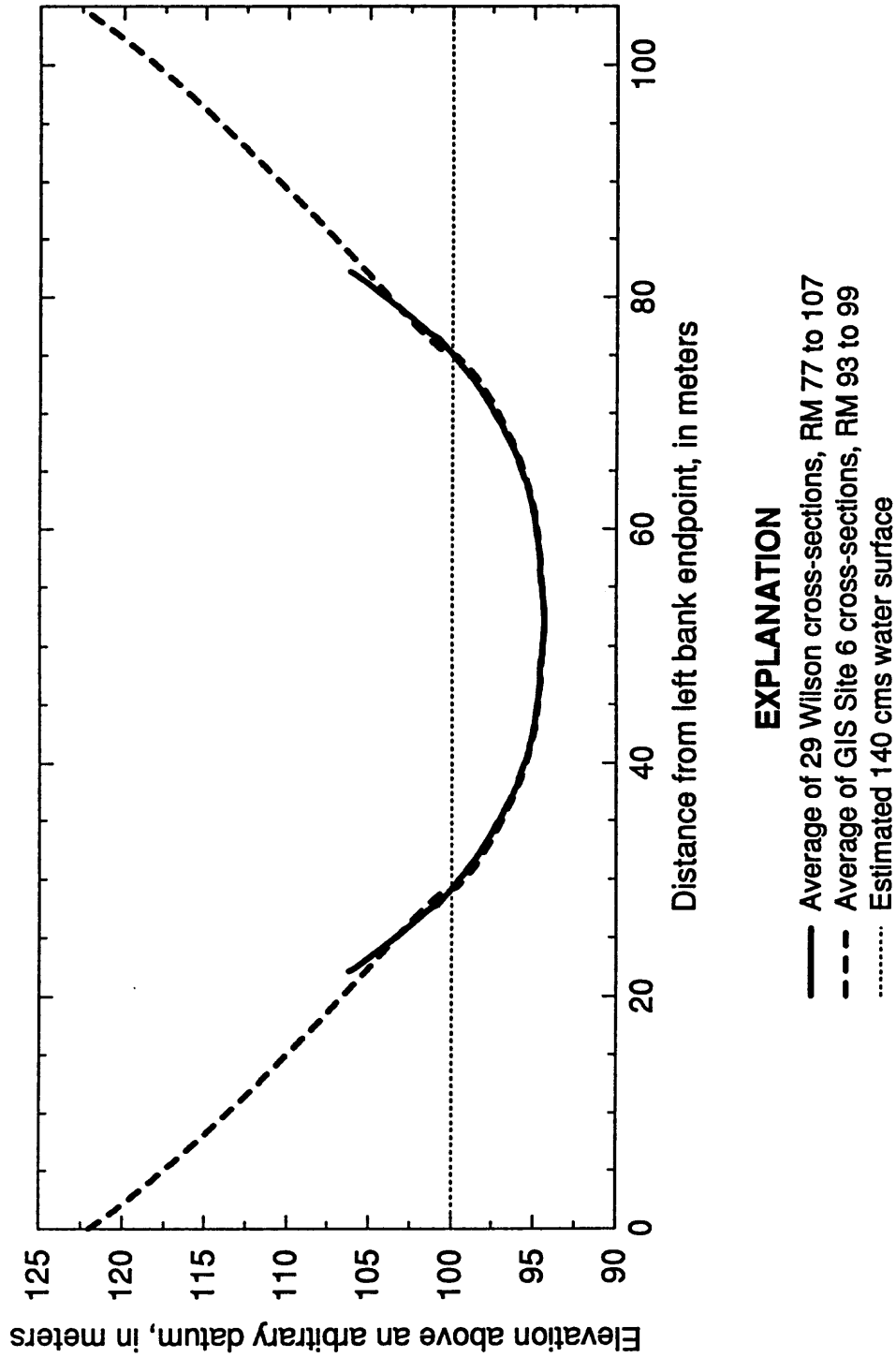


Figure 22. Comparison of the average shapes calculated from the Wilson cross-sections and the GIS cross-sections for morphologically similar reach RM 77 to 107. The width of the average shape of the GIS Site 6 cross-sections at 140 m³/s was multiplied by 0.617 to match the width of the average shape from the Wilson cross-sections at that discharge.

Morphologically Similar Reach RM 107 - 140:

The river-level geology in this reach is complicated by the fact that the river travels through several different types of rock within a short distance -- twice through the Vishnu Schist and Tapeats Sandstone, and once through the Unkar Group and Bass Limestone. GIS data are available from two sites in this reach: Site 7, RM 120 to 123, in the Tapeats Sandstone; and Site 8, RM 133 to 138, in the Bass Limestone. Because the riverbed through a significant portion of the reach is Vishnu Schist (18.2 of 53 km, or 11.3 of 33 miles), the average shape from Site 6 (with its width adjusted as described above) was used along with the average shapes from Sites 7 and 8 to compute the average shape for this morphologically similar reach. For the cross-sections through the limestone and schist, the average shape from all the Wilson cross-sections was added below the 140 m³/s water surface. For the cross-sections in the Tapeats Sandstone, however, the average shape at 140 m³/s from two other reaches also in Tapeats Sandstone (RM 50 to 63.3 and 169 to 190) was added to each cross-section.

The resulting average shape for this reach is slightly wider (by 5.1 m) than the average of the 25 Wilson cross-sections through the same reach. Adjusting the average width of the GIS cross-sections at 140 m³/s by the difference in width between the two shapes (a factor of 0.919) results in good agreement between the two average shapes (figure 23).

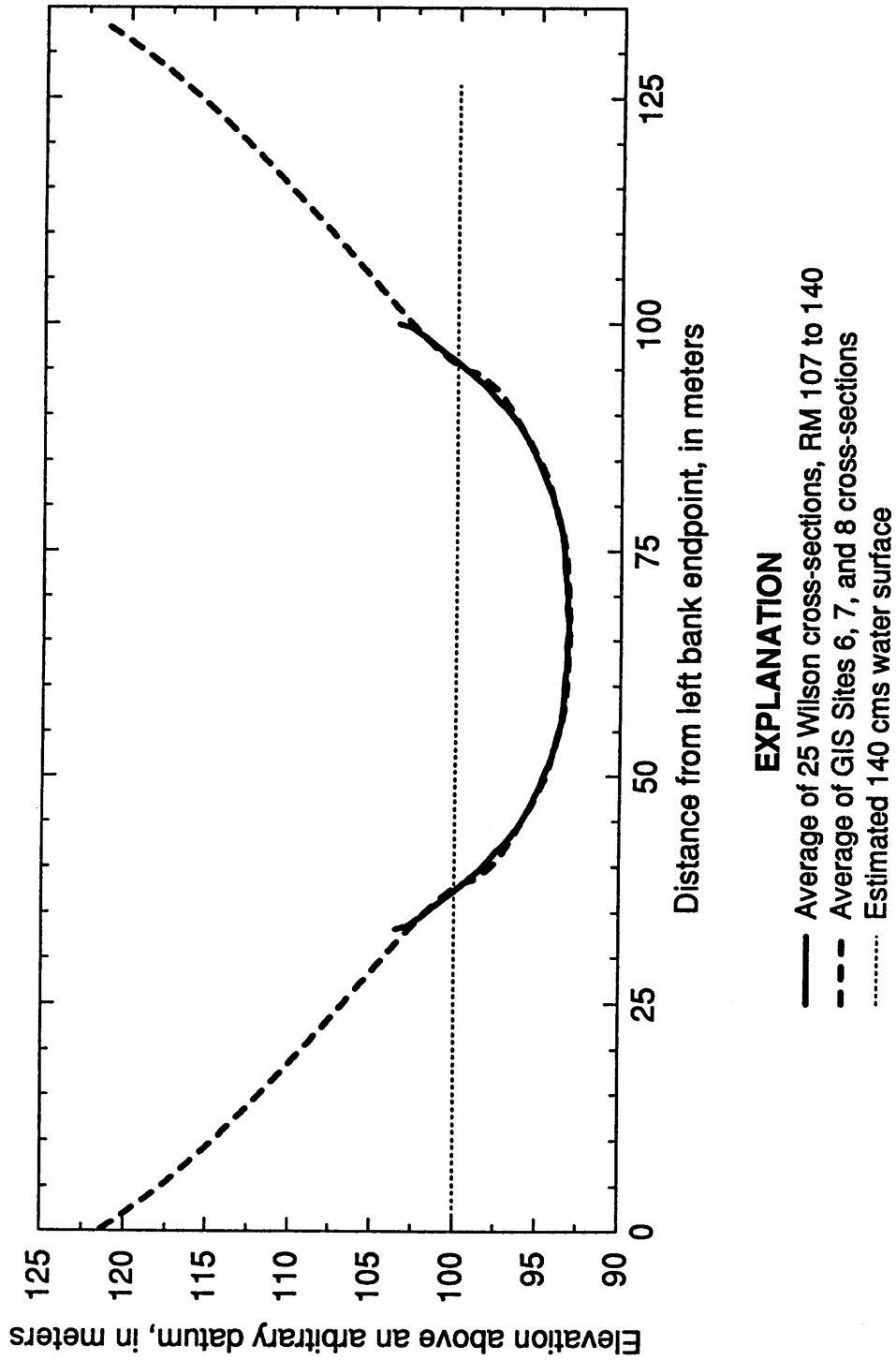


Figure 23. Comparison of the average shapes calculated from the Wilson cross-sections and the GIS cross-sections for morphologically similar reach RM 107 to 140. The width of the average shape of the GIS Site 6, 7, and 8 cross-sections at 140 m³/s was multiplied by 0.919 to match the width of the average shape from the Wilson cross-sections at that discharge.

Morphologically Similar Reach RM 140 - 169:

The dominant river-level rock type between RM 140 and 169 is the Cambrian limestone of the Muav Formation. GIS Site 9, RM 143 to 145, contains sufficient data to represent this reach well. The average shape added to each cross-section below the 140 m³/s water surface was the average of all the Wilson cross-sections. The difference in channel width at 140 m³/s between the average shape from the GIS cross-sections and the average shape from the Wilson cross-sections is only 0.76 m (a 1.3% difference). The average channel width of the GIS cross-sections at 140 m³/s was therefore multiplied by 1.013 to match that of the Wilson cross-sections. The presence of Kanab Creek within the limited GIS reach results in an asymmetric shape, which is unlikely over the distance of the entire morphologically similar reach (29 miles, or 47 km). Therefore, the shape was averaged left and right to obtain the average shape for the morphologically similar reach (figure 24).

Morphologically Similar Reach RM 169 - 190:

Between RM 169 and 190, the river-level rock types include Bright Angel Shale, Tapeats Sandstone, and lava over these Cambrian clastic rocks. GIS Site 10 (RM 179-181), which provides representative cross-sections for this reach, is within the segment with lava over the clastic rocks, near Lava Falls. The average shape added below the 140 m³/s water surface to each cross-section is that of the average of the 16 Wilson cross-sections, RM 169 to 190. The difference in width at 140 m³/s between these two average shapes is about 2.8 m (about a 3.4% difference). Therefore, the average width of the Site 10 GIS cross-sections at 140 m³/s was multiplied by 1.035 to match the width of the average of the Wilson cross-sections, RM 169 to 190.

The presence of Prospect Canyon on the left bank at about RM 179.3 leads to an asymmetric average shape of the GIS cross-sections. Again, the average shape for the entire morphologically similar reach is more likely symmetric, as indicated by the

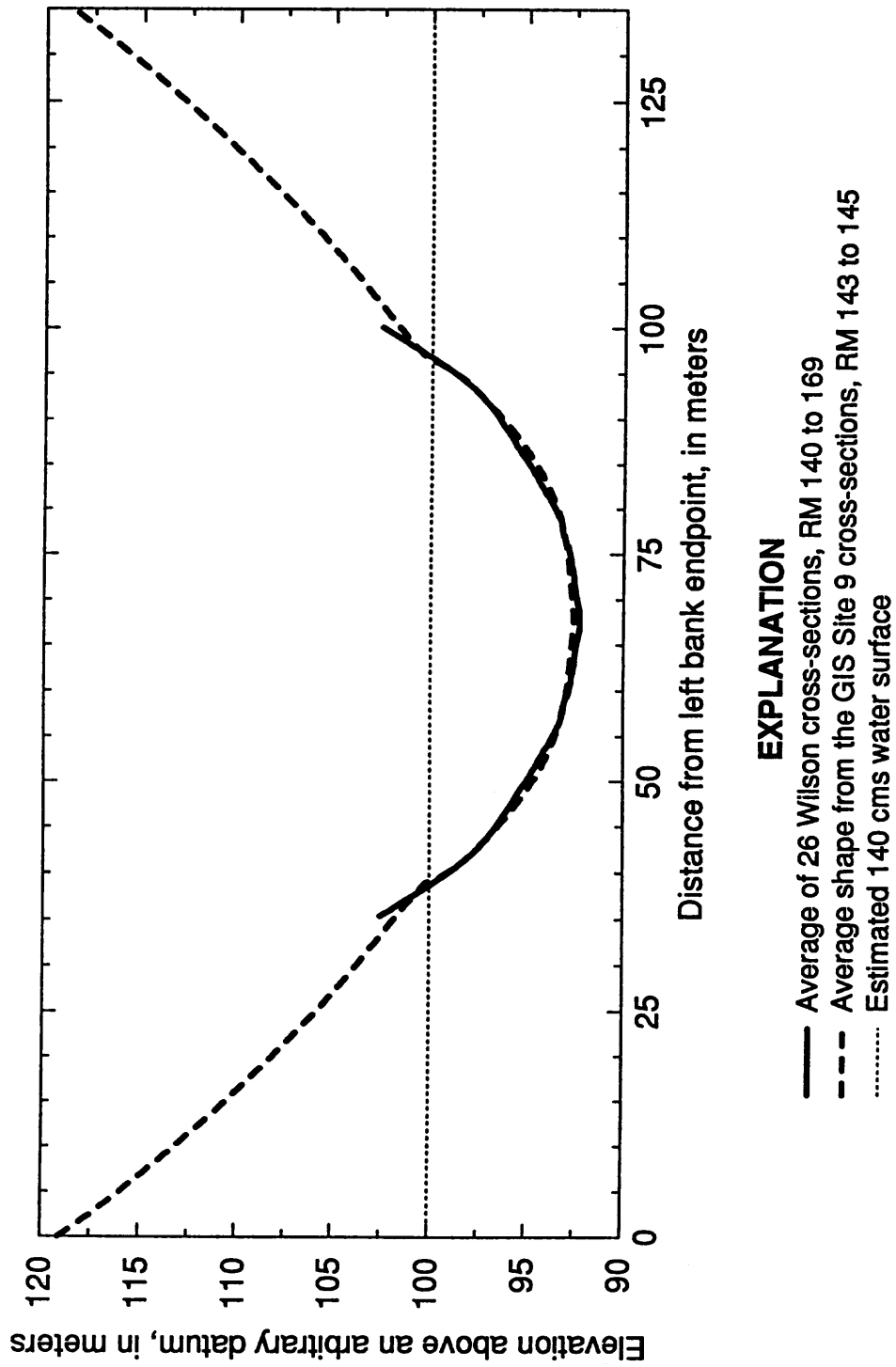


Figure 24. Comparison of the average shapes calculated from the Wilson cross-sections and the GIS cross-sections for morphologically similar reach RM 140 to 169. The width of the average shape of the GIS Site 9 cross-sections at 140 m³/s was multiplied by 1.013 to match the width of the average shape from the Wilson cross-sections at that discharge.

average of the Wilson cross-sections in this reach. Therefore, the shape for this reach was averaged left and right about the center of the $140 \text{ m}^3/\text{s}$ water surface (figure 25).

Morphologically Similar Reach, RM 190 - 225:

While the rock type at river-level through much of this reach is Vishnu Schist, the presence of Tapeats Sandstone above the schist results in a wider average shape than that found in other reaches through the schist (e.g., the Granite Gorge). The Tapeats Sandstone also produces a relatively broad, flat channel bottom, as it does in other locations. GIS Site 11, RM 207 to 210, is located where the Vishnu Schist is at river level and provides a representative shape for this morphologically similar reach. The average shape added to each GIS cross-section below the $140 \text{ m}^3/\text{s}$ water surface is the average shape from the 29 Wilson cross-sections between RM 190 and 225. The width of the average shape of these Wilson cross-sections at $140 \text{ m}^3/\text{s}$ (89.74 m) is 10.6 m greater than the average of the Site 11 GIS cross-sections. Therefore, the average width from the GIS cross-sections at $140 \text{ m}^3/\text{s}$ was multiplied by 1.134 in order to match the average width of the Wilson cross-sections at this discharge. In addition, the average shape from the GIS cross-sections is asymmetric because of the presence of the Granite Park Fault through much of the GIS reach. Granite Park Canyon runs along this fault, opening up to a wide, relatively flat area along the left bank of the river. Therefore, the shape was averaged left and right to produce a symmetric shape for the 56 km (35-mile) long reach. A comparison of the average shape computed from the GIS cross-sections with the average of the Wilson cross-sections (figure 26) shows good agreement between the two below the $140 \text{ m}^3/\text{s}$ water surface. Above that stage, the average channel shape from the GIS cross-sections becomes wider than the average of the Wilson cross-sections.

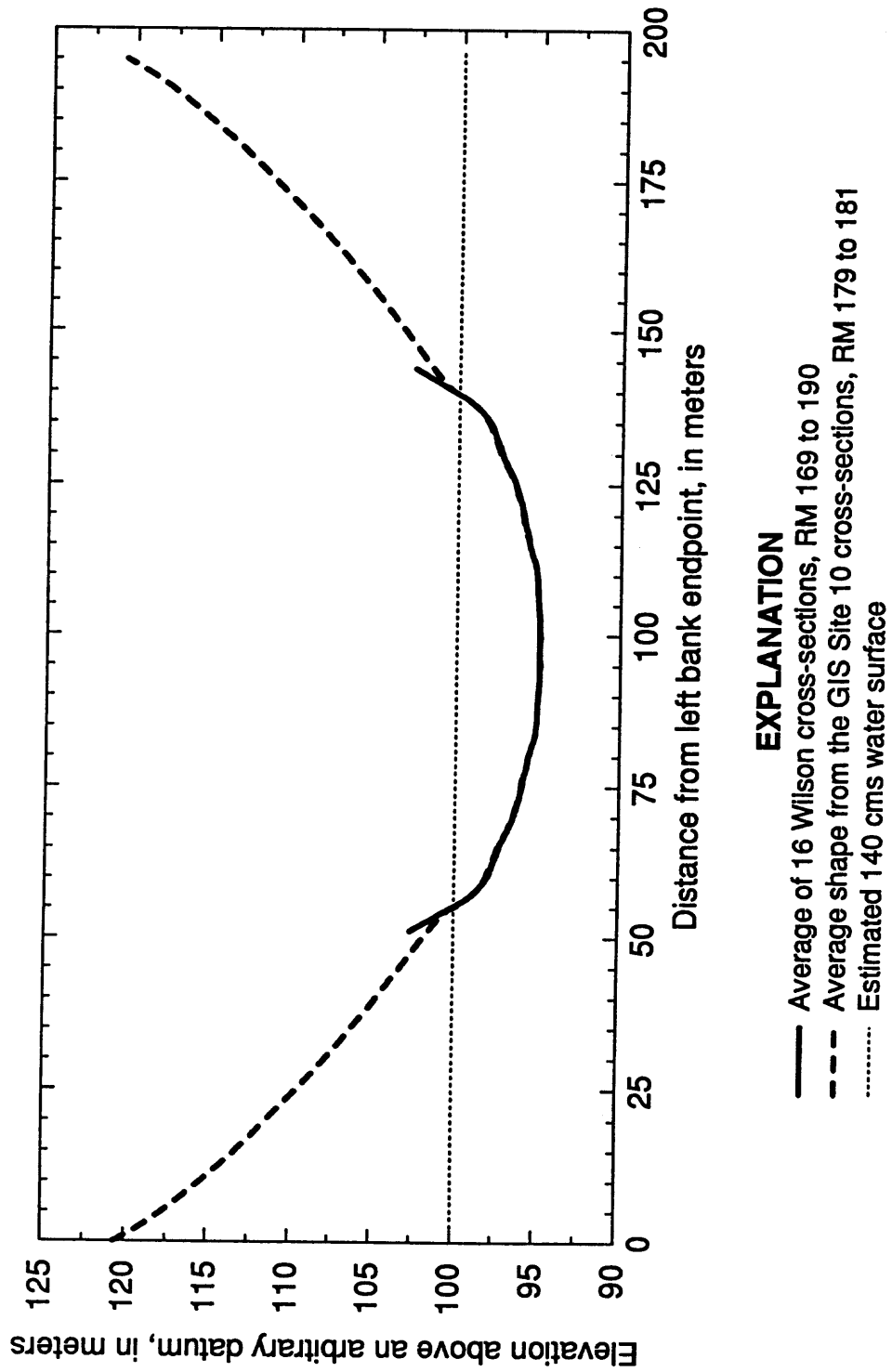
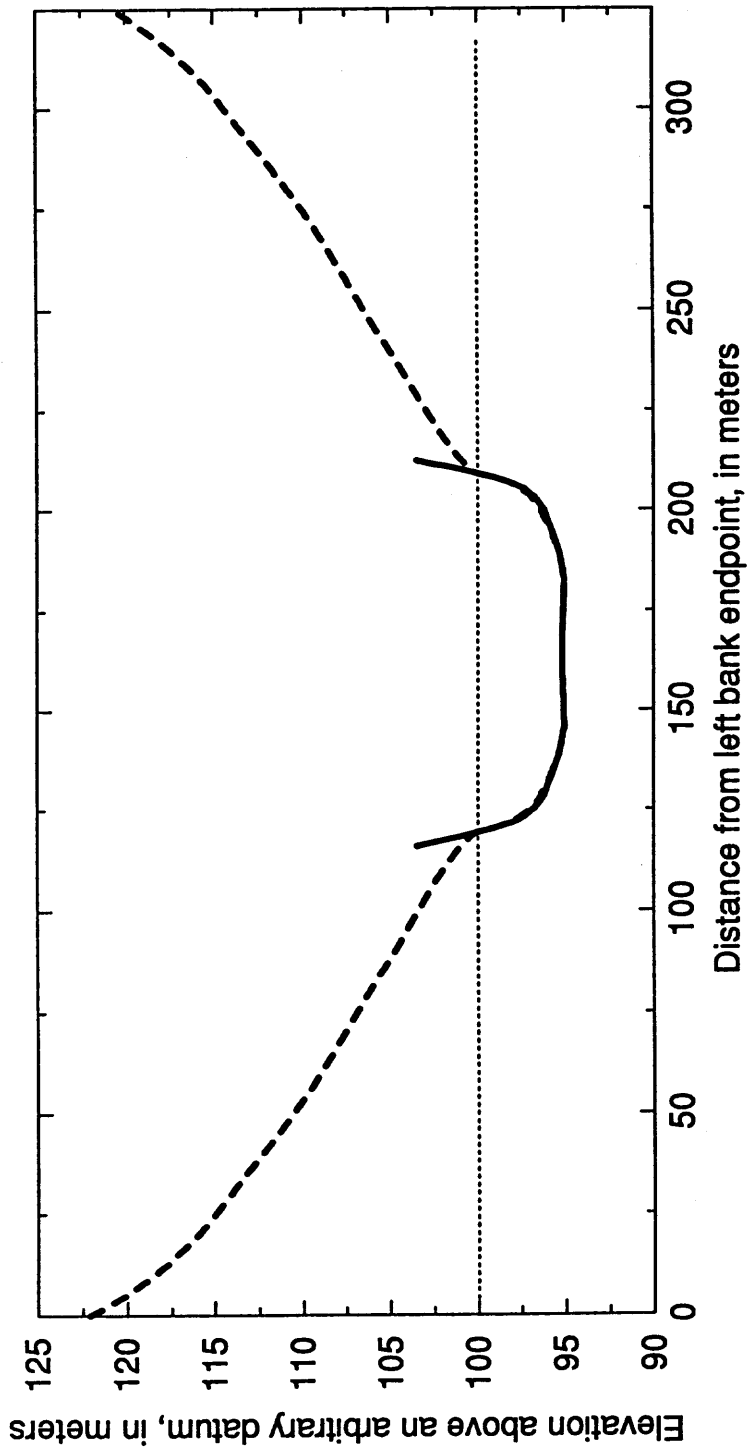


Figure 25. Comparison of the average shapes calculated from the Wilson cross-sections and the GIS cross-sections for morphologically similar reach RM 169 to 190. The width of the average shape of the GIS Site 10 cross-sections at 140 m³/s was multiplied by 1.035 to match the width of the average shape from the Wilson cross-sections at that discharge.



EXPLANATION

- Average of 30 Wilson cross-sections, RM 190 to 225
- - - Average shape from the GIS Site 11 cross-sections, RM 207 to 210
- Estimated 140 cms water surface

Figure 26. Comparison of the average shapes calculated from the Wilson cross-sections and the GIS cross-sections for morphologically similar reach RM 190 to 225. The width of the average shape of the GIS Site 11 cross-sections at 140 m³/s was multiplied by 1.134 to match the width of the average shape from the Wilson cross-sections at that discharge.

Computing the Single Weighted Average Channel Shape

An average channel shape for the entire 362-km (225-mile) reach was calculated using weighted average shapes of the morphologically similar reaches obtained from the GIS data as discussed in the previous section. The weighting applied to the average shape of each morphologically similar reach was found by dividing the number of river miles within the morphologically similar reach by the total 225 miles (table 5). Two of the morphologically similar reaches (RM 50 - 63.3 and RM 107 - 140) include more than one GIS reach, and two other reaches are represented by the average shape from three GIS reaches where the river-level rock is limestone. In each of those cases, an average shape for the morphologically similar reach was found first using weighted averages of the individual GIS reaches.

The average shape for the morphologically similar reaches containing multiple GIS reaches was found by weighting the individual GIS reaches according to the percent of the total distance in that morphologically similar reach for which the river-level rock type is the same as in the GIS reach. For example, the channel shape for the reach RM 50 to 63.3 is represented in part by cross-sections from Site 4, in the Bright Angel Shale, and in part by the cross-sections from Site 5, in the Tapeats Sandstone. A total of 9.3 miles, or 69.9%, of the 13.3-mile reach are in the Bright Angel Shale, while 4 miles of the reach, or 30.1%, are in the Tapeats Sandstone. The average shape for morphologically similar reach RM 50 to 63.3 was then found by averaging the Site 4 average shape, weighted by 0.699, and the Site 5 average shape, weighted by 0.301. For the two morphologically similar reaches represented by the average of all the limestone reaches (RM 0 - 11 and RM 23 - 50), the average shapes of the individual limestone reaches were all weighted equally (by 0.333) to obtain the representative shape.

Table 5. Calculated weighting factors for the average shapes representing the morphologically similar reaches

Morphologically Similar Reach (RM)	% of 225 Miles	Representative GIS Reach(es)	% of GIS data representing the MSR	Weighting Factor
0 - 11	4.9	Site 3, RM 42-48	33.3	.049
		Site 8, RM 133-138	33.3	
		Site 9, RM 143-145	33.3	
11 - 23	5.3	Site 6, RM 93-99	100	.053
23 - 50	12.0	Site 3, RM 42-48	33.3	.120
		Site 8, RM 133-138	33.3	
		Site 9, RM 143-145	33.3	
50 - 63.3	5.9	Site 4, RM 51-56	69.9	.059
		Site 5, RM 60-63.3	30.1	
63.3 - 77	6.1	Site 5, RM 63.3-72	100	.061
77 - 107	13.3	Site 6, RM 93-99	100	.133
107 - 140	14.7	Site 6, RM 93-99	37.2	.147
		Site 7, RM 120-123	39.5	
		Site 8, RM 133-138	22.4	
140 - 169	12.9	Site 9, RM 143-145	100	.129
169 - 190	9.3	Site 10, RM 179-181	100	.093
190 - 225	15.6	Site 11, RM 207-210	100	.156

The weighting factors were applied to both the widths and elevations at each fraction of cross-stream distance for the average shapes of each morphologically similar reach. The widths and elevations at specified fractions of cross-stream distance were then summed to produce the single average channel shape (figure 27).

Discussion of the Break in Slope of the Average Channel Shape

A comparison of the single average shape computed from the GIS cross-sections with that obtained from the Wilson cross-sections shows good agreement between the two up to a center depth of about 6.7 m, corresponding to a discharge of about 310 m³/s (11,000 ft³/s). A break in the slope of the side of the average channel shape computed from the GIS cross-sections begins at a center depth of 7.1 m, which corresponds to a discharge of about 380 m³/s (13,400 ft³/s). This break in slope, also seen in the average shape computed for each morphologically similar reach, would be consistent with a transition from the dominant effects of channel-forming processes to those of hillslope processes. Evidence showing that the break in slope exists in the topography as defined in the GIS model and is not simply an artifact of the method used to calculate the average channel shape is presented below. The same break in slope is not present in the average of the Wilson cross-sections. However, the linear slopes of the banks in these cross-sections are the result of a lack of measurements near the edges of the water, as explained below. Geomorphic conditions that contribute to the break in slope are also discussed below.

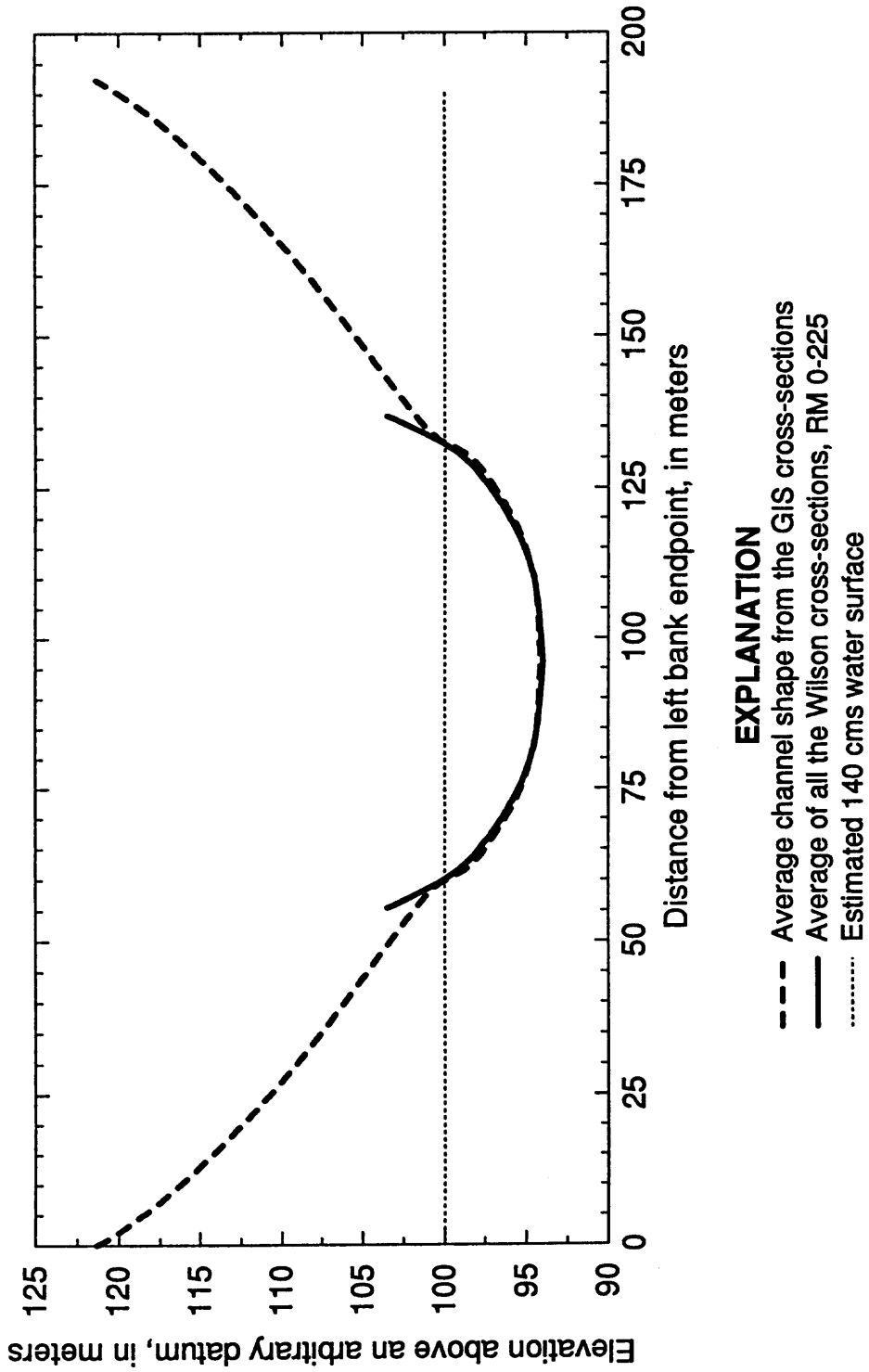


Figure 27A. Comparison of the average channel shape calculated for the entire 362-km (225-mile) reach using the GIS cross-sections and the average channel shape calculated from the Wilson cross-sections. The break in slope of the average shape from the GIS cross-sections occurs at a center depth of about 7.1 m, which corresponds to a discharge of about 380 m³/s (13,400 ft³/s).

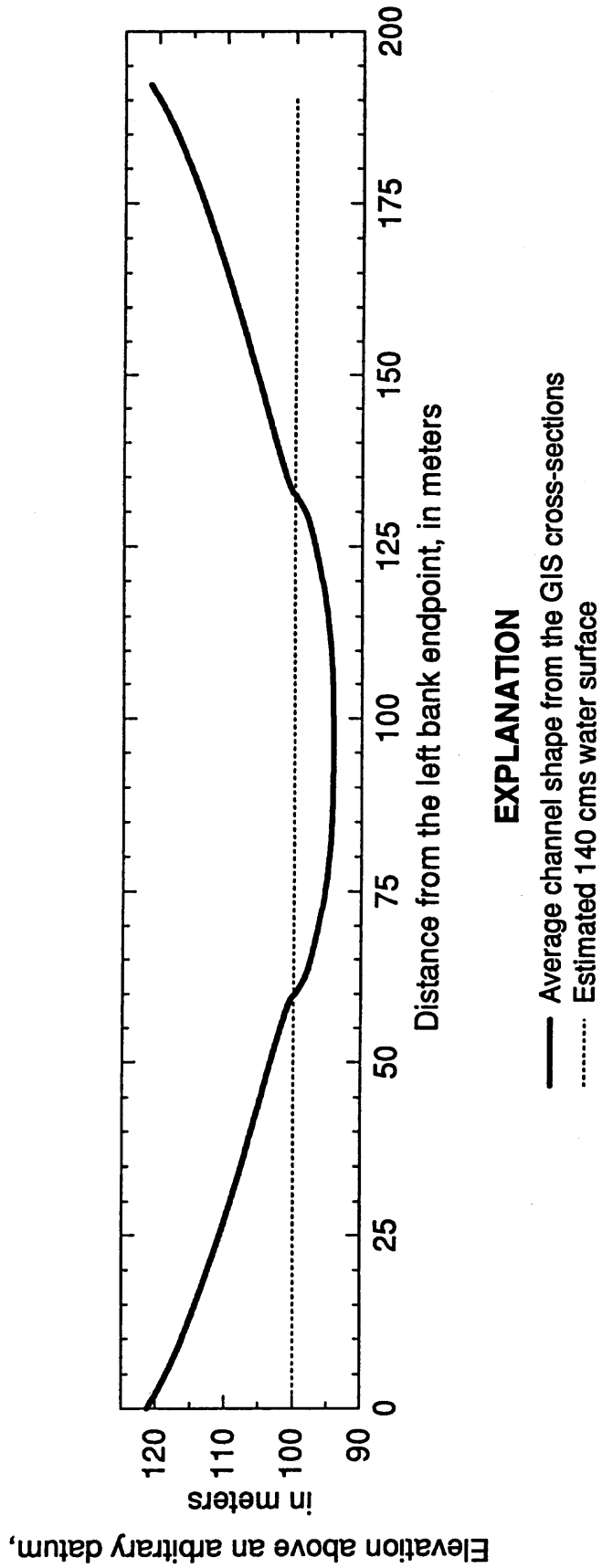
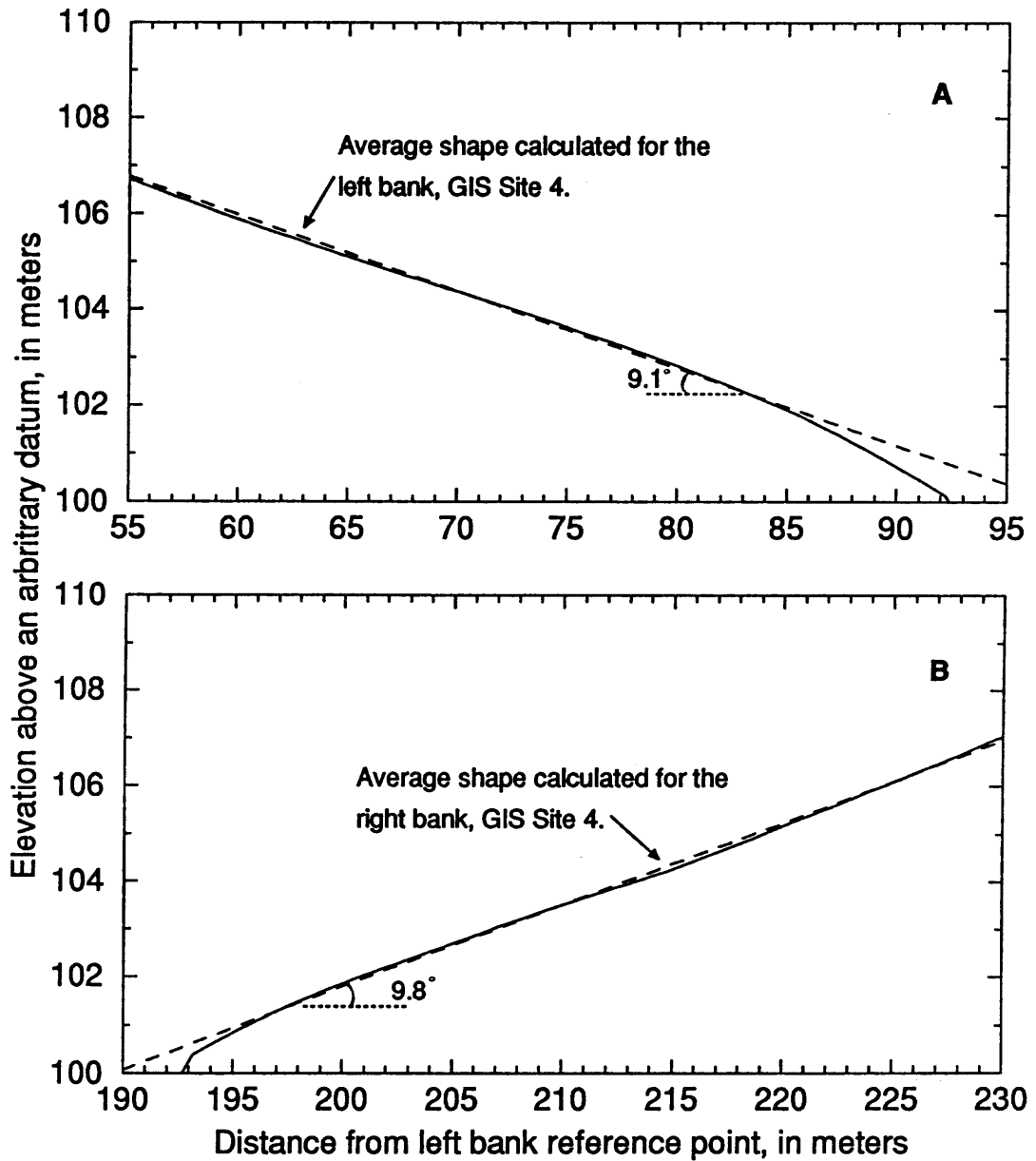


Figure 27B. Average channel shape calculated for the entire 362-km (225-mile) reach using the GIS cross-sections, plotted with no vertical exaggeration.

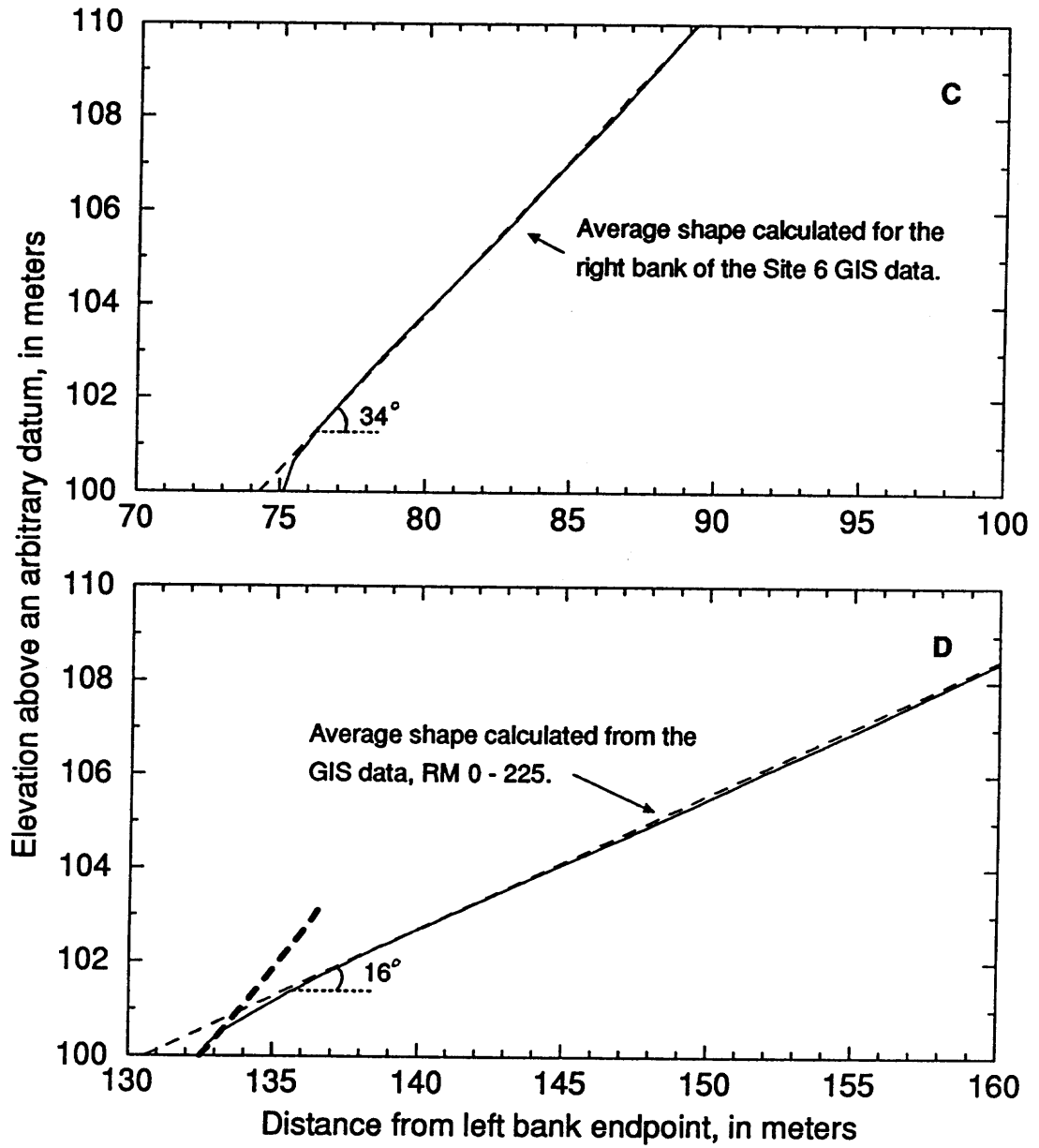
The break in the slope of the side of the channel was found by calculating average shapes using only the topographic data in the GIS database. The method used to average the cross-sections within a particular GIS reach initially averaged the data in three separate segments: 1) the left bank GIS data; 2) the segment below the 140 m³/s (5,000 ft³/s) water surface, where shape was estimated using the Wilson cross-sections; and 3) the right bank GIS data. While the average shapes for the morphologically similar reaches have been averaged left and right, the average shape for each GIS reach was computed initially without averaging left and right of the center of the 140 m³/s (5,000 ft³/s) water surface. The break in slope of the side of the channel can be seen in the average shape calculated from the Site 4 (RM 51 to 56) cross-sections (figure 28). For each bank, the average shape was computed separately using only the GIS data. Above the break in slope, the average channel bank is essentially linear over about a 7-m change in elevation, with a slope of 9.8° on the right bank and 9.1° on the left bank. The slope of the linear segment of the channel bank above the break was also calculated for the narrowest GIS reach with the steepest bank, Site 6 (RM 93 to 99), and for the single average shape computed from the GIS cross-sections. For the average shape computed from the Site 6 data, the channel slope between center depths of 7.1 and 17 m is about 34° (figure 28). For the average channel shape for the entire 362-km (225-mile) reach, the slope above the break is about 16°. In each case, the break in slope occurs between one and two meters above the 140 m³/s (5,000 ft³/s) water surface, where the GIS and the Wilson data sets were matched. Because the slope break is above the matching point, it is clearly present in the GIS data.



EXPLANATION

- - - Linear regression for 102 m < elev. < 108 m
- Average shape computed from the GIS data

Figure 28. Examples showing the average channel shape above the 140 m³/s (5,000 ft³/s) water surface. A, Left bank of GIS Site 4 (RM 51 - 56). B, Right bank of GIS Site 4. C, Right bank of GIS Site 6 (RM 93 - 99). D, Right bank of the average channel shape computed for RM 0 - 225. In each case, the break in slope of a linear segment of the bank occurs one to two meters above the 140 m³/s (5,000 ft³/s) water surface.



EXPLANATION

- Average channel shape from the GIS cross-sections
- - - Average of all the Wilson cross-sections, RM 0-225
- - - Linear regression for 101 m < elev. < 110 m

Figure 28, continued.

The same break in slope is not evident in the average of the Wilson cross-sections because these measurements did not extend to the edge of the channel, and the break in slope typically would fall within the gap in data between the edge of the water surface and the first point measured on either bank. These cross-sections were measured using depth-sounding equipment mounted in a small boat. Identification of the location of the boat in the cross-stream direction was based in part on the assumption of a constant boat speed between reference points (Wilson, 1986). When approaching the edge of the channel, the boat slowed down to turn, so that identification of its location became less accurate. Also, rapid changes in depth near the edge of the channel combined with the less accurate navigation to result in poor resolution of the channel shape near the edges of the water.

To compute the average of the Wilson cross-sections, depth between the edge of the water surface and the first point identified below it was estimated using a linear interpolation. For example, there are no depth measurements within 6.1 m (20 ft) of the edge of the water surface for cross-section S-9 at RM 7.4 (figure 29). The closest points to the edges of the water were 4.8 m (16 ft) and 3.4 m (11 ft) below the water surface on the left and right banks, respectively. The Wilson cross-sections were measured at discharges close to $790 \text{ m}^3/\text{s}$ ($28,000 \text{ ft}^3/\text{s}$). Based on the width and shape of the channel at this cross-section, the $140 \text{ m}^3/\text{s}$ ($5,000 \text{ ft}^3/\text{s}$) water surface is estimated to be less than 3 m below the $790 \text{ m}^3/\text{s}$ ($28,000 \text{ ft}^3/\text{s}$) water surface. As stated above, the break in slope was found to be 1 to 2 m above the $140 \text{ m}^3/\text{s}$ ($5,000 \text{ ft}^3/\text{s}$) water surface in each morphologically similar reach. The lack of depth measurements in the Wilson cross-sections close to the edges of the channel means that the break in slope could not be detected from these cross-sections, and that the average shape computed from them would necessarily have a linear slope above the $140 \text{ m}^3/\text{s}$ ($5,000 \text{ ft}^3/\text{s}$) water surface.

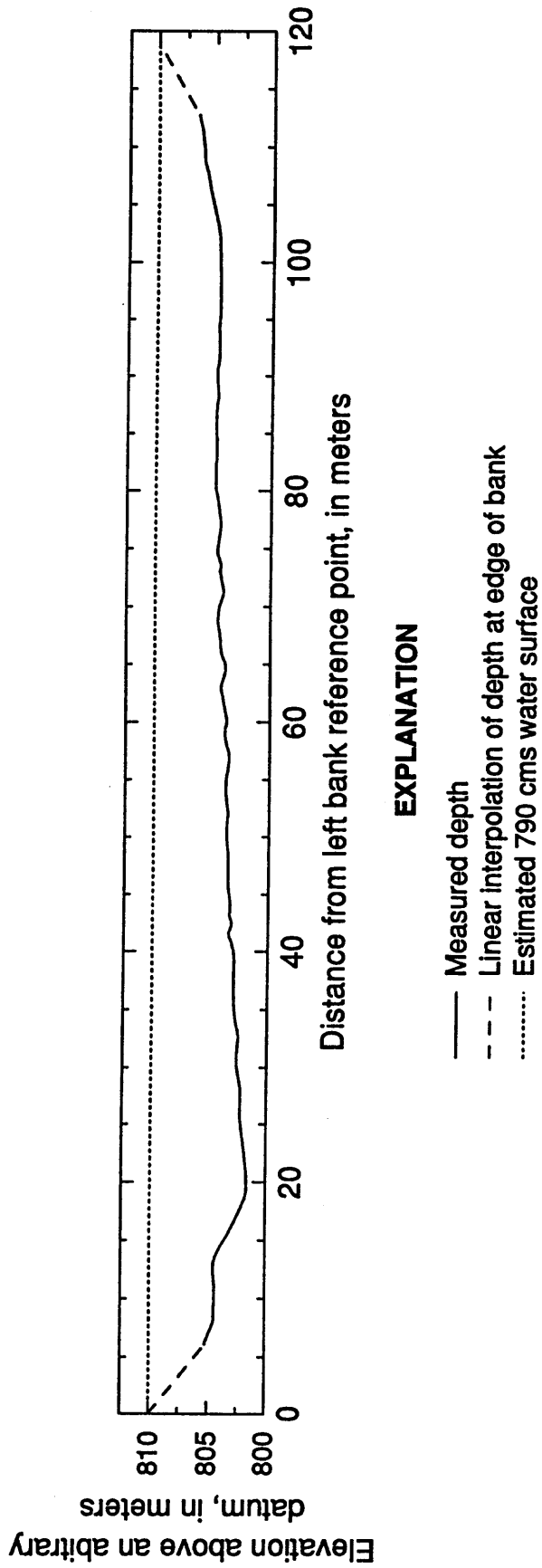


Figure 29. Wilson cross-section S-9, at RM 7.4, shown with no vertical exaggeration. There are no depth measurements within 6.1m of the water's edge on either bank. Depth near the water's edge was estimated using a linear interpolation from the water's edge to the next known point.

The geomorphology of the Colorado River channel through Marble and Grand Canyons is influenced by both river-channel and hillslope processes. The river is incised in bedrock, but the average channel shape computed from the GIS data for high flows is not entirely in a bedrock channel. The geomorphology of the Colorado River in the Grand Canyon has been described in detail by Howard and Dolan (1981), but will be discussed generally here in order to explain why the break in slope of the side of the channel exists. In the 3.3 million years since the Colorado River through Marble and Grand Canyons cut down to near its present grade (Lucchitta, 1972), talus slopes have developed from rockfall at the base of near-vertical cliffs, and boulders have been carried from side canyons into the main channel by numerous debris flows. The talus slopes extend well above the pre-dam high water zone in many areas, as indicated by stable bands of riparian vegetation above the 2,800 m³/s (100,000 ft³/s) waterline (Carothers and Brown, 1991). The linear to concave shape of the channel above the break in slope results from the presence of both bedrock channel walls and talus slopes, and, in some areas, sand deposited by previous high flows.

The present-day channel includes many alluvial sand deposits, both those associated with flow around debris fans and those along the channel margins. The availability of sand, both on the bed of the channel and along the channel margins, also strongly affects the shape of the active channel. For example, Howard and Dolan (1981) found the shape of the bottom of the channel in the cliff-bordered reaches between RM 1 and RM 10 to be nearly flat and dominated by sand. They did not provide data that could be used to reconstruct their channel profiles and estimate bed elevation changes between the time of their measurements and the measurement of the Wilson cross-sections. However, assuming their assessment is correct, a qualitative comparison of the shape of the channel then and when the Wilson cross-sections were measured can be made. Howard and Dolan's profile measurements were made prior to the exceptionally high dam releases in 1983 through 1985. As previously mentioned,

the highest release from Glen Canyon Dam occurred in June, 1983, when the instantaneous discharge at Lees Ferry peaked at $2,760 \text{ m}^3/\text{s}$ ($97,300 \text{ ft}^3/\text{s}$). Cross-sections measured by Wilson (1986) in April and May, 1984, indicate the average shape of the channel bed through this same reach was well-rounded. This is likely the result of the evacuation of sand along the bed through this reach during the high release of 1983, without subsequent replacement of the sand through inflow from the Paria River at RM 1.

Schmidt and Graf (1990) noted significant aggradation of sand at many beaches downstream from Lees Ferry, particularly in wide reaches, following the 1983 high flows. They calculated the planimetric area covered by alluvial sand deposits in reaches extending a total of about 158 km (98.1 miles) from aerial photographs taken in October, 1984, at low discharges (about $170 \text{ m}^3/\text{s}$, or $6,000 \text{ ft}^3/\text{s}$). The mean area per kilometer of all types of sand deposits ranged from $18,000 \text{ m}^2 / \text{km}$ in a narrow reach (RM 140 to 160) to about $26,900 \text{ m}^2 / \text{km}$ in a wide reach (RM 41 to 62), with the total area covered by the alluvial deposits through the 158 km being about $764,000 \text{ m}^2$. The data presented are not sufficient to calculate volumes of sand in these deposits. Although the volume of sand has not been computed, the area covered by these deposits indicates a significant amount of sand was present along the channel margins at that time.

The break in the slope of the channel occurs at a stage corresponding to about the mean daily flow after the closure of the dam, which Howard and Dolan (1981) stated was $360 \text{ m}^3/\text{s}$. The mean daily discharge was also computed from the record of the gaging station Colorado River at Lees Ferry and its associated stage-discharge relation for October 1, 1985 through September 30, 1995, and again found to be $360 \text{ m}^3/\text{s}$. As previously mentioned, the break in slope begins at a stage corresponding to a discharge of about $380 \text{ m}^3/\text{s}$ ($13,400 \text{ ft}^3/\text{s}$). Because of the presence of extensive alluvial sand deposits within this system, I believe the 'U' in the middle of the channel exists

because of sediment transport conditions dominated by the mean daily post-dam discharge. As indicated by the Wilson cross-sections and detailed bathymetric surveys (Graf et.al., 1995b), the shape of the bed through Marble and Grand Canyons is highly irregular. Wilson's general descriptions of his measured profiles included bowl-shaped, trapezoidal, flat, and V-shaped, with the calculated spatial average of all the profiles having a U shape. The geomorphic conditions described above, then, combined with complex physical processes, have resulted in the present-day characteristic channel shape presented here.

Specification of Channel Shape for the Flow Model

The one-dimensional unsteady flow model uses the inflow hydrograph converted to stage as the upstream boundary condition. Therefore, equations relating area and hydraulic radius to depth are needed to provide inputs to solve the flow equations. The needed relations were obtained by fitting equations to the channel characteristics of the average shape. Because the average channel shape has a distinct change in slope of the side of the channel at a center depth of about 7.1 m, separate functions are needed to relate area and hydraulic radius to depth above and below this center depth.

Area as a function of depth was found by first determining the relation between channel width and depth, then integrating to find the relation between area and depth. The following relations were derived for width as a function of depth

$$b = 44.152 + 16.268 \ln h \qquad h \leq 6.95 \text{ m}; \quad (1a)$$

$$b = 16.250 + 9.247h - 0.09988h^2 \qquad 6.95 \text{ m} < h, \quad (1b)$$

where b is the width of the channel and h is the flow depth. The two curves match at a center depth of 6.95 m, so this value determines which relation will be used rather than separating the functions at a depth of 7.1 m. Integrating the above equations leads to relations for area as a function of depth which are

(2)

$$A = 44.152(h - h_0) + 16.268(h(\ln h - 1) - h_0(\ln h_0 - 1)) + A_0$$

$$h \leq 6.95 \text{ m}; \quad (2a)$$

$$A = 16.250(h - h_{0b}) + 4.6235(h^2 - h_{0b}^2) - 0.033295(h^3 - h_{0b}^3) + A_{0b}$$

$$6.95 \text{ m} < h, \quad (2b)$$

where h is the flow depth, h_0 and A_0 are the depth and area at which the roughness parameter, β , is nominally 0 and are equal to 4.311 and 211.8, respectively. The values of h_{0b} and A_{0b} are 6.95 and 402.2, respectively, with the value of A_{0b} calculated using equation (2a) for a depth of 6.95 m.

Estimation of the Channel Roughness

In addition to the need for information concerning average channel shape for high flows is the need for a way to relate stage to discharge for the average shape. The one-dimensional unsteady flow model uses a non-dimensional friction coefficient that is a function of the channel roughness and varies with stage to relate stage to discharge. This friction coefficient, β , is defined by

$$\beta = \frac{u}{u_*} \quad (3)$$

where u is the average velocity and u_* is the shear velocity. The shear velocity is defined as $(\tau/\rho)^{1/2}$, where τ is the bed shear stress and ρ is the density of water. For the original model, a wetted-perimeter-averaged shear velocity for steady, uniform flow was used to calculate β (Wiele and Smith, 1996). The equation for this shear velocity is

$$u_* = \left[gR \left(S - \frac{\partial e}{\partial x} \right) \right]^{1/2} \quad (4)$$

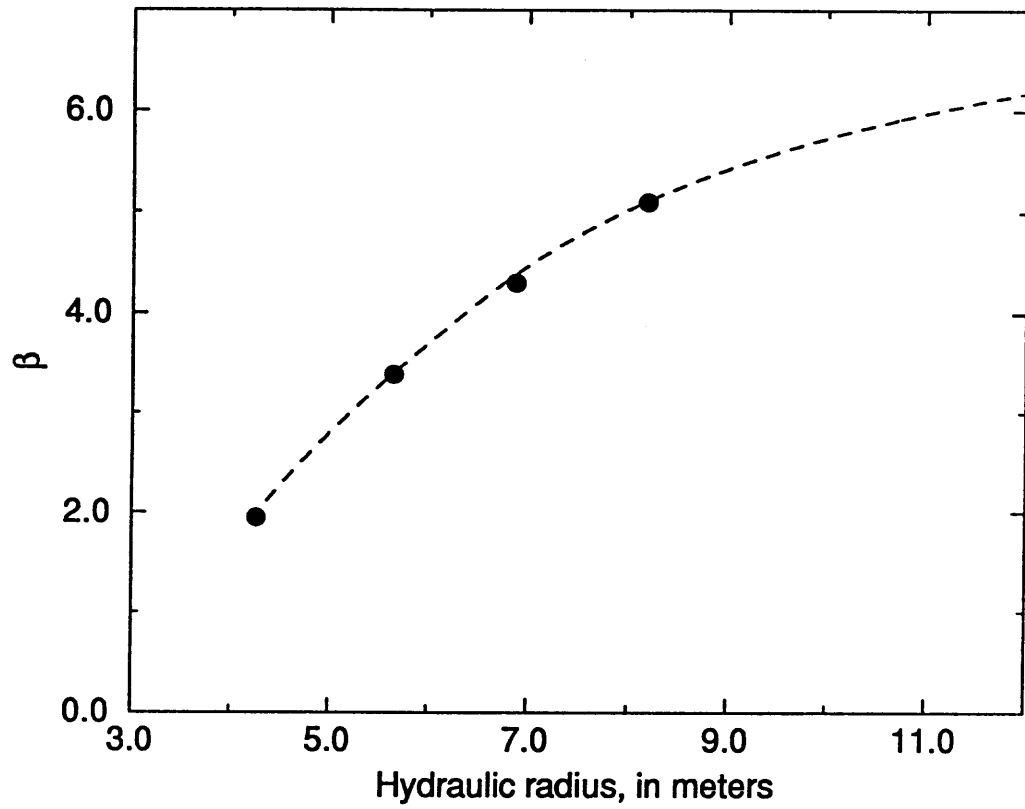
where g is the acceleration due to gravity, R is the reach-averaged hydraulic radius, S is

the average water surface slope (0.00155) between Lees Ferry and Diamond Creek, and $\partial e/\partial x$ is the additional slope of the water surface with respect to the average slope due to the shape of the wave. This friction coefficient varies as a function of stage and includes the effects of local accelerations due to expansion and contraction of the channel. The dominant large-scale roughness elements include boulders on the bed and in debris fans, and, for higher flows, talus slopes and side channels.

A relation between the hydraulic radius, R , and the friction coefficient, β , was developed for the original model using β calculated directly from areas from measured channel cross-sections and a reach-averaged flow velocity measured by dye-tracing at a known, steady discharge. A smooth logarithmic function was fitted to the two known points and an estimated value of roughness at 142 m³/s. This function has since been updated using measured wave speeds from the 1996 high flow release from Glen Canyon Dam (Wiele and Griffin, 1997). The revised roughness relation (figure 30) for the original channel shape is

$$\beta = -5.252 + 4.932 \ln R \quad (5)$$

The geometric properties of the average shape from the Wilson cross-sections were used to determine hydraulic radius as a function of the flow depth for the original version of the flow model (Wiele and Smith, 1996).



EXPLANATION

- roughness relation for the original channel shape
- values from dye studies and measured cross-sections at known discharges

Figure 30. Roughness relation for the original channel shape from the average of the Wilson cross-sections, revised using measured wave speeds from the 1996 high flow release from Glen Canyon Dam.

The numerical method used to solve the flow equations in the original version of the model was also modified because the sharp curvature of the hydrograph from the high flow release produced excessive numerical diffusion (Wiele and Griffin, 1997). Changing from a fully implicit numerical scheme to the Crank-Nicholson scheme (Anderson and others, 1984), which time-centers the solution by averaging an explicit solution and an implicit solution at each step, reduced the excessive numerical diffusion. Prediction of wave propagation under more extreme conditions, such as the high flow release, was improved by this modification.

Determination of the Friction Coefficient using Measured Wave Speeds

Hydraulic geometry for the high discharge average channel shape was found using data available from an experimental high flow release from Glen Canyon Dam along with previously measured flow velocities and cross-section areas at known discharges. During the experimental high release, conducted in March and April, 1996, the high flow was preceded by a steady discharge of 226 m³/s (8,000 ft³/s), then increased to 1,270 m³/s (45,000 ft³/s) over a period of about 12 hours. Discharge from the dam was held constant at 1,270 m³/s for about 7 days, then decreased back to 226 m³/s over a period of about 46 hours. This gradual decrease in discharge enabled the use of gaging station records to calculate a kinematic wave speed over the range of discharge of the wave between Lees Ferry at RM 0 (gaging station number 09380000) and Diamond Creek at RM 225 (RK 362; gaging station number 09404200). Discharge was computed from stage measurements and the associated stage-discharge relations at these gaging stations (figure 31). Because of the slow, steady decrease in discharge during the falling limb of the high release, both diffusion and the additional slope of the water surface due to the wave were negligible. The celerity of the wave, dQ/dA , was therefore essentially that of a purely kinematic wave.

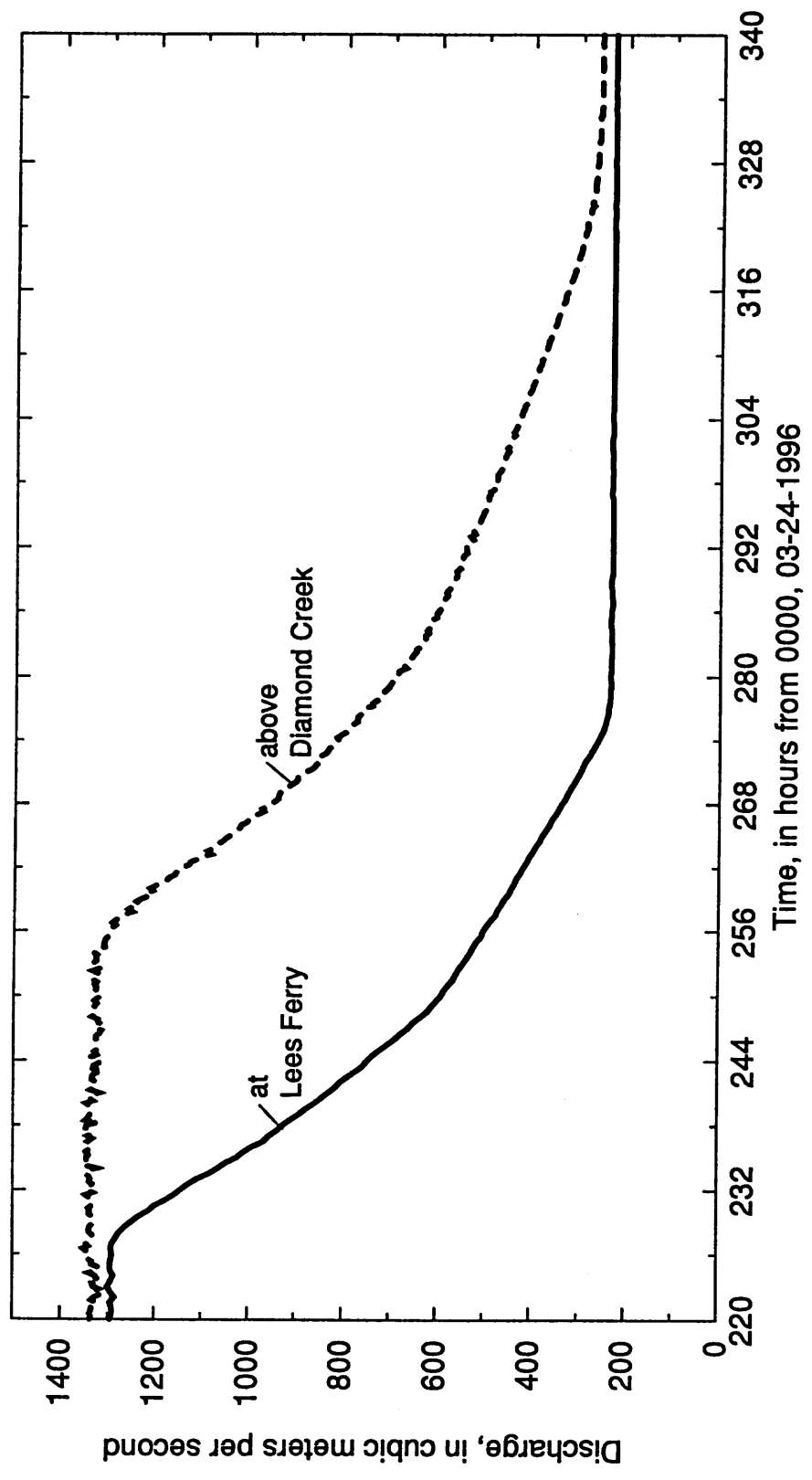


Figure 31. Hydrographs computed from the records of the streamflow-gaging stations at Lees Ferry (RM 0) and above Diamond Creek near Peach Springs (RK 362, RM 225), for the falling limb of the 1996 high flow release.

A kinematic wave has only one wave velocity at each point, and this velocity can be determined from a combination of the continuity and momentum equations, with momentum reduced to $\tau = \rho gRS$ (Lighthill and Whitham, 1955). The combined form of the equation is

$$\frac{dA}{dt} + \frac{dQ_k}{dx} = 0 \quad (6)$$

This equation can be rearranged to solve for the wave speed, c , at a point on a hydrograph:

$$c = \frac{dQ_k}{dA} = -\frac{dx}{dt} \quad (7)$$

where the wave speed is dependent upon the discharge and the channel hydraulic geometry. The wave speed can be determined by finding the amount of time required for a specific discharge to travel the known distance from one gaging station to the next, $\Delta x/\Delta t$, where $\Delta x/\Delta t \approx dx/dt$. Using the gaging station data, Δx is the distance between two gaging stations and Δt the amount of time required for a specific discharge to travel from one gaging station to the next. The reach-averaged wave speed, dQ_k/dA , as a function of discharge during the falling limb of the high flow was then found for the reach from Lees Ferry to Diamond Creek, 362 km downstream (figure 32).

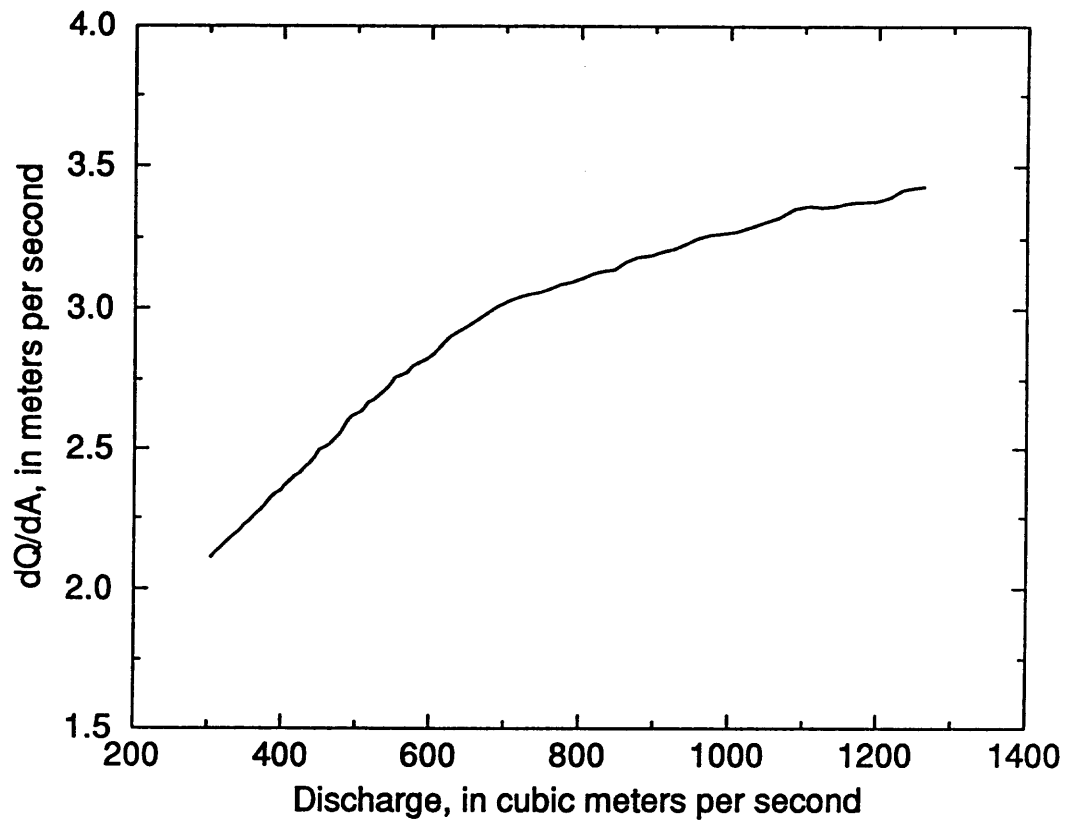


Figure 32. Wave speed calculated from records of the streamflow-gaging stations at Lees Ferry and above Diamond Creek, recorded during the falling limb of the 1996 high flow release.

The relation between area and discharge was found by integrating dQ_k/dA over the range of the wave, using known values of area at given discharges to determine the integration constant. The known values of area and discharge come from measured flow velocities from dye studies conducted at average steady discharges of 432 m³/s (15,300 ft³/s; Graf, 1995) and 1,290 m³/s (45,500 ft³/s; Graf, personal commun.), and from the Wilson cross-sections measured at about 800 m³/s (28,000 ft³/s; Wilson, 1986). Integration of $dA/dQ = f(Q_k)$ is easier than integrating $dQ/dA = f(Q_k)$ because it allows for separation of variables. Therefore, $1/c$ derived from the streamflow-gaging station records was plotted as a function of Q_k , and three lines were fitted to the data (figure 33). The relations for wave speed as a function of discharge and the range of discharges over which they apply are:

(8)

$$c = 1/(a_0 + a_1 \ln Q_k) \quad Q_k \leq 623.5 \text{ m}^3/\text{s}; \quad (8a)$$

$$c = 1/(b_0 + b_1 \ln Q_k + b_2 (\ln Q_k)^2) \quad 623.5 \text{ m}^3/\text{s} < Q_k \leq 715 \text{ m}^3/\text{s}; \quad (8b)$$

$$c = 1/(c_0 + c_1 \ln Q_k) \quad 715 \text{ m}^3/\text{s} < Q_k, \quad (8c)$$

where

$$a_0 = 1.491$$

$$a_1 = -0.1781$$

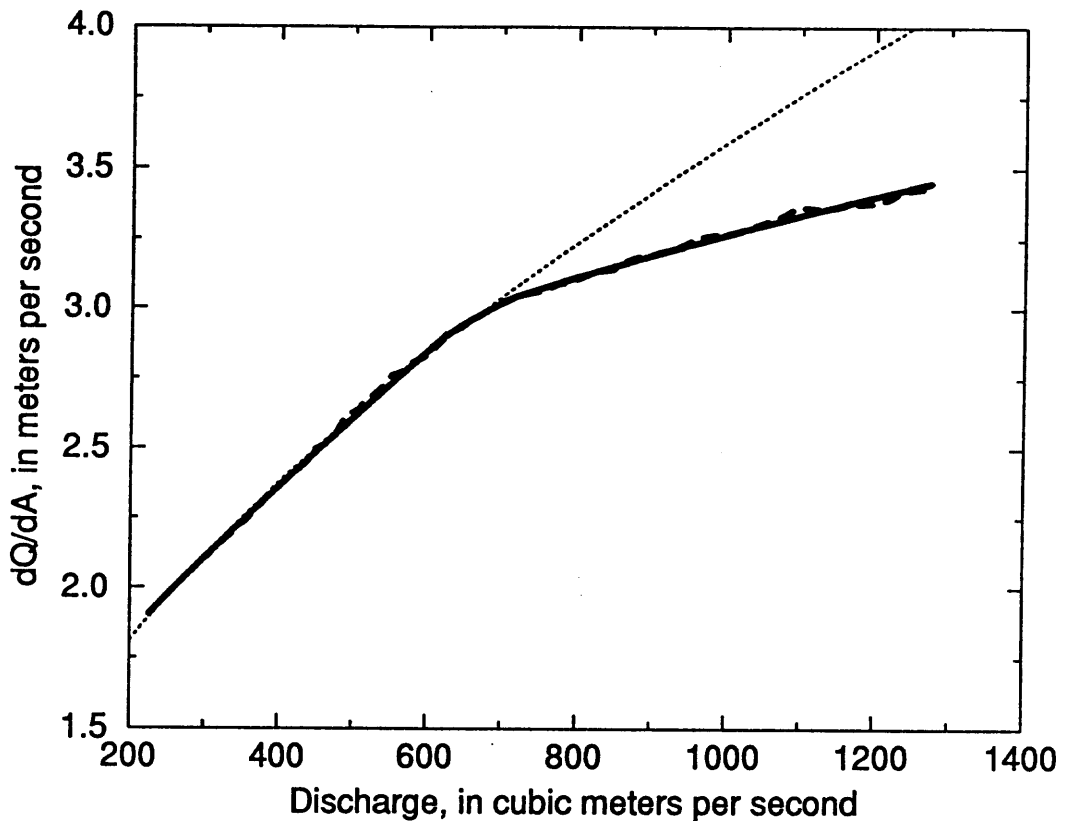
$$b_0 = 9.164$$

$$b_1 = -2.599$$

$$b_2 = 0.1909$$

$$c_0 = 0.7774$$

$$c_1 = -0.06821$$



EXPLANATION

- wave speed calculated from the original model functions
- - - dQ/dA calculated from gaging station records
- 3 regression curves fit to the calculated dQ/dA

Figure 33. Comparison of wave speed calculated from the records of the streamflow-gaging stations at Lees Ferry and above Diamond Creek, recorded during the 1996 high flow release, and the calculated least-squares regression curves for these data. The wave speed calculated using functions in the original version of the one-dimensional unsteady flow model is also shown. The break in slope of the wave speed calculated from the gaging station records from the 1996 high flow release is likely related to the break in slope of the average high-discharge channel shape. As stage increases above the break in the slope of the channel, the rate of increase in dQ_k/dA is reduced based on the proportion of flow over the sides of the channel.

The equations $1/c = f(Q_k)$ were then integrated to obtain relations between discharge and cross-section area. The results of the integrations are equations in the form $A = f(Q_k) + A_0$, where the value of the constant (A_0) is unknown. However, the value of this constant of integration can be determined using measured reach-averaged flow velocities for known discharges along with the relation $u = Q/A$. For example, the dye study performed in 1991 measured flow velocity in the Colorado River below Glen Canyon Dam at an average steady discharge of $432 \text{ m}^3/\text{s}$ ($15,300 \text{ ft}^3/\text{s}$; Graf, 1995). The reach-averaged flow velocity was found to be 0.99 m/s . The cross-section area corresponding to that velocity and discharge is then 436 m^2 . By substituting the known values of discharge and area into the equation $A_0 = A - f(Q_k)$, the value of A_0 was then found for $Q \leq 623.5 \text{ m}^3/\text{s}$. Matching the equations for the higher ranges of discharge at their limits leads to the following equations for calculating area as a function of discharge:

(9)

$$A = 182.32 + a_0 Q_k + a_1 Q_k (\ln Q_k - 1) \quad Q_k \leq 623.5 \text{ m}^3/\text{s}; \quad (9a)$$

$$A = -33.528 + b_0 Q_k + b_1 Q_k (\ln Q_k - 1) + b_2 Q_k ((\ln Q_k)^2 - 2 \ln Q_k + 2) \quad 623.5 \text{ m}^3/\text{s} < Q_k < 715 \text{ m}^3/\text{s}; \quad (9b)$$

$$A = 254.97 + c_0 Q_k + c_1 Q_k (\ln Q_k - 1) \quad 715 \text{ m}^3/\text{s} < Q_k. \quad (9c)$$

The values of the coefficients for these equations are the same as those for equations 8a, b, and c for wave speed as a function of discharge. Using these relations and the average shape of the channel computed from the GIS cross-sections, a relation between the friction coefficient and hydraulic radius was derived, which is described in the next section.

Finding β for a Specific Discharge

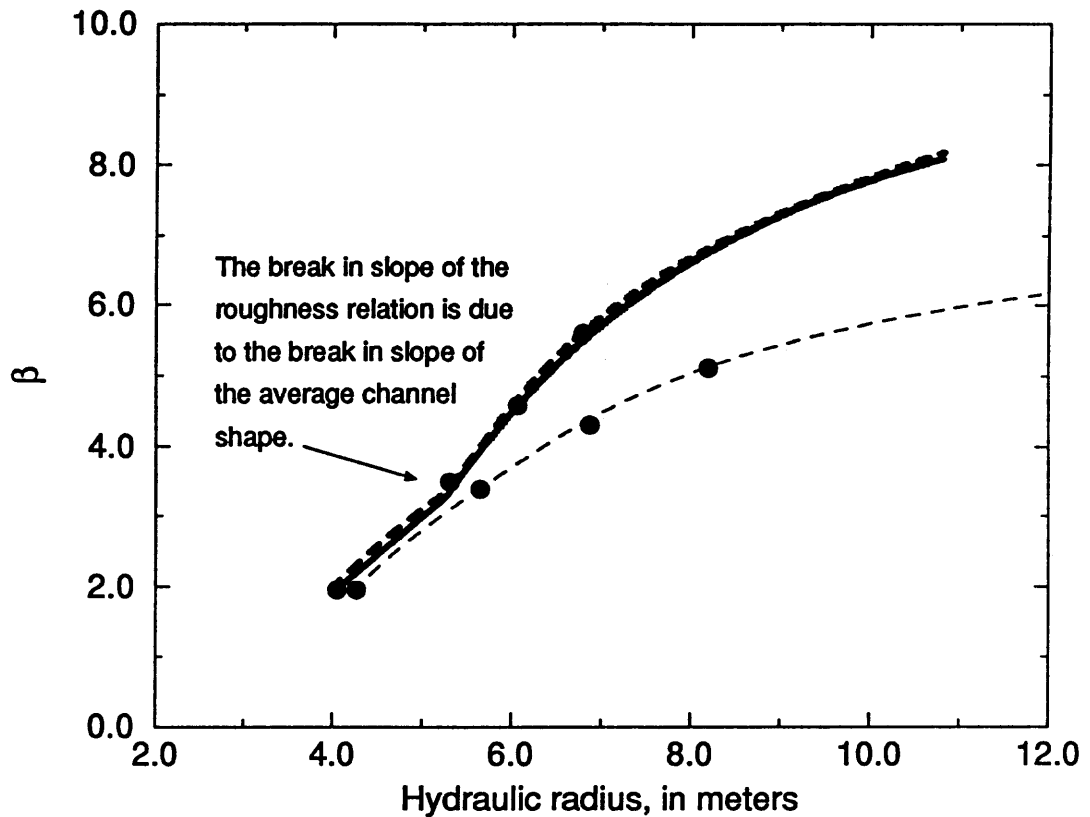
Once the relation between discharge and area was found, the friction coefficient, β , over the range of discharge released during the 1996 high flow was calculated for the new channel shape using the equation:

$$\beta = \frac{Q_k}{A(gRS)^{1/2}} \quad (10)$$

This equation is derived from the relations

$$u = \frac{Q_k}{A} = \beta u_* = \beta(gRS)^{1/2} \quad (11)$$

where the area, A , and hydraulic radius, R , have been related to stage for the specified channel shape, and area was computed from discharge using equations 9a-c. For a purely kinematic wave, the additional slope of the water surface due to the wave is negligible, and is not included in the shear velocity term. For the purpose of the 1d, unsteady flow model, the friction coefficient was then defined as a function of the hydraulic radius using the calculated values of β to compute least-squares regression curves. The break in slope of the side of the channel also affects the relation between hydraulic radius and the roughness parameter. Two separate curves were fitted to the data above and below the hydraulic radius corresponding to a center depth of 7.2 m. Because there are no data for area as a function of discharge above the maximum discharge of the 1996 high flow release (1270 m³/s), a linear extrapolation was made to extend the relation above this discharge. As a result, three separate relations are needed to define roughness as a function of hydraulic radius (figure 34).



EXPLANATION

- beta calculated from new channel shape and area as a function of discharge
- regression curves for calculated beta as a function of hydraulic radius
- values from dye studies and measured cross-sections at known discharges
- roughness relation for the original channel shape

Figure 34. Roughness (β) as a function of hydraulic radius calculated for the new channel shape from the average of the GIS cross-sections, compared to the roughness relation for the original channel shape calculated from the Wilson cross-sections. The points plotted for known values are for the same discharges, but plot on the different curves because of the different relations between area and hydraulic radius for the two average channel shapes. For flows above $1,290 \text{ m}^3/\text{s}$ ($45,500 \text{ ft}^3/\text{s}$), the roughness relation is based in part on a linear extrapolation of the area-discharge relation.

Equations for the lines fitted to the three segments of the data are:

(12)

$$\beta = -2.3765 + 1.0723R \quad R \leq 5.26 \text{ m}; \quad (12a)$$

$$\beta = -24.836 + 24.054 \ln R - 4.2945(\ln R)^2 \quad 5.26 \text{ m} < R \leq 9.50 \text{ m}; \quad (12b)$$

$$\beta = -2.9165 + 4.6559 \ln R \quad 9.50 \text{ m} < R; \quad (12c)$$

where 5.26 m is the hydraulic radius corresponding to a center depth of 7.2 m, with a predicted discharge of 398 m³/s (14,100 ft³/s). Curves 12b and 12c match at a hydraulic radius of about 9.50 m, which corresponds to a center depth of 15.8 m and discharge of about 3,900 m³/s (138,000 ft³/s). The values of roughness obtained for hydraulic radii greater than 6.80 m (center depth of about 10.5 m) using equation 10 result from extrapolating the relation between discharge and area above the range of discharge of the high flow release (1,290 m³/s, or 45,500 ft³/s). Equation 12c, then, is based entirely on the extrapolated area-discharge relation along with the average channel shape from the GIS cross-sections. The correlation coefficients for each of the regressions were greater than 0.99.

The one-dimensional unsteady flow model was modified to incorporate the new shape functions for the average channel shape computed from the GIS cross-sections and the relations derived for calculating roughness as a function of hydraulic radius. Geometric and hydraulic properties determined for the new characteristic channel shape and roughness for selected discharges are shown in table 6. Discharge as a function of stage is also shown in figure 35. The modified model was then applied to several test cases, including dam releases and pre-dam floods. The model results are discussed in the next chapter.

Table 6. Geometric and hydraulic properties of the average channel shape from the GIS cross-sections

Discharge (m ³ /s)	Discharge (ft ³ /s)	Average velocity (m/s)	Shear velocity (m/s)	Area (m ²)	Center depth (m)	Average depth (m)	Top width (m)	Hydraulic radius (m)	Wetted perimeter (m)	Friction coefficient
141.5	4,996	.4818	.2461	293.7	5.481	4.089	71.83	3.981	73.78	1.958
431.2	15,230	.9888	.2847	436.1	7.389	5.512	79.12	5.333	81.77	3.473
792.7	27,990	1.405	.3031	564.4	8.900	6.228	90.63	6.040	121.8	4.635
1292	45,620	1.804	.3215	716.2	10.48	7.015	102.1	6.798	105.4	5.611
2550	90,040	2.436	.3547	1047	13.42	8.561	122.3	8.271	126.6	6.868
3400	120,100	2.733	.3716	1244	14.97	9.403	132.3	9.075	137.1	7.355
5661	199,900	3.318	.4056	1705	18.21	11.25	151.5	10.82	157.6	8.181
8498	300,000	3.868	.4371	2197	21.29	13.09	167.8	12.56	174.9	8.850
14,140	499,300	4.720	.4812	2996	25.77	15.92	188.2	15.24	196.6	9.808

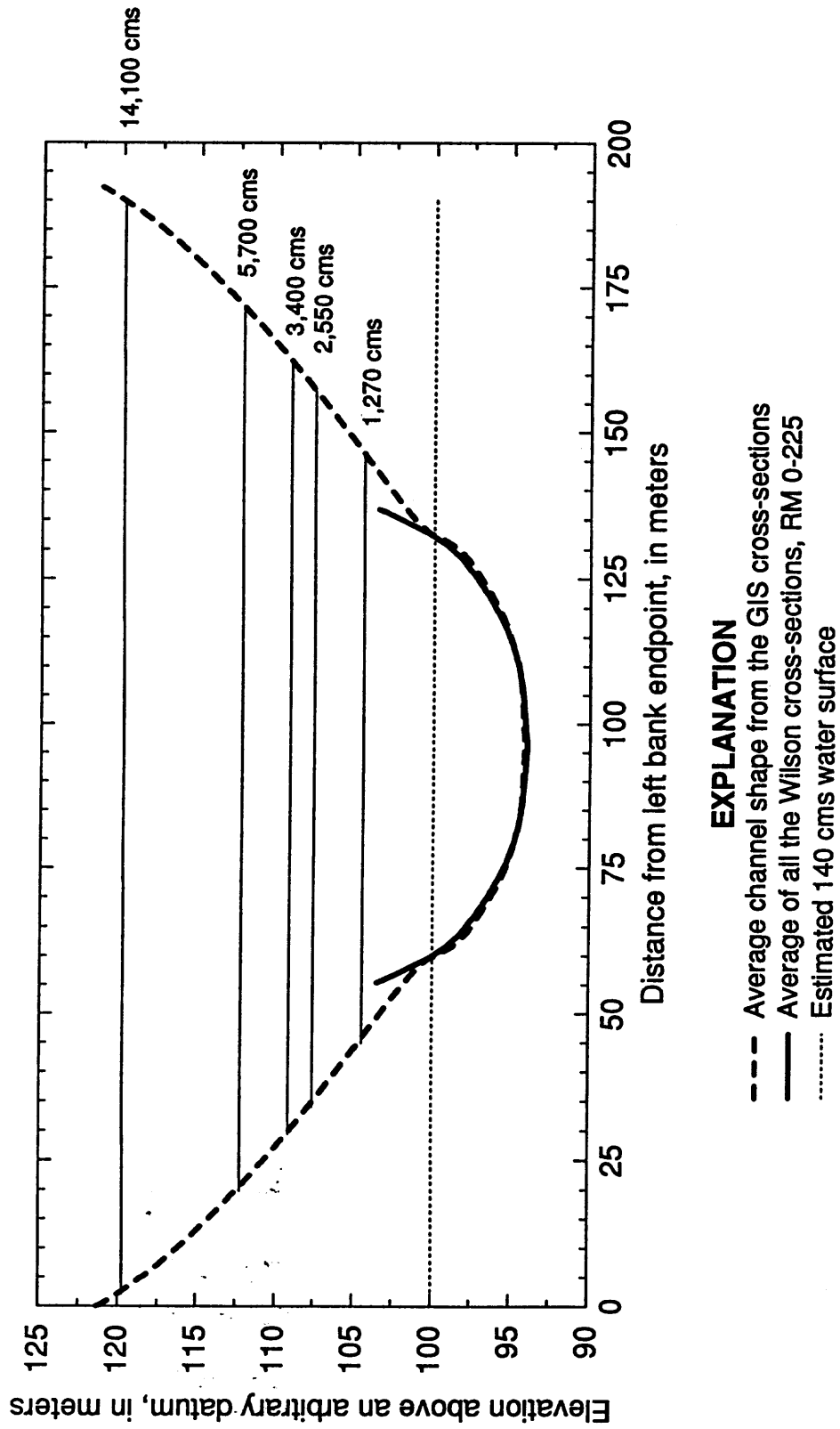


Figure 35. Predicted discharge as a function of stage for the average channel shape calculated from the GIS cross-sections.

CHAPTER 3

RESULTS

Application of the Revised Flow Model

The one-dimensional unsteady flow model was modified using the equations for the new channel shape and roughness derived in the previous section. The revised model was then applied to several different flow conditions, both pre- and post-dam, and compared to hydrographs computed from gaging station records for these flows to check the accuracy of the model results. These cases include: 1) the 1996 high flow ($1,270 \text{ m}^3/\text{s}$; $45,000 \text{ ft}^3/\text{s}$) dam release; 2) a week of normal dam operations; and 3) two pre-dam flood events. In each case, the input hydrograph was the discharge computed from the record of the gaging station and the stage-discharge relation at Lees Ferry, Arizona. The original version of the model was also run for each case to provide a comparison with the new model results. In addition, results from the model version revised using the 1996 high flow release data and the Crank-Nicholson numerical scheme, but still using the average channel shape from the Wilson cross-sections, were included in the comparison.

Application of the Revised Model to the 1996 High Flow Release

The revised model was applied to the 1996 high flow release in order to check whether or not it provides accurate predictions of the timing and rate of the initial rise in discharge at the gaging station locations. Because of the steepness of the rising limb, diffusion effects were large and had a strong affect on the rate at which the wave travelled downstream. Therefore, comparison of model results with hydrographs computed from the gaging station records on the rising limb serves as an independent

test of the hydraulic geometry derived using the falling limb of the hydrographs computed from the gaging station records. The average absolute time error on the rising and falling limbs of the high flow release show significant improvement of the revised models over the original model (tables 7 and 8). On the rising limb, the error was normalized by the travel time of the mid-point of the wave to each gaging station location. Time error on the falling limb was normalized by the time of fall at the particular gaging station location. The normalized error provides a means of comparing the error at each gaging station location to the error at the other locations (Wiele and Griffin, 1997).

Table 7. Error of the original and revised models on the rising limb of the 1996 high flow release

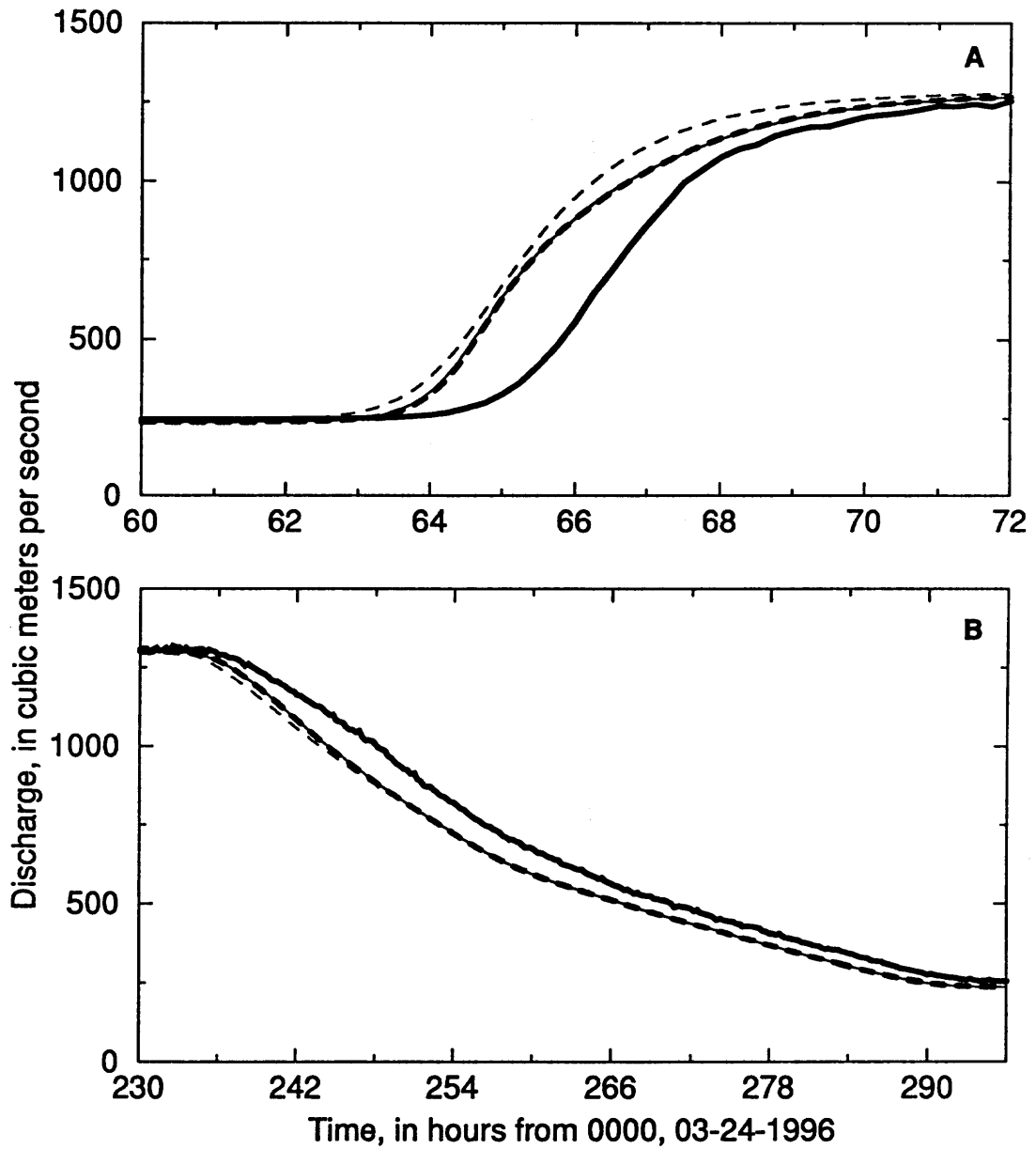
Gaging station location	Original model		Revised model with original channel shape		Revised model with new channel shape	
	average absolute error (hours)	error normalized by wave travel time	average absolute error (hours)	error normalized by wave travel time	average absolute error (hours)	error normalized by wave travel time
above the Little Colorado River, 09383100	1.7	0.16	1.0	0.10	1.1	0.10
near Grand Canyon, 09402500	1.1	0.080	0.57	0.040	0.51	0.035
above Diamond Creek, near Peach Springs, 09404200	1.6	0.045	0.32	0.0092	0.40	0.011

Table 8. Error of the original and revised models on the falling limb of the 1996 high flow release

Gaging station location	Original model		Revised model with original channel shape		Revised model with new channel shape	
	average absolute error (hours)	error normalized by time of fall	average absolute error (hours)	error normalized by time of fall	average absolute error (hours)	error normalized by time of fall
above the Little Colorado River, 09383100	3.6	0.069	3.2	0.062	3.2	0.062
near Grand Canyon, 09402500	1.4	0.026	1.1	0.021	0.99	0.019
above Diamond Creek, near Peach Springs, 09404200	1.4	0.020	0.77	0.011	0.72	0.011

At Diamond Creek, the original model predicted the mid-point of the rising limb of the high flow release would arrive about 1.6 hours earlier than the gaging station records indicate, while the revised model with the new channel shape predicted the arrival of the wave about 0.40 hour late. This time error (0.40 hour) is only about 1.1% of the wave travel time from Lees Ferry to Diamond Creek (about 35 hours). Results of the original model, revised using roughness derived from the high flow measured wave speed and the Crank-Nicholson numerical method for solving the flow equation, are also included in the comparison. This revised version of the original model, which uses the average channel shape from the Wilson cross-sections, produced results similar to those of the revised model using the new channel shape obtained from the GIS cross-sections. For both revised versions of the model, the roughness relations were derived from the channel geometry and wave speed as a function of discharge, which was determined empirically from the falling limb of the high flow release. As a result, the two revised versions of the model, with the original and new channel

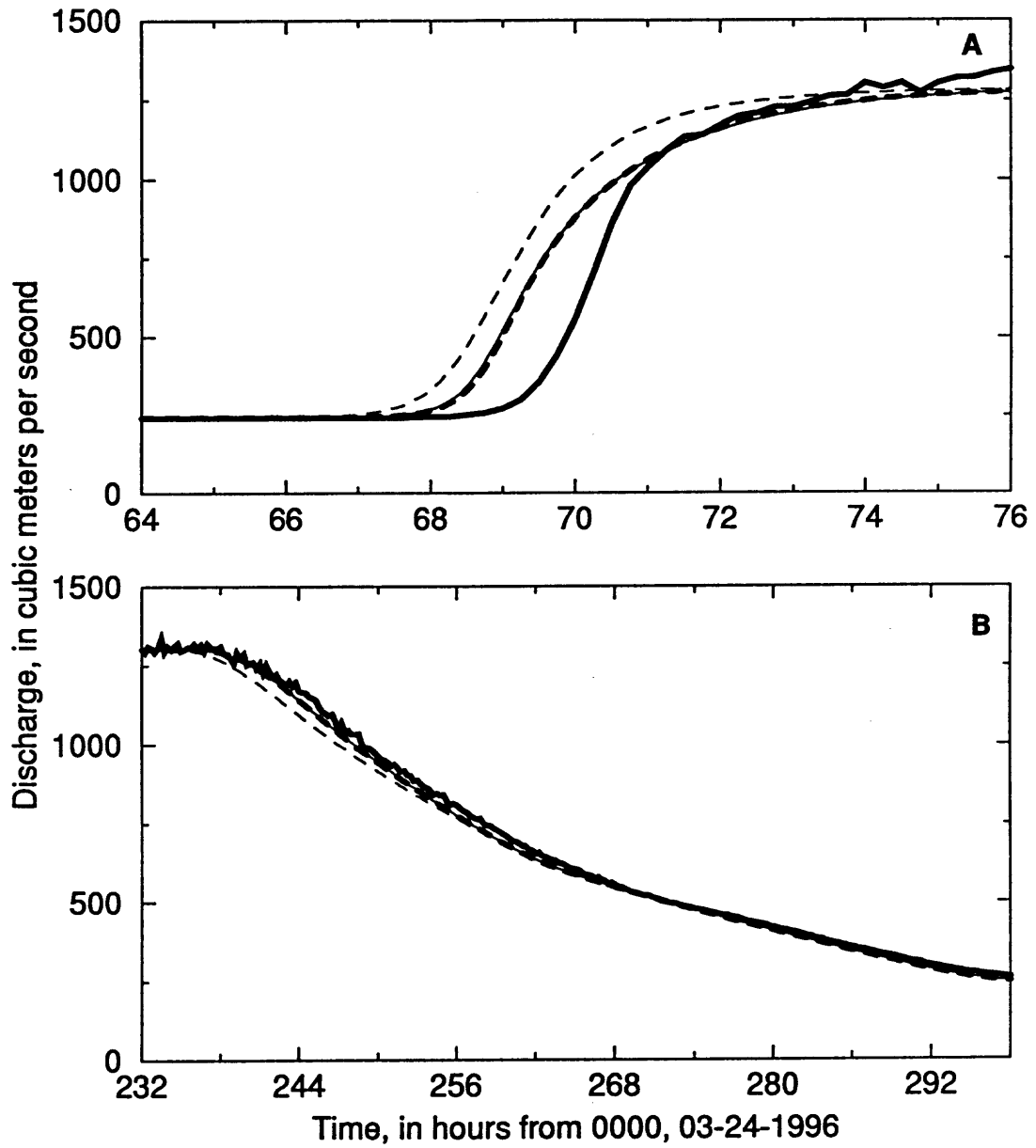
shapes, are expected to and do produce similar results. Comparisons of hydrographs computed from the streamflow-gaging station records and their associated stage-discharge relations with hydrographs calculated by the three different model versions also show the improvement of the revised model results over those from the original model (figures 36-38).



EXPLANATION

- hydrograph from gaging station record
- - - hydrograph from original model
- - - hydrograph from revised model with original channel shape
- . - . hydrograph from revised model with new channel shape

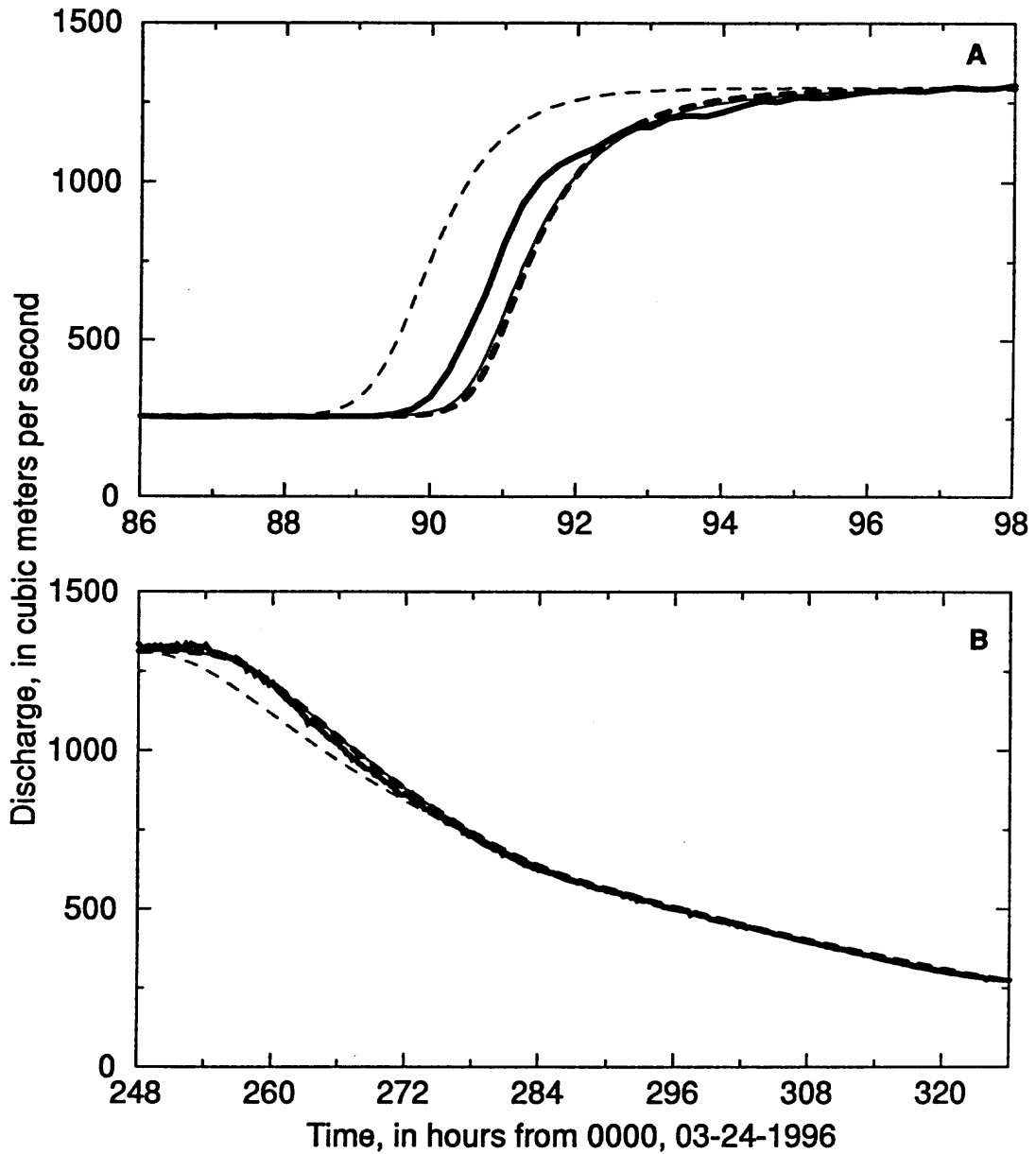
Figure 36. Calculated hydrographs and hydrographs computed from stage records and the stage-discharge relation at streamflow-gaging station Colorado River above the Little Colorado River near Desert View (RK 98, RM 61) for the 1996 high flow release. A, rising limb. B, falling limb. Note the difference in time scales.



EXPLANATION

- hydrograph from gaging station record
- - - hydrograph from original model
- - - hydrograph from revised model with original channel shape
- · - hydrograph from revised model with new channel shape

Figure 37. Calculated hydrographs and hydrographs computed from stage records and the stage-discharge relation at streamflow-gaging station Colorado River near Grand Canyon (RK 142, RM 88) for the 1996 high flow release. A, rising limb. B, falling limb. Note the difference in time scales.



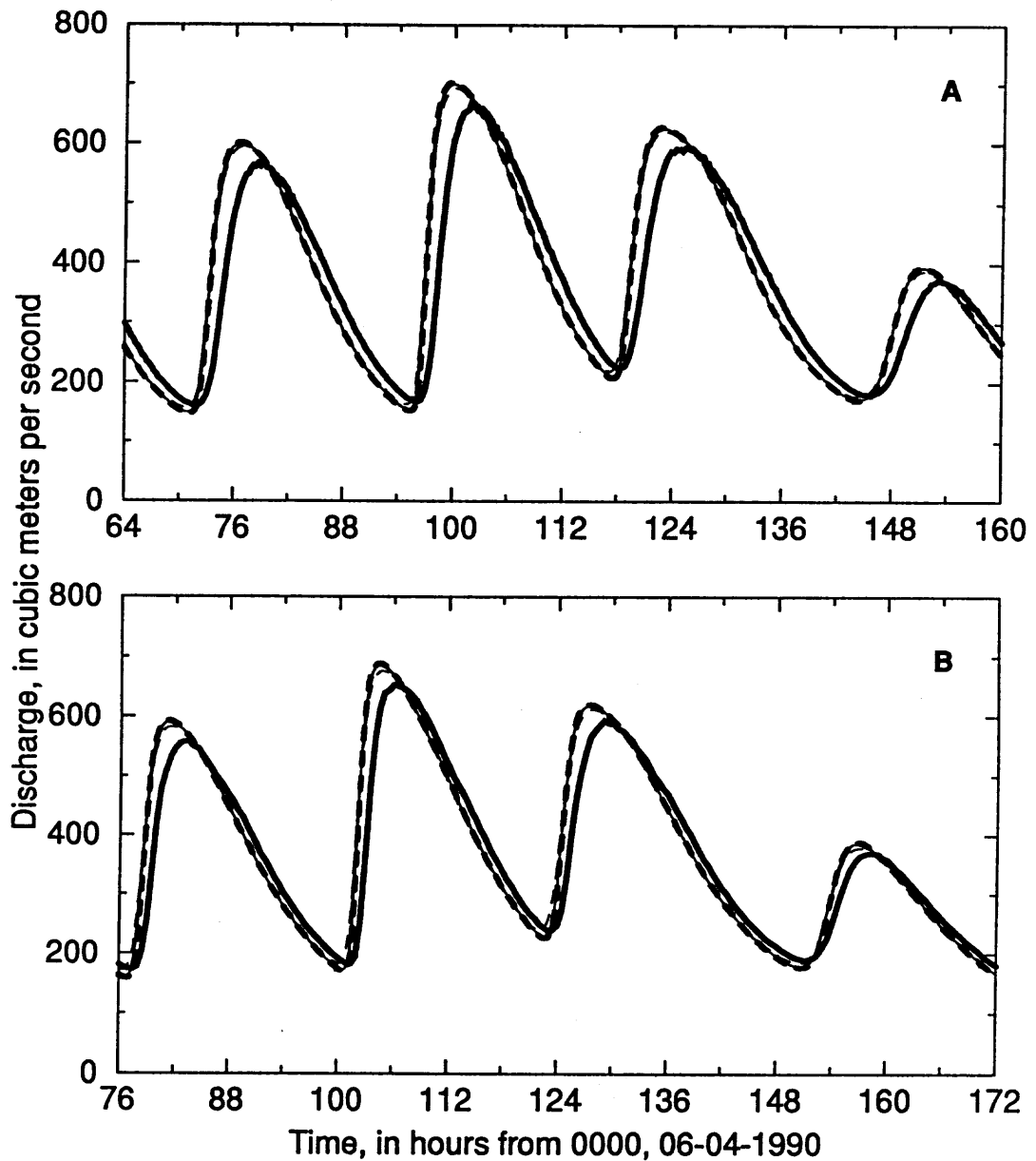
EXPLANATION

- hydrograph from gaging station record
- - - hydrograph from original model
- - - hydrograph from revised model with original channel shape
- · - hydrograph from revised model with new channel shape

Figure 38. Calculated hydrographs and hydrographs computed from stage records and the stage-discharge relation at streamflow-gaging station Colorado River above Diamond Creek near Peach Springs (RK 362, RM 225) for the 1996 high flow release. A, rising limb. B, falling limb. Note the difference in time scales.

Application of the Revised Model to Normal Dam Operations

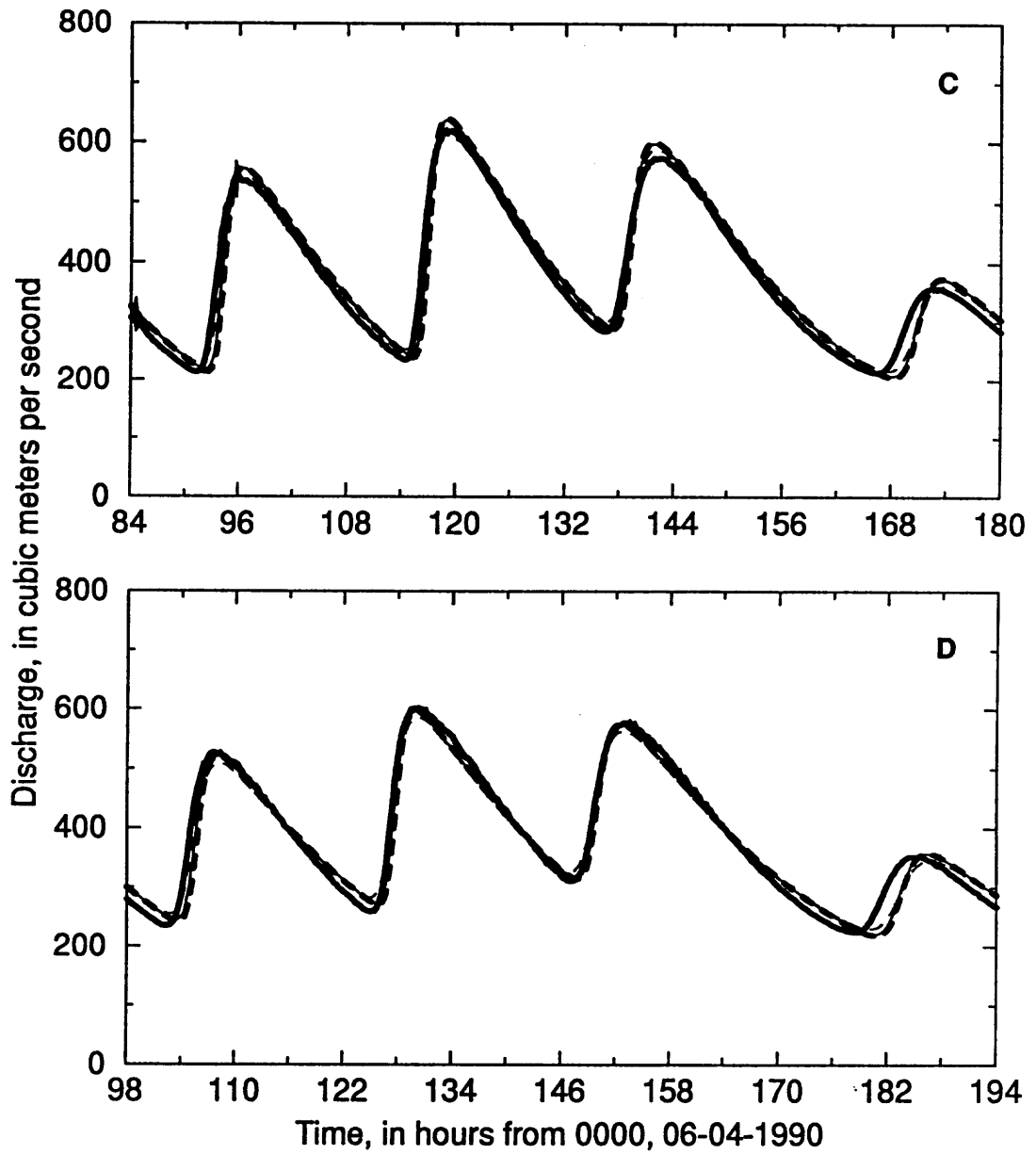
The revised versions of the model were run for a week of normal dam operations to show that they still provide reasonable results for low fluctuating flows (below 790 m³/s) as well as for high flows. Hydrographs were calculated for discharge released from the dam between 06-04-1990 and 06-20-1990, during which the maximum daily discharge at Lees Ferry was about 600 m³/s (21,000 ft³/s) and daily minimum discharge was about 120 m³/s (4,200 ft³/s). On weekends, the daily peak discharge dropped to about 450 m³/s (16,000 ft³/s), while the minimum discharge remained about the same. During this period, the streamflow-gaging station 09404120, Colorado River above National Canyon near Supai (RK 267, RM 166) was also operational, and results at this location were included in the comparison. All three model versions produced similar results at the four gaging station locations downstream from Lees Ferry (figure 39). Therefore, the modifications made to the model to accommodate high flows did not adversely affect the results for low fluctuating flows.



EXPLANATION

- hydrograph from the gaging station record
- - - hydrograph from the original model
- hydrograph from the revised model with the original channel shape
- - - hydrograph from the revised model with the new channel shape

Figure 39. Calculated hydrographs and hydrographs determined from stage records and the stage-discharge relation at Colorado River streamflow-gaging stations during a period of normal dam operations. A, above the Little Colorado River near Desert View (RK 98, RM 61). B, near Grand Canyon (RK 142, RM 88). C, above National Canyon near Supai, (RK 267, RM 166). D, above Diamond Creek near Peach Springs (RK 362, RM 225)



EXPLANATION

- hydrograph from the gaging station record
- - - hydrograph from the original model
- hydrograph from the revised model with the original channel shape
- - - hydrograph from the revised model with the new channel shape

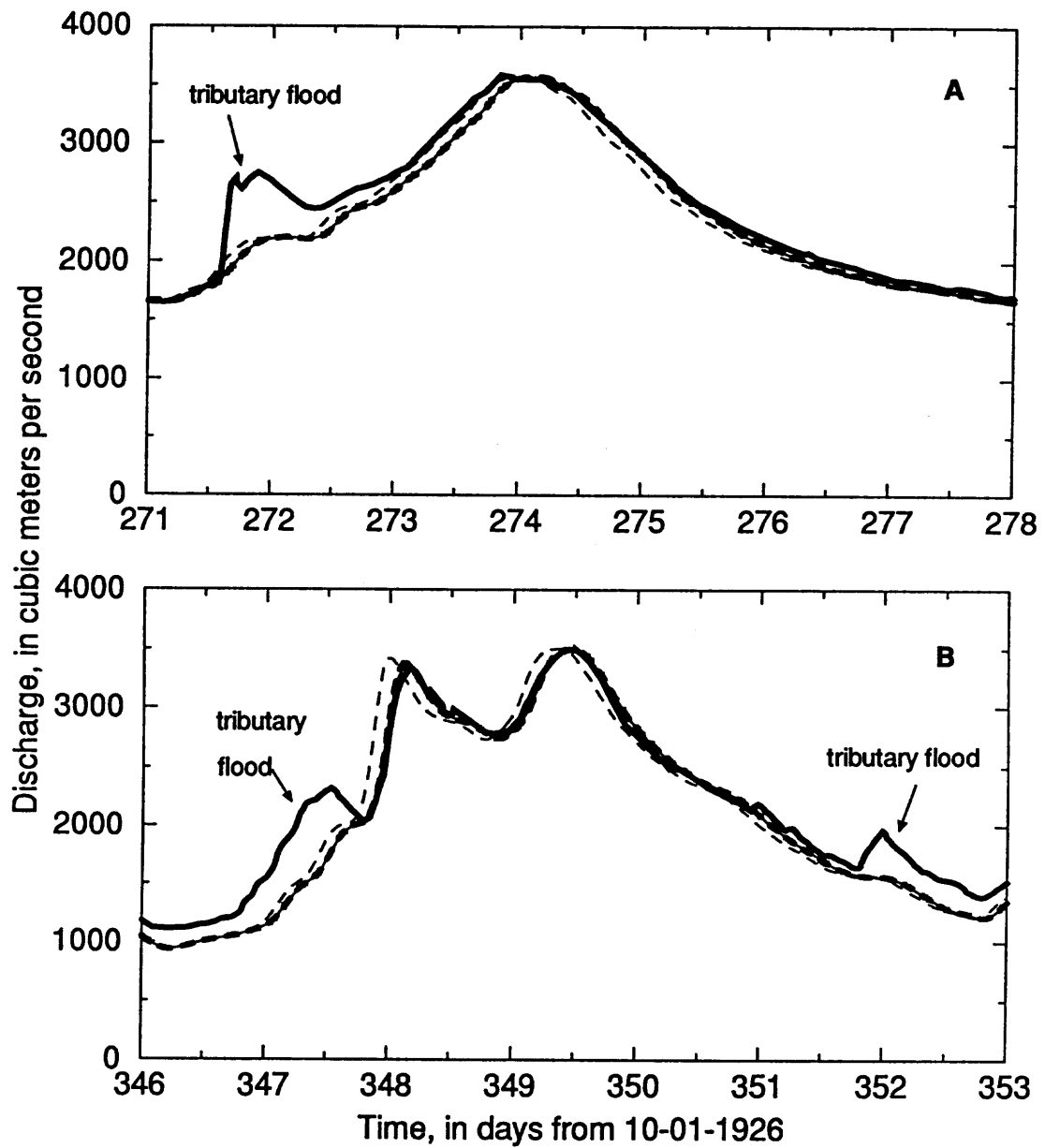
Figure 39, Continued.

Application of the Revised Model to Two Pre-dam Flood Events

Discharge hydrographs computed from the records of the gaging stations at Lees Ferry and near Grand Canyon have been obtained for two periods in 1927 during which floods of the Colorado River reached magnitudes greater than $3,400 \text{ m}^3/\text{s}$ ($120,000 \text{ ft}^3/\text{s}$). These hydrographs were computed from stage records in digital form and the stage-discharge relations for the streamflow-gaging stations in effect during those periods (digital and written records provided by D. Topping, USGS, Boulder). Although no reach-averaged flow velocity measurements have been made above $1,270 \text{ m}^3/\text{s}$ ($45,000 \text{ ft}^3/\text{s}$), the relations used to calculate wave speed and area from discharge as well as the channel roughness as a function of hydraulic radius were extrapolated upward to estimate the hydraulic properties of the channel for higher flows. The estimate of the stage for a $3,400 \text{ m}^3/\text{s}$ flow for the average shape from the GIS cross-sections (15 m) falls within the range of the data used to compute the average shape. Therefore, the relations used to represent this shape were not extrapolated for the higher flow. The average increase in stage from a discharge of $790 \text{ m}^3/\text{s}$ ($28,000 \text{ ft}^3/\text{s}$), the discharge at which the Wilson cross-sections were measured, to a discharge of $3,400 \text{ m}^3/\text{s}$ is estimated to be about 6.1 m.

The hydrograph computed from the gaging station record and associated stage-discharge relation at Lees Ferry was again used as the input hydrograph for each model application (i.e., the upstream boundary condition). Written records for the gaging stations indicate there were large tributary inflows (especially from the Paria and Little Colorado Rivers) during each of these events. Comparison of the gaging station records at Lees Ferry and near Grand Canyon also clearly indicate the presence of unsteady inflows from tributaries during these flood events. However, detailed digital records of the tributary inflows are not available, so no additional unsteady inflows were added when the models were applied to these flows.

Comparison of model-calculated hydrographs and the hydrographs computed from the stage record and associated stage-discharge relation at the streamflow-gaging station near Grand Canyon show significant improvement of the revised versions of the model over the original version (figure 40). This improvement is most apparent for the second flood event, between September 11 and 17, 1927, because tributary inflow during the rising limb of the first event resulted in an increase in discharge as a function of time for the rising limb near Grand Canyon, above what was predicted from the hydrograph at Lees Ferry. For the second flood event, the original version of the model predicted the arrival of the flood peak about 3.9 hours earlier than the arrival of the flood peak determined from the gaging station records. However, the two revised versions of the model, with the original channel shape and the new channel shape from the GIS cross-sections, predicted the arrival of the flood peak 0.7 and 0.9 hours early, respectively. The revised versions of the model, then, provide significant improvement in the prediction of the progress of flood waves from Lees Ferry through Marble and Grand Canyons.



EXPLANATION

- hydrograph from the gaging station near Grand Canyon
- - - hydrograph from the original model
- hydrograph from the revised model with the original channel shape
- - - hydrograph from the revised model with the new channel shape

Figure 40. Calculated hydrographs and hydrographs determined from stage records and the stage-discharge relations at Colorado River near Grand Canyon (RK 142, RM 88). A, from 29 June through 5 July, 1927. B, from 11 September through 17 September, 1927. The results from the two revised models are nearly the same, and show substantial improvement over the results from the original model.

CHAPTER 4

SUMMARY AND CONCLUSIONS

The objectives of this study were to derive a characteristic channel shape for high-discharge flows in the Colorado River through Marble and Grand Canyons and to relate stage to discharge for this characteristic shape. To meet these objectives, a dense set of cross-sections was first extracted from topography in the GCES/GIS database. A method was then developed to average the cross-sections, and a characteristic high-discharge channel shape for the river corridor between Lees Ferry and Lake Mead was derived. Comparisons of the average shapes computed from the GIS data for each of 10 morphologically similar reaches show good agreement with the average shapes calculated using the 199 measured Wilson cross-sections in the same reaches. A break in the slope of the average channel shape was shown to exist in the GIS topography, and to occur at a stage at which the estimated discharge is about the mean daily post-dam discharge ($360 \text{ m}^3/\text{s}$). Evidence indicates the break in slope is consistent with a transition from the dominant effects of channel-forming processes to those of hillslope processes. Channel roughness as a function of stage for discharges up to $1,300 \text{ m}^3/\text{s}$ was derived for the average channel shape using measured wave speed as a function of discharge from the 1996 high flow release.

Also as part of this work, an existing one-dimensional unsteady flow model was modified with functions for the new channel shape and roughness, which resulted in significant improvement of the model's ability to predict the progress of high discharge (above $790 \text{ m}^3/\text{s}$) waves from Glen Canyon Dam to Diamond Creek. Application of the model to pre-dam floods showed that extrapolation of the roughness relation produced improved predictions for discharges as high as $3,400 \text{ m}^3/\text{s}$. The

revised model version using an extrapolation of the average shape calculated from the Wilson cross-sections along with the roughness relation developed for that shape produced results similar to those from the model version with the new shape and roughness. However, it is expected that the new shape from the GIS data will produce better results in a one-dimensional sediment transport model than the extrapolated shape from the Wilson cross-sections, with its continuous steep banks. This conclusion is based on the observed distribution of alluvial sand deposits and sediment transport during the 1996 high flow release.

The results of this work show it is feasible to obtain an average channel shape from GIS data, even when coverage of the reach of interest is limited. In this case, only about 20% of the 362-km (225-mile) reach from Lees Ferry to Diamond Creek is covered by the GIS data. Therefore, extracting topographic information from a GIS database can be used as an alternative to extensive field measurements to derive an average channel shape to use for modeling flow and sediment transport.

Future Work

Further improvement of the one-dimensional unsteady flow model is expected to be achieved by modifying the model to apply to shorter reaches using average channel shapes calculated from the GIS cross-sections for the morphologically similar reaches. Stage measurements recorded during the 1996 high flow release by a number of temporary stage gages installed along the Colorado River between Glen Canyon Dam and Lake Mead can be used to estimate wave speed as a function of discharge for the shorter reaches. During the high flow release, 30 stage-gaging stations spaced a minimum of 8 km (5 miles) apart collected data (personal communication, R. Gauger, USGS, WRD, Flagstaff, Arizona). Stage-discharge relations have not been developed for these gaging stations, so the data simply show stage as a function of time. However, wave speed at the maximum and minimum stages (and discharges) can be

determined from these records. Wave speed for specific reaches can be estimated, then, and used along with average shapes calculated from the GIS cross-sections for the same reaches to determine hydraulic geometry for the reaches. The one-dimensional unsteady flow model can then be modified to route the dam release from reach to reach. This should improve the accuracy of the model as well as enable an estimate of stage as a function of discharge for specific reaches.

Modification of the one-dimensional unsteady flow model to include sediment transport is needed to improve prediction of the availability of sediment, primarily sand, in the channel. Use of high flow releases as a dam management tool is dependent in part on the ability to predict accurately the availability of sand on the channel bed for redistribution to the channel margins. While the influx of sediment from the two primary contributing tributaries, the Paria and Little Colorado Rivers, can be estimated from gaging station records, the ability to predict how sand is redistributed downstream is currently limited. A pool-scale model has been developed that predicted accurately the bed-evolution in a short reach just downstream from the Little Colorado River resulting from a high influx of sediment to the Colorado River during a flood of the Little Colorado River in January, 1993 (Wiele et al., 1996). This model also can be applied in other reaches where bed topography is available, but its accuracy depends in part on the accuracy of the estimate of sediment influx to the reach. By adding sediment transport to the one-dimensional unsteady flow model, better estimates of sand redistribution through the system will be possible.

Another possible extension of this work concerns using variations in topography to estimate channel roughness. Roughness in this system is dominated by large-scale channel features, such as boulders on the bed and debris fans, rather than by bed roughness. Therefore, it should be possible to use the variations in topography, particularly variations in river width with stage, to estimate the channel roughness for both limited reaches of the Colorado River through Marble and Grand Canyons as well

as the entire 362-km reach between Lees Ferry and Diamond Creek. Future work using the GIS data should include a detailed analysis of the topographic variations and an attempt to correlate these variations with large-scale channel roughness.

REFERENCES

- Akima, H., 1978, Bivariate interpolation and smooth surface fitting for irregularly distributed data points, *ACM Transactions for Mathematical Software*, 4, p. 148-159.
- Anderson, D.A., Tannehill, J.C., and Pletcher, R.H., 1984, *Computational Fluid Mechanics and Heat Transfer: Hemisphere*, Washington, D.C.
- Belknap, B. and Evans, L.B., 1989, *Belknap's Waterproof Grand Canyon River Guide*, Westwater Books, Evergreen, Colorado.
- Beus, S.S., and Morales, M., ed., 1990, *Grand Canyon Geology*, Oxford University Press, New York.
- Burkham, D.E., 1986, Trends in selected hydraulic variables for the Colorado River at Lees Ferry and near Grand Canyon, Arizona -- 1922 - 1984, in *Glen Canyon Environmental Studies Report 7* (NTIS PB 88-216098/AS): Salt Lake City, Utah, Bureau of Reclamation.
- Carothers, S.W. and Brown, B.T., 1991, *The Colorado River through Grand Canyon*, The University of Arizona Press, Tucson, Arizona.
- Environmental Systems Research Institute, Inc., 1991, *ARC/INFO® User's Guide, Rev. 6, Surface Modeling with TIN*, ESRI, Inc., Redlands, California.
- Environmental Systems Research Institute, Inc., 1993, *Understanding GIS, the ARC/INFO® Method, Rev. 6 for Workstations*, Longman Scientific and Technical (Copublished in the US with John Wiley and Sons, Inc.) New York.
- Environmental Systems Research Institute, Inc., 1994, *ArcDoc Version 7.0*, ESRI, Inc., Redlands, California.
- Graf, J.B., 1995, Measured and predicted velocity and longitudinal dispersion at steady and unsteady flow, Colorado River, Glen Canyon Dam to Lake Mead. *Water Resources Bulletin*, vol. 31, no. 2: p. 265-281.
- Graf, J.B., Jansen, S.M.D., Fisk, G.G., and Marlow, J.E., 1995a, Topography and bathymetry of the Colorado River, Grand Canyon National Park, Little Colorado River to Tanner Rapids, U.S. Geological Survey Open-File Report 95-726, 7 sheets.
- Graf, J.B., Marlow, J.E., Fisk, G.G., and Jansen, S.M.D., 1995b, Sand-storage changes in the Colorado River downstream from the Paria and Little Colorado Rivers, June 1992 to February 1994, U.S. Geological Survey Open-File Report 95-446.
- Griffin, E.R. and Wiele, S.M., 1996, Calculated Hydrographs for unsteady research flows at selected sites along the Colorado River downstream from Glen Canyon Dam, Arizona, 1990 and 1991, U.S. Geological Survey Water-Resources Investigations Report 95-4266.
- Harden, D.R., 1990, Controlling factors in the distribution and development of incised meanders in the central Colorado Plateau. *Geological Society of America Bulletin*, v. 102, p. 233-242.
- Hereford, R., Thompson, K.S., Burke, K.J., and Fairley, H.C., 1996, Tributary debris fans and the late Holocene alluvial chronology of the Colorado River, eastern Grand Canyon, Arizona. *Geological Society of America Bulletin*, v. 108, no. 1, p. 3-19.

- Howard, A. and Dolan, R., 1981, Geomorphology of the Colorado River in the Grand Canyon. *Journal of Geology*, v. 89, no. 3, p. 269-298.
- Kaplinski, M., Hazel, J.E. Jr., Beus, S.S., 1995, Monitoring the effects of interim flows from Glen Canyon Dam on sand bars in the Colorado River corridor, Grand Canyon National Park, Arizona, final report to Glen Canyon Environmental Studies.
- Kundu, P.K., 1990, *Fluid Mechanics*, Academic Press, Inc., San Diego, CA.
- Leopold, L.B. and Maddock, T. Jr., 1953, The hydraulic geometry of stream channels and some physiographic implications, U.S. Geological Survey Professional Paper 252.
- Leopold, L.B., Wolman, M.G. and Miller, J.P., 1964, *Fluvial Processes in Geomorphology*, W. H. Freeman and Company, San Francisco.
- Lighthill, M.J. and Whitham, G.B., 1955, On kinematic waves, I: flood movement in long rivers. *Proc. Royal Society London A*, 229, p. 281-316.
- Lucchitta, I., 1972, Early history of the Colorado River in the Basin and Range Province. *Geological Society of America Bulletin*, v. 83, p. 1933-1948.
- McCullagh, M.J. and Ross, C.G., Delaunay triangulation of a random data set for isarithmic mapping, *Cartographic Journal*, 17, p. 93-99.
- McKee, E.D. and McKee, E.H., 1972, Pliocene uplift of the Grand Canyon region-- Time of drainage adjustment. *Geological Society of America Bulletin*, v. 83, p. 1923-1932.
- Middleton, G.V. and Wilcock, P.R., 1994, *Mechanics in the Earth and Environmental Sciences*, Cambridge University Press, Cambridge, UK.
- O'Connor, J.E., Ely, L.L., Wohl, E.E., Stevens, L.E., Melis, T.S., Kale, V.S., and Baker, V.R., 1994, A 4500-year record of large floods on the Colorado River in the Grand Canyon, Arizona. *The Journal of Geology*, vol. 102, p. 1-9.
- Randle, T.J. and E.L. Pemberton, 1987, Results and Analysis of STARS modeling efforts of the Colorado River in Grand Canyon, Glen Canyon Environmental Studies, Bureau of Reclamation, Salt Lake City, Utah.
- Schmidt, J.C. and Graf, J.B., 1990, Aggradation and degradation of alluvial sand deposits, 1965 to 1986, Colorado River, Grand Canyon National Park, Arizona, U.S. Geological Survey Professional Paper 1493.
- Schmidt, J.C. and Leschin, M.F., 1995, Geomorphology of post-Glen Canyon Dam fine-grained alluvial deposits of the Colorado River in the Point Hansbrough and Little Colorado River confluence study reaches in Grand Canyon National Park, Arizona, report to Glen Canyon Environmental Studies.
- Smith, J.D., and Wiele, S.M., 1995, Flow and sediment transport in the Colorado River between Lake Powell and Lake Mead, in preparation.
- Stevens, L., 1983, *Colorado River in Grand Canyon, A Guide*. Red Lake Books, Arizona.
- Vieux, V.E., 1993, Geographic Information Systems and non-point source water quality and quantity modelling, in *Terrain Analysis and Distributed Modelling in Hydrology*, K.J. Beven and I.D. Moore, ed., John Wiley and Sons, New York.

- Werth, L.F., Wright, P.J., Pucherelli, M.J., Wegner, D.L., and Kimberling, D.N., 1993, Developing a geographic information system for resources monitoring on the Colorado River in the Grand Canyon, Report Number R-93-20, Dept. of the Interior, Bureau of Reclamation, Denver, Colorado.
- Wiele, S.M., Graf, J.B., and Smith, J.D., 1996, Sand deposition in the Colorado River in the Grand Canyon from flooding of the Little Colorado River. American Geophysical Union, *Water Resources Research*, v. 32, no. 12, p. 3579-3596.
- Wiele, S.M. and Griffin, E.R., 1997, Extended range of a one-dimensional flow model of the Colorado River between Glen Canyon Dam and Lake Mead, Arizona, in preparation.
- Wiele, S.M. and Smith, J.D., 1996, A reach-averaged model of diurnal discharge wave propagation down the Colorado River through the Grand Canyon. American Geophysical Union, *Water Resources Research*, v. 32, no. 5, p. 1375-1386.
- Williams, G.P., 1978, Hydraulic geometry of river cross sections---Theory of minimum variance, U.S. Geological Survey Professional Paper 1029.
- Wilson, R.P., 1986, Sonar patterns of Colorado riverbed, Grand Canyon, *Proceedings of the Fourth Federal Interagency Sedimentation Conference, 2*, Las Vegas, Nevada.

Appendix A. Locations of GIS reaches in relation to river level geology and geomorphology (modified from Smith and Wiele, 1995).

Span of Morphologically Similar Reach (River Miles)	Span of Reach (River Kilometers)	Dominant Rock Types	Distribution of GIS Reaches
0 - 11 0.8 - 1.5 1.5 - 3.8 3.8 - 5.5 5.5 - 11.2	0 - 18 1.3 - 2.4 2.4 - 6.2 6.2 - 9.0 9.0 - 18.0	Mixed Permian Rocks Kaibab Limestone Toroweap Limestone Coconino Sandstone Hermit Shale	 Site 2, RM 0 - 2 Lees Ferry
11 - 23	18 - 37	Pennsylvanian Clastic Rocks Supai Group	
23 - 50 23.2 - 33.9 33.9 - 48.8	37 - 81 37.4 - 54.5 54.5 - 78.8	Mid and Lower Paleozoic Limestones Redwall Limestone Muav Limestone	 Site 3, RM 42 - 48 President Harding Rapid & Point Hansbrough
50 - 63.3 48.8 - 59.3 59.3 - 63.3	81 - 101.8 78.8 - 95.5 95.5 - 101.8	Cambrian Sedimentary Rocks Bright Angel Shale Tapeats Sandstone	 Site 4, RM 51 - 56 Nankoweap  Site 5, RM 60 - 63.3 Little Colorado River
63.3 - 77	101.8 - 124	PreCambrian Sedimentary Rocks Unkar Group	 Site 5, RM 63.3 - 72 above Carbon Creek to Cardenas Creek

Appendix A. Locations of GIS reaches in relation to river level geology and geomorphology (modified from Smith and Wiele, 1995).

Span of Morphologically Similar Reach (River Miles)	Span of Reach (River Kilometers)	Dominant Rock Types	Distribution of GIS Reaches
77 - 107	124 - 172	PreCambrian Metamorphic Rocks Vishnu Schist and Zoroaster Granite	 Site 6, RM 93 - 99 Granite Rapid to Crystal Rapid
107 - 140 106.7 - 109.6 109.6 - 117.3 117.3 - 127.1 127.1 - 130.7 130.7 - 137.5 137.5 - 139.7	172 - 225 171.8 - 176.4 176.4 - 188.8 188.8 - 204.5 204.5 - 210.3 210.3 - 221.3 221.3 - 224.8	Basal Cambrian and Mixed PreCambrian Rocks Unkar Group Vishnu Schist Tapeats Sandstone Vishnu Schist Bass Limestone Tapeats Sandstone	 Site 7, RM 120 - 123 Blacktail Canyon  Site 8, RM 133 - 138 Tapeats and Deer Creeks
140 - 169	225 - 272	Cambrian Limestone Muav Formation	 Site 9, RM 143 - 145 Kanab Creek

Appendix A. Locations of GIS reaches in relation to river level geology and geomorphology (modified from Smith and Wiele, 1995).

Span of Morphologically Similar Reach (River Miles)	Span of Reach (River Kilometers)	Dominant Rock Types	Distribution of GIS Reaches
<p>169 - 190 169.1 - 176.6</p> <p>176.6 - 178.8 178.8 - 190.1</p>	<p>272 - 306 272.1 - 284.2</p> <p>284.2 - 287.7 287.7 - 305.9</p>	<p>Cambrian Clastic Rocks Bright Angel Shale</p> <p>Tapeats Sandstone Lava over Cambrian Rocks</p>	<p> Site 10, RM 179 - 181 Lava Falls</p>
<p>190 - 225</p> <p>190.1 - 207.8</p> <p>207.8 - 225.0</p>	<p>306 - 362</p> <p>305.9 - 334.4</p> <p>334.4 - 362.4</p>	<p>Basal Cambrian and PreCambrian Metamorphic Rocks Tapeats Sandstone over Vishnu Schist</p> <p>Vishnu Schist</p>	<p> Site 11, RM 207 - 210 Granite Park</p>

Note: The placement of the GIS reach names and shaded boxes in the table is intended to show their approximate locations in relation to the distribution of rock types at river level.